Chem Soc Rev

REVIEW ARTICLE

View Article Online
View Journal | View Issue

Check for updates

Cite this: Chem. Soc. Rev., 2018, 47, 8349

Functionalised heterogeneous catalysts for sustainable biomass valorisation

Putla Sudarsanam,*[a] Ruyi Zhong,[bc] Sander Van den Bosch,[a] Simona M. Coman,[d] Vasile I. Parvulescu*[d] and Bert F. Sels*[a]

Received 16th May 2018

DOI: 10.1039/c8cs00410b

rsc.li/chem-soc-rev

Efficient transformation of biomass to value-added chemicals and high-energy density fuels is pivotal for a more sustainable economy and carbon-neutral society. In this framework, developing potential cascade chemical processes using functionalised heterogeneous catalysts is essential because of their versatile roles towards viable biomass valorisation. Advances in materials science and catalysis have provided several innovative strategies for the design of new appealing catalytic materials with well-defined structures and special characteristics. Promising catalytic materials that have paved the way for exciting scientific breakthroughs in biomass upgrading are carbon materials, metal–organic frameworks, solid phase ionic liquids, and magnetic iron oxides. These fascinating catalysts offer unique possibilities to accommodate adequate amounts of acid–base and redox functional species, hence enabling various biomass conversion reactions in a one-pot way. This review therefore aims to provide a comprehensive account of the most significant advances in the development of functionalised heterogeneous catalysts for efficient biomass upgrading. In addition, this review highlights important progress ensued in tailoring the immobilisation of desirable functional groups on particular sites of the above-listed materials, while critically discussing the role of consequent properties on cascade reactions as well as on other vital processes within the bio-refinery. Current challenges and future opportunities towards a rational design of novel functionalised heterogeneous catalysts for sustainable biomass valorisation are also emphasized.

Open Access Article. Published on 18 September 2018. Downloaded on 21/02/2026 10:11:12 PM.
This article is licensed under a Creative Commons Attribution-NonCommercial 3.0 Unported Licence.

1. Introduction

Rapid population growth and vast economic developments elicited an unforeseen increase in global energy demand that is estimated to double between 2000 and 2035.[1] Fossil fuel sources, such as crude oil, coal, and natural gas currently hold the major share of energy supply. However, fossil fuels are non-renewable and global petroleum production is predicted to peak by 2020 due to increasing demand for chemical industries, before decaying.[2] The first oil crisis in 1973 raised an awareness about the limited availability of traditional oil and gas sources.[3] Another major concern of the 21st century is the increasing levels of greenhouse gas emissions (*e.g.*, CO_2) caused by the enormous consumption of fossil fuels.[4,5] Global CO_2 emissions reached an all-time record of 41.5 ± 4.4 billion tonnes in 2017, contributing to an atmospheric CO_2 concentration of 408 ppm, the highest since the beginning of the industrial revolution.[6–8] If this situation continues, global average temperatures are estimated to increase drastically in the range of 2.5–5.4 °C above pre-industrial levels by 2050.[2] Global warming is a major threat to humankind as well as to the biosphere, as witnessed by the increased rate and intensity of many climate catastrophes in recent times. In order to control global warming, several countries have issued stringent regulations to reduce the utilisation of fossil fuels, moving towards a carbon-neutral society. In December 2015, the 21st Conference of the Parties to the United Nations Framework Convention on Climate Change (COP21/CMP11, Paris) led to an agreement between 195 countries to reduce CO_2 emissions, with a target to limit global temperatures to below 1.5 °C above pre-industrial levels.[9] The European Union also set the exacting ecological targets, for example a 20% reduction in CO_2 emissions by 2020 compared to 1990 levels.[10] Part of the European Union goal is also to expand the renewable energy market share to 20% of the total energy supply by 2020. In view of these concerns and challenges, there has been a growing research interest towards the use of clean, sustainable resources for the production of fuels and chemicals.

[a] Centre for Surface Chemistry and Catalysis, Faculty of Bioscience Engineering, KU Leuven, Celestijnenlaan 200f, B-3001, Heverlee, Belgium. E-mail: sudarsanam.putla@kuleuven.be, putla2007@gmail.com, bert.sels@biw.kuleuven.be; Fax: +32 16 321 998; Tel: +32 16 321 610
[b] Department of Chemistry, Southern University of Science and Technology, Shenzhen, 518055, China
[c] Dalian Institute of Chemical Physics, Chinese Academy of Sciences, Dalian 116023, China
[d] University of Bucharest, Department of Organic Chemistry, Biochemistry and Catalysis, B-dul Regina Elisabeta 4-12, Bucharest 030016, Romania

Open Access Article. Published on 18 September 2018. Downloaded on 21/02/2026 10:11:12 PM.
This article is licensed under a Creative Commons Attribution-NonCommercial 3.0 Unported Licence.

Various renewable resources, such as wind, geothermal, solar, hydropower, and biomass are available for the production of energy and/or chemicals (Fig. 1). As a highly abundant, natural carbon source, biomass is considered as a promising renewable alternative to fossil fuels that can be transformed into a wide range of value-added chemicals, clean solvents, and high-energy density fuels.[1,11–16] Global annual production of biomass is estimated to be greater than 10 billion tons (dry basis), equating to more than 10% of global energy supply.[17–19] Untapped biomass sources could generate a huge amount of energy, equivalent to more than 2 billion tons of standard coal.[19] The National Renewable Energy Action Plans estimated that biomass would provide around 42% of the total renewable energy needed for electricity, heating, and cooling by 2020.[20] Several biomass resources, such as animal waste, agricultural crops, wood, and aquatic plants are available for the production of sustainable chemicals.[21] These biomass feedstocks can be harnessed within a relatively short period, boosting environmental credentials.

A large number of technologies based on biological, thermal, and chemical processes have been developed for biomass valorisation (Fig. 2).[22,23] Among those, chemical processing of biomass

Putla Sudarsanam

Dr Putla Sudarsanam (1986), currently Marie Curie Postdoctoral Researcher at KU Leuven (Belgium), obtained his PhD degree in Chemistry (2015) from CSIR-Indian Institute of Chemical Technology (India) under the guidance of Dr B. Mahipal Reddy. His research mainly focuses on developing novel heterogeneous solid catalysts for biomass valorisation, sustainable organic transformations, and automotive exhaust gas purification. He authored about 46 peer-reviewed journal articles with an h-index of 24 and more than 1360 citations. He has been received several awards/fellowships, such as Marie Skłodowska-Curie Fellowship-2016 (Belgium), Young Scientist Award-2017 to participate in the 67th Nobel Laureate Meeting (Germany), Leibniz-DAAD Postdoc Fellowship-2016 (Germany), Best PhD Thesis Award-2015 (Catalysis Society of India), EuropaCat PhD Student Award-2013 (XIth European Congress on Catalysis, France) and Endeavour Research Fellowship-2013 (Australia).

Ruyi Zhong

Ruyi Zhong (1987), currently a joint postdoc of Southern University of Science and Technology and Dalian Institute of Chemical Physics, Chinese Academy of Sciences, obtained her PhD degree in 2017 at the Centre for Surface Chemistry and Catalysis under the guidance of Prof. Bert Sels. Her research focuses on the synthesis and functionalization of mesostructured silica–carbon nanocomposites and their application in biomass conversion. Her expertise includes solid acid catalysis in biomass-related reactions, templated synthesis of mesostructures, tuning surface properties of composite catalysts and various characterization methods.

Sander Van den Bosch

Sander Van den Bosch (1990), currently postdoctoral researcher at KU Leuven, obtained his PhD degree in 2017 at the Centre for Surface Chemistry and Catalysis under the guidance of Prof. Bert Sels. His research focuses on the improved valorisation of lignin for future biorefining, using innovative lignin-first strategies. His expertise includes heterogeneous catalysis for biomass conversions, lignin chemistry, and biomass characterisation.

Simona M. Coman

Simona M. Coman (1969), obtained her PhD degree in 2001 in the field of heterogeneous hydrogenation catalysis. After several research stages in KU Leuven, Belgium, a post-doctoral stage in UC Louvain-la-Neuve, Belgium and a research fellowship of AvH Foundation, in HU Berlin, Germany, she became, in 2008, full professor at University of Bucharest. In 2012, she was awarded the "Gheorghe Spacu" award in the field of Chemical Sciences by the Romanian Academy. Her areas of research interest include heterogeneous catalysis for fine chemical and pharmaceutical intermediates and the biomass conversion. She authored about 90 peer-reviewed papers with an h index of 23.

This journal is © The Royal Society of Chemistry 2018

Open Access Article. Published on 18 September 2018. Downloaded on 21/02/2026 10:11:12 PM.
This article is licensed under a Creative Commons Attribution-NonCommercial 3.0 Unported Licence.

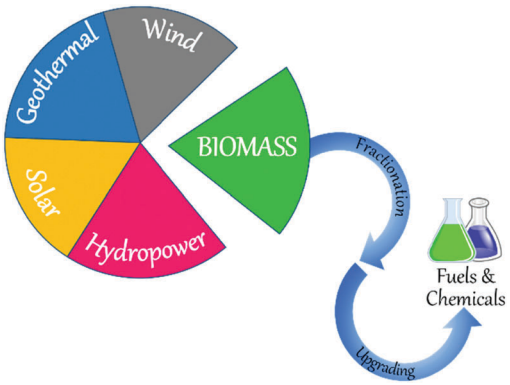

Fig. 1 Available renewable energy sources and valorising biomass into fuels and chemicals.

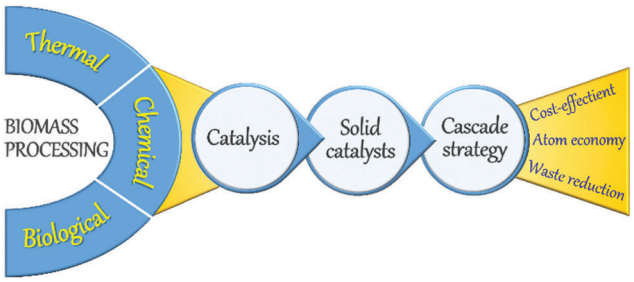

Fig. 2 Concept of sustainable biomass processing.

is of paramount research interest as the resulting products can exhibit relatively equating characteristics to petro-based products. Various kinds of chemical processes, such as fast pyrolysis, hydro-processing, oxidation, dehydration, hydrolysis, (trans)esterification, isomerisation, and many others have been reported, in which the application of a catalyst is crucial to enhance reaction rates and to obtain high yields of desirable products in a short time period. Indeed, catalysis is a key technology in modern chemical industry and plays an essential role in the production of a vast majority of bulk and commodity chemicals.[3] Catalysis greatly contributes to the development of new, greener, and potential chemical processes, offering feasible alternatives to stoichiometric reactions, thus acting as a driving force towards a more sustainable chemical industry.[24–26] Homogeneous and heterogeneous catalysts are both used in petrochemical industry as well as in biomass upgrading. Homogeneous catalysts, where the active sites are in the same phase as the reactants, can interact efficiently with the reaction substrates, typically resulting in higher turnover frequency (TOF) rates compared to heterogeneous catalysts. However, homogeneous catalysts are often associated with high toxicity, corrosivity, energy-intensive separation and purification procedures, and inefficient reusability. Stringent government regulations have therefore directed chemical industries to search for alternative catalytic materials. In this respect, heterogeneous catalysis, where the catalyst exists in a different phase (typically solids) as the reactants (mostly liquids or gasses), could offer tremendous potentials for several energy- and environmental-related applications including biomass upgrading.[27–30] Availability of facile preparation methods, low production costs, remarkable robustness, high resistance to common reaction conditions (moisture, air, pressure, and temperature) and durable lifetime are some of the primary advantages of heterogeneous solid catalysts. More importantly, solid catalysts can be efficiently recovered from reaction mixtures and can be readily reused in multiple catalytic cycles, making the process cost-effective and more sustainable.

Vasile I. Parvulescu

Vasile I. Parvulescu received his PhD from the Polytechnic University of Bucharest in 1986 with a thesis investigating the selectivity of bi- and multi-metal catalysts in hydrogenation of aromatic hydrocarbons. After several years as high-signor researcher at the Institute of Inorganic and Rare Metals, in 1992 he joined the University of Bucharest, where he becomes full professor in 1999. He is currently director of the Department of Organic Chemistry, Biochemistry and Catalysis. His scientific interest concerns the study of heterogeneous catalysts for green and fine chemistry and environmental protection. He authored more than 370 papers, 27 patents, and 7 books. He was awarded by the Romanian Academy ("Nicolae Teclu" Award, 1990), Romanian President (Knight for Merits, 2008) and The National Grand Lodge of Romania ("Grigore Moisil" award for exact sciences, 2015).

Bert F. Sels

Bert F. Sels (1972), currently full professor at KU Leuven, obtained his PhD degree in 2000 in the field of heterogeneous oxidation catalysis. He was awarded the DSM Chemistry Award in 2000, the Incentive Award by the Belgian Chemical Society in 2005, and the Green Chemistry Award in 2015. He is currently director of the Centre for Surface Chemistry and Catalysis, designing heterogeneous solid catalysts for future challenges in industrial organic and environmental catalysis. His expertise includes heterogeneous catalysis in bio-refineries, design of hierarchical zeolites and carbons and the spectroscopic and kinetic study of active sites for small-molecule activation. He authored about 300 peer-reviewed journal articles with an h index of 70 and more than 16 700 citations, and filed 25 patents.

Open Access Article. Published on 18 September 2018. Downloaded on 21/02/2026 10:11:12 PM.
This article is licensed under a Creative Commons Attribution-NonCommercial 3.0 Unported Licence.

One-pot cascade catalytic reactions play a pivotal role towards sustainable biomass valorisation (Fig. 2).[31–34] Cascade reactions can improve the atom economy or the E-factor ($kg_{waste}/kg_{product}$) by limiting the number of energy-intensive steps needed for the isolation and purification of intermediate products as well as for the catalysts recovery. In this context, the versatile application of multifunctional solid catalysts with adequate amounts of acid, base or redox active sites is essential. Advances in the fields of chemistry, materials science, spectroscopy, and catalysis enabled us to get a profound understanding of key steps involved in the rational design of new, multifunctional solid catalysts as well as in the heterogeneous catalytic reactions. Important aspects are fine-tuning of catalyst properties, efficient functionalisation of solid catalysts, behaviour of reactants/intermediates/products with the solid surface, and the modifications in catalyst properties during and after the reaction. This in-depth understanding has provided several innovative strategies, paving the way for the development of state-of-the-art solid phase catalysts, which are highly valuable not only for petrochemicals production and environmental pollution control, but also for sustainable biomass valorisation.

Over the last few years, a variety of functionalised heterogeneous catalysts has been developed for biomass upgrading, including zeolites, carbon materials, mesoporous silica, metal–organic frameworks, metal oxide supported metals, solid phase ionic liquids, magnetic iron oxides, and organic polymers.[21,30,35] In particular, carbon materials, metal–organic frameworks, solid phase ionic liquids, and magnetic iron oxides have received great attention because of exciting scientific breakthroughs and their extensive catalytic applications in biomass valorisation (Fig. 3). Accommodating ample amounts of acid–base and redox functional species is one of the unique features of these materials, making them capable of catalyzing various biomass conversion reactions in a one-pot way. For instance, carbon materials (*e.g.*, activated carbon, graphene, carbon nanotubes, carbon nanofibers, and mesoporous carbons) can play a vital role in biomass valorisation because of their fascinating characteristics associated with tailorable porosity, rich surface chemistry, high specific surface area, and remarkable hydrophobicity.[35] In addition, new functional carbon-based materials can be synthesised through pyrolysis of renewable biomass molecules (cellulose, sucrose, glucose, *etc.*) and their subsequent application as catalyst support or catalytically active phase in the biomass valorisation will be an added advantage in the context of sustainable biomass upgrading.

Metal–organic frameworks (MOFs), an extraordinary family of crystalline porous materials, are of particular research interest for biomass upgrading and considered as a promising alternative to typical porous zeolite and silica catalysts.[36–38] MOFs are composed of metal nodes and organic ligands, which virtually contain considerable amounts of acid–base and redox species. In addition, the distinctive features of MOFs allow to immobilise desired functional acid–base groups ($–SO_3H$, $–NH_2$, *etc.*) or active metal nanoparticles (Ru, Pd, Cu, *etc.*) on particular sites of the MOFs. The properties of resulting functionalised MOFs could be significantly different from the pristine analogues, due to the existence of synergistic host-dopant interactions.

Solid phase ionic liquids (SILs), such as supported ILs and polymerised ILs have drawn great attention for both fundamental research and practical applications including catalytic biomass upgrading.[39–42] They not only retain the individual properties of ILs and supports/polymers, but also endow novel functional active sites due to the cooperative effect of ILs with supports/polymers. Solid phase ILs can also overcome negative aspects of pristine ILs, such as high preparation costs, active phase leaching, and poor recovery/recycling. Particular interactions between the anionic and cationic parts of ILs can show a conceivable constructive effect in stabilising acid–base and active metal centers, which could be beneficial for cascade biomass upgrading.[43]

Biomass valorisation often entails the processing of larger molecules in viscous or solid reaction mixtures. The separation of solid catalysts from such type of reaction mixtures requires energy-intensive steps, making the process more complex and expensive. To overcome these concerns, the use of magnetic solid catalysts in biomass conversions is a potential approach. Magnetic catalysts can be efficiently separated from the reaction mixture using an external magnetic field, without affecting their catalytic properties.[30,44,45] Particularly, core–shell $Fe_3O_4@SiO_2$ magnetic nanomaterials have received a great deal of interest in biomass valorisation.[46–48] In addition to the benefits of catalyst separation, the existence of silanol groups in $Fe_3O_4@SiO_2$ can offer facile routes for selective anchoring of acid, base or metal active species that may assist to achieve promising results in biomass conversion reactions.

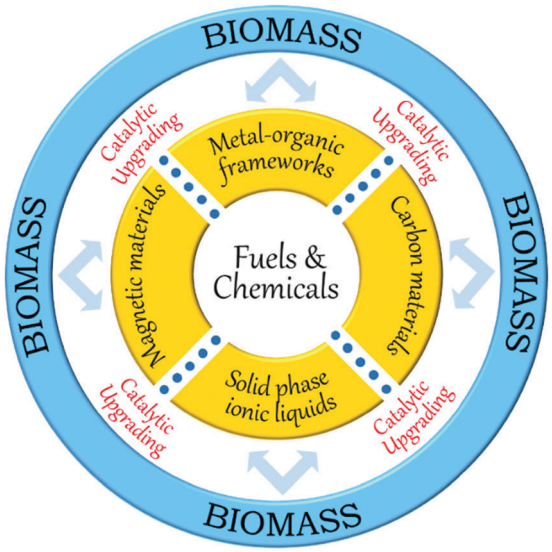

Fig. 3 Schematic overview of this review.

1.1 Scope of the review

Over the last few years, numerous research efforts have been undertaken towards developing a variety of heterogeneous catalysts for biomass upgrading reactions. Accordingly, several review articles have been reported on this topic. For instance,

 This journal is © The Royal Society of Chemistry 2018

Open Access Article. Published on 18 September 2018. Downloaded on 21/02/2026 10:11:12 PM.
This article is licensed under a Creative Commons Attribution-NonCommercial 3.0 Unported Licence.

Zhang *et al.*[49] provided a review on the importance of liquid state ionic liquids for the processing of renewable energy into fuels and chemicals. At the same time, Herbst *et al.*[36] summarised several catalytic applications of MOFs for biomass conversions. In 2016, Liu *et al.*[50] provided a review on the catalytic applications of magnetic materials for biomass upgrading. In another review, Lam and Luong have discussed the role of carbon materials as catalyst supports and as active phase catalysts for the transformation of biomass to fuels and chemicals.[35] Li *et al.*[51] reported a critical review, focusing on the valorisation of lignocellulose to biofuels using solid catalysts. Recently, Trombettoni *et al.*[52] reviewed various catalytic applications of sulfonated resin-based solid acids for biomass upgrading. Although these reviews provide useful implications and insights in the respective fields, there seems to remain an unexplored potential in the field of functionalised heterogeneous catalysts for the cascade processing of biomass valorisation. At the same time, there are concerns regarding the added-value of functionalised heterogeneous catalysts for biorefinery industry with respect to pristine analogues. Based on the above background, this review aims to revise and critically evaluate the most significant findings and advances related to the applications of carbon materials, MOFs, solid phase ionic liquids, and magnetic iron oxides for biomass conversions. Throughout the review, special attention has been drawn to facile approaches developed for the immobilisation of functional active sites on the above-listed materials as well as to understand the role of ensuing properties on chemical reactions and mechanisms in biomass valorisation. In addition to one-pot cascade reactions, also other types of vital reactions that normally take place in bio-refineries will be covered. Finally, a summarised overview will highlight the challenges and opportunities of future research towards rational design of promising functionalised heterogeneous catalysts in the context of sustainable biomass upgrading. Considering the significance of tailored catalytic functionalities for efficient biomass upgrading, materials characterization techniques (spectroscopy, microscopy, and sorption) are vital to identify structure–property relationships. This elaborate research field is beyond the scope of the present review, though several recent articles and reviews have already discussed the theory and the application of relevant characterization tools, applicable for the functionalised catalysts reported in this review.[53–58]

2. Carbon-based catalysts

Over the last three decades, carbon materials have been intensely investigated in the fields of materials science, nanotechnology, and catalysis, which can be attributed to their fascinating characteristics associated with textural, conductivity, stability, and hydrophobicity.[59–62] They have found versatile applications, for example as catalyst support and as active phase in catalysis, as electrode in energy storage devices, in water purification, in gas separation, and as soil additive. Carbon can exhibit three states of hybridisation, namely sp, sp^2, and sp^3, which drive the formation of well-defined pentagonal, hexagonal or heptagonal structures.[60] These 'magic' configurations allow the development of a variety of advanced carbon materials, such as fullerenes, carbon nanotubes, graphene, and mesoporous carbon. Although these materials solely consist of carbon atoms, they possess unique properties due to the extraordinary arrangement of carbon atoms with a flexible geometry. The scientific community has recognised the importance of carbon materials with two prestigious Nobel prizes: (1) fullerenes – 1996 (Chemistry, Prof. Robert F. Curl Jr., Prof. Harold W. Kroto and Prof. Richard E. Smalley) and (2) graphene – 2010 (Physics, Prof. Andre Geim and Prof. Konstantin Novoselov).[60,61]

2.1 Factors affecting the catalytic activity of carbon materials in biomass upgrading

Carbon materials have emerged as promising catalyst supports as well as metal-free active phase catalysts for various biomass transformation reactions.[35,63,64] They exhibit a broad spectrum of crucial catalytic properties: (i) large specific surface area, (ii) tailorable porous structures and surface chemistry, (iii) excellent chemical stability in acid or base media, (iv) remarkable hydrothermal stability, and (v) efficient functionalisation. Many types of conventional carbon materials, such as activated carbon, carbon black, glassy carbon, pyrolytic carbon, and polymer-derived carbon have been employed for stabilizing catalytic active phases. Owing to high specific surface area and rich surface chemistry, these carbon materials allow the formation of highly dispersed metal particles (Pd, Ru, Ni, Cu, Ag, Fe, *etc.*) throughout the catalyst matrix, resulting in enhanced resistance to sintering even at higher metal loadings and elevated temperature conditions.

Advances in materials science and nanotechnology have provided several innovative strategies for the development of new carbon materials, such as carbon nanotubes, graphene, and mesoporous carbons that can be used as catalyst supports or active catalysts.[35,63,64] Carbon nanotubes (CNTs) are characterized by a hexagonal arrangement of sp^2 carbons with well-controlled cavity geometries. CNTs can be classified as single-walled and multi-walled CNTs based on the number of carbon layers present in the tubular wall. Single-walled CNTs are semiconductive with diameters of around 0.4–2 nm, whereas multi-walled CNTs are metallic.[65] Interestingly, the cavities of CNTs can prevent the aggregation of active metal NPs during catalyst synthesis or catalytic reactions.[66,67] Graphene is a two-dimensional material consisting of a single layer of carbon atoms in hexagonal sp^2 hybridisation.[64] Two types of C–C bonds, namely in-plane σ-bond and out of-plane π bond are typically found in graphene. The electronic properties of graphene, controlled by out of-plane π-bonds, play a crucial role in enhancing the interactions of graphene with metallic NPs, and consequently the catalytic performance of graphene in biomass conversions. Mesoporous carbons, mesostructured carbon-based composites, and carbon nanofibers have also received great attention for catalytic biomass upgrading.[68–70] Owing to unique shape- and porosity-controlled properties, these carbon materials could offer strong active phase-support

Open Access Article. Published on 18 September 2018. Downloaded on 21/02/2026 10:11:12 PM.
This article is licensed under a Creative Commons Attribution-NonCommercial 3.0 Unported Licence.

interactions, which can lead to unusual catalytic activities and selectivities in biomass upgrading.

Defect sites and surface chemistry are the key parameters that determine the catalytic efficiency of carbon materials in biomass conversions. For example, defect sites incorporated into the sp^2 framework of CNTs, graphene or activated carbon can strongly influence surface properties and catalytic functionalities.[71] Heteroatom doping is an appealing strategy, which exploits defect structures in carbon materials.[72–74] Various elements, including nitrogen, phosphorus, boron, and sulphur have been successfully doped into carbon materials. Interestingly, structural and electronic properties of doped carbon materials can be considerably different from the pristine analogues, due to the synergistic host–dopant interactions. For instance, doping with electron rich nitrogen can adjust the spin density and the charge distribution of carbon atoms. This will lead to enhanced π-binding ability and improved basicity on the carbon surface.[72] In addition, N-doping can assist in the formation of new surface nucleation sites and multiple active centres around the N-rich sites.[73] In contrast, boron doping generates acid sites in carbon materials. The presence of such functional sites on the carbon surface not only contributes to improved interactions between the carbon support and the dispersed metal NPs, but also enables the use of carbon materials as promising metal-free catalysts.

In order to further improve the catalytic activity and selectivity of pristine or doped carbon materials, the immobilisation of various acid (nitro, sulphate, or phosphate) or base functionalities (–SO_3Na, –COONa, –ONa, or –NH_2) on the carbon surface has been carried out using appropriate synthesis methods.[35] Anchoring of acid functional groups on the carbon surface can occur through strong C–S, C–C, C–O, or C═O bonds.[35,75] Hence, these functional carbon materials can act as stable solid Brønsted acids for various important biomass conversion reactions, such as esterification, transesterification, etherification, hydrolysis, and dehydration. For instance, acid-bearing carbon catalysts showed good activity for the dehydration of 2-propanol to propylene in the presence of water vapour, a vital reaction for upgrading biomass-derived oxygenates.[76] Base functionalised carbons have also been found excellent catalytic efficiencies, for example in biodiesel synthesis.[77] However, these functionalised carbons suffer from several drawbacks, especially in the case of acid groups. For example, acid-bearing carbon materials are usually prepared by sulfonation of partially carbonized organic molecules using highly concentrated hazardous liquid acids, such as H_2SO_4 or HNO_3.[78] These protocols show adverse effects on the structure as well as on the stability of carbon materials, which in turn could lead to inefficient recovery of the catalyst from the reaction mixture. Besides, oxygen-containing groups present on the carbon surface may promote side reactions during biomass valorisation (Fig. 4).[35] This will lead to a low selectivity of desired products and can even irreversibly poison the catalyst. In order to circumvent these problems, several promising strategies have been suggested, such as selective deposition of –SO_3H groups on carbon edges, or deprotonation–carbometalation, followed by base functionalisation, *etc.*[77,78]

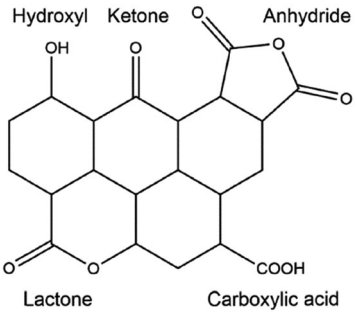

Fig. 4 Presence of various oxygen-containing groups in an activated carbon material. Reproduced with permission from ref. 35. Copyright (2014) American Chemical Society.

The simultaneous functionalisation of carbon materials with acid or base species as well as with active metal particles will lead to the design of novel bifunctional catalysts. Bi-functional catalysts have the advantages of integrating several catalytic processes in a one-pot way for sustainable biomass upgrading. For instance, both metallic and acid properties are essential for the direct conversion of levulinic acid to γ-valerolactone. Compared to metal oxides, carbon supports show a stronger ability to stabilise both acid and metal sites because of their high hydrothermal stability and rich surface chemistry. Wang *et al.*[79] developed a facile synthesis procedure for developing a graphene-supported Ru/SO_3H bi-functional catalyst. In this process, Ru NPs are initially deposited on graphene, followed by its functionalisation with benzenesulfonic acid groups (Fig. 5). This bifunctional catalyst showed a high selectivity to γ-valerolactone *via* the Ru catalysed hydrogenation of levulinic acid to 4-hydroxyvaleric acid and the subsequent acid catalysed dehydration to γ-valerolactone. The presence of tailorable porous structures is also crucial for efficient functionalisation of carbon materials, which was well-documented in the case of mesoporous carbon-based composites.[80] For example, a porous graphite-like carbon network incorporated in a Sn(IV)-grafted MCM-41 was found to show a good catalytic performance for the conversion of sugars into ethyl lactate in ethanol, which was

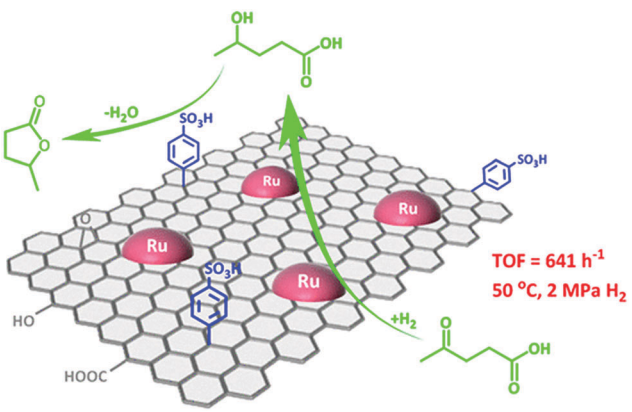

Fig. 5 Graphene-based metal/acid bi-functional catalyst for one-pot conversion of levulinic acid to γ-valerolactone. Reproduced with permission from ref. 79. Copyright (2017) American Chemical Society.

This journal is © The Royal Society of Chemistry 2018

Open Access Article. Published on 18 September 2018. Downloaded on 21/02/2026 10:11:12 PM.
This article is licensed under a Creative Commons Attribution-NonCommercial 3.0 Unported Licence.

attributed to synergistic effect of Lewis and weak Brønsted acid sites.[81]

In general, high production costs and low yields are the major drawbacks in the synthesis of carbon materials. Especially, in the case of CNTs and graphene, high synthesis costs strongly limit their practical applications in biomass conversions. It is therefore indispensable to use low-cost, abundant, and sustainable substrates for the preparation of carbon-based catalysts. Noticeably, recent studies have provided several facile routes for the transformation of bio-based molecules into new carbon materials with prolific functional sites.[82–84] A key advantage of such synthesis processes is that the raw material (biomass) is abundant and renewable. To enhance the activity of biomass-derived carbon catalysts for biomass conversions, various acid–base functional molecules can be immobilised by either *ex situ* or *in situ* methods. Devi *et al.*[85] developed a highly stable carbon catalyst derived from glycerol (a major by-product in biodiesel synthesis) incorporating various basic functionalities. The synthesis procedure involves an *in situ* carbonisation and sulfonation of glycerol to obtain a SO_3H–carbon catalyst, followed by a controlled treatment with aqueous NaOH solution. The resulting solid base catalyst showed good performance in the transesterification of sunflower oil with methanol to produce biodiesel, in which glycerol is formed as a by-product that can be used again for the synthesis of carbon-based catalysts, hereby greatly improving process economy and sustainability.

The strong hydrophobic nature of carbon materials is another key driving force that boosts their catalytic applications for biomass upgrading processes. Owing to high resistance capacity towards water, which is the preferred solvent in many bio-refinery processes, carbon surfaces can efficiently prevent the leaching of active phase during catalytic reactions, thus improving the catalyst recyclability, a critical benchmark for industrial applications.[76] Moreover, high hydrothermal stability of carbon materials is another significant advantage over other catalytic materials, for example zeolites, which suffer from irreversible deactivation due to deterioration of their crystalline structure in the presence of water. Interestingly, the hydrophilic character of carbon materials can be improved by employing an oxidation treatment in order to facilitate immobilisation of desired functional groups on the carbon surface.[86] The catalytic efficiency of several classes of carbon-based materials tested in biomass valorisation was critically discussed in the following paragraphs. In addition, an overview of the most significant catalytic results achieved in carbon catalysed biomass conversions is provided in Table 1.

2.2 Conventional carbon based catalysts

Carbon black and activated carbon have been widely used as supporting materials for the synthesis of promising heterogeneous catalysts because of their low preparation cost and high specific surface area.[35,86] Carbon black is an amorphous solid with planar layers of sp^2-hybridised carbon. Pyrolysis of hydrocarbon precursors or organic polymers at elevated temperatures is typically used for the synthesis of carbon black. Activated carbon is also an amorphous solid, though with a characteristic twisted geometry of planar-layered structures, which are cross-linked by aliphatic bridging groups that provide a high density of defect sites. Both physical and chemical activation processes are used for the preparation of activated carbons. The raw material is initially pyrolysed at 600–900 °C in the physical activation, and then exposed to an oxidising atmosphere (oxygen or steam) at desirable temperatures. In contrast, chemical activation involves impregnation of carbon precursors with an acid, a strong base, or a salt, followed by a carbonisation step in the range of 450–900 °C. Chemical activation is the preferred process due to the mild conditions (*i.e.*, lower temperatures and shorter times) required for the synthesis of activated carbon.

2.2.1 Reductive catalytic fractionation of lignocellulose. Lignocellulose is the most abundant biomass feedstock, with an annual growth of 170 billion tons and it does not directly compete with food supplies because of its non-edible nature.[87–89] Lignocellulose is mainly composed of three biopolymers (Fig. 6): cellulose (30–50%, polymer of glucose), hemicellulose (20–35%, polymer of C_5 and C_6 carbohydrates), and lignin (15–30%, aromatic polymer). Hence, the efficient fractionation of lignocellulose into separated streams of these three polymers is often the entry point for a fruitful bio-refinery as it opens the possibility of subsequent transformations to high-value chemicals and fuels. In this context, reductive catalytic fractionation (RCF) of lignocellulose has received tremendous attention, providing a stable lignin oil containing high-value phenolic mono-, di- and oligomers as well as a valorisable solid carbohydrate pulp that can be used for the production of paper, fine chemicals, or biofuels.[90] The Sels group has made significant advancements on this novel ''lignin-first'' bio-refinery concept using carbon supported metal catalysts. For instance, RCF of birch wood was studied in the presence of a Ru/C catalyst using H_2 pressure and methanol as a solvent.[91] The obtained lignin oil mainly contains phenolic monomers (50% yield based on the original lignin content), next to phenolic dimers and oligomers. Several key parameters were optimised to achieve promising results in terms of delignification efficiency and yields of phenolic monomers. A negligible decrease in phenolic monomers yield from 50% to 48% was observed after a recycling test of Ru/C catalyst (entry 1, Table 1). The subsequent valorisation of carbohydrates pulp to sugar polyols further revealed the versatile role of the Ru/C catalyst. The effect of several bio-based solvents in RCF process of birch wood was also studied using a Pd/C catalyst.[92] Among the solvents tested, methanol and ethylene glycol showed highest lignin-first delignification efficiency values, which are highly dependent on the reaction time and the temperature. On the other hand, the synergetic effect of alcohol/water mixture was recognized in RCF process of poplar wood using a Pd/C catalyst.[93] Results showed improved delignification of lignocellulose in the presence of low water concentrations solvent mixtures, while higher water concentrations favor solubilisation of both lignin and hemicellulose, giving a pure cellulosic residue. Sels *et al.*[94] also studied effect of acidic and alkaline additives on the RCF process

Open Access Article. Published on 18 September 2018. Downloaded on 21/02/2026 10:11:12 PM.
This article is licensed under a Creative Commons Attribution-NonCommercial 3.0 Unported Licence.

Table 1 Catalytic applications of the most significant carbon-based materials in biomass valorisation

Entry	Catalyst	Reaction	Product	Reaction conditions	Catalytic activity		Recycling results	Ref.
					Conv. %	Yield %		
1	5 wt% Ru/C	Reductive fractionation of birch wood sawdust	Lignin phenolic monomers	2 g birch sawdust, 0.3 g Ru/C, 40 mL MeOH, 250 °C, 12 MPa H_2 at 250 °C, 3 h	93[a]	50	Negligible decrease in phenolic monomers yield (48%) after a recycling test	91
2	Ru/activated carbon	Continuous-flow hydrogenation of cellulose oligomers	C_6 sugar alcohols	25 vol% of 2-propanol in water, 180 °C, pH = 2.7, 5 h, liquid hourly space velocity of 4.7 h^{-1}, 60 bar Ar at RT[b]	—	36.4%	Stable catalytic activity during 12 h time-on-stream	103
3	Carbon encapsulated Fe NPs	Hydrogenation of levulinic acid	γ-Valerolactone	5 g levulinic acid, 0.2 g catalyst, 45 mL H_2O, 170 °C, 5 bar H_2 at RT, 3 h	99.5	99	5 (stable catalytic activity)	104
4	Ni–$Fe_{0.5}$/activated carbon	Hydrogenation of ethyl levulinate	γ-Valerolactone	100 mg ethyl levulinate, 40 mg catalyst, 10 mL H_2O, 100 °C, 4 MPa H_2 at RT, 6 h	99.3	99	5 (catalyst deactivation, due to leaching of active sites)	106
5	N-Doped carbon decorated Cu/MgAlO	Hydrogenolysis of HMF[c]	DMF[d] DMTHF[e]	0.5 g HMF, 0.1 g catalyst, 10 mL cyclohexanol, 220 °C, N_2 atm	100	96[f] 94.6[g]	5 (stable catalytic activity)	110
6	Fe/N-doped carbon	Hydrogenation of furfural	Furfuryl alcohol	0.5 mmol furfural, 50 mg catalyst, 3 mL of 2-butanol, 160 °C, 15 h	91.6	76	5 (catalyst deactivation, due to changes in structure of active phases and pores blocking)	111
7	MoC_x NPs/hollow carbon spheres	Hydrodeoxygenation of phenol	Benzene	3 mmol phenol, 30 mg catalyst, 5 mL *n*-octane, 350 °C, 80 bar H_2 at 350 °C, 4 h	87	74	Negligible catalytic loss after a recycling test	119
8	Sulfonated carbon	Transesterification of purified palm oil	Biodiesel	12 : 1 molar ratio of methanol to oil, 0.5 wt% catalyst based on oil, 270 °C, 30 min	—	95	3 (significant decrease in biodiesel yields from 95% to 45%, due to leaching of acidic species)	123
9	Pt_9Sn_1/C	Oxidation of glycerol	Glyceric acid	5 mmol glycerol, 100 mg catalyst, 10 mL water, 60 °C, O_2 (15 mL min^{-1}), 8 h	91	50	4 (stable catalytic activity after treating the catalyst at 400 °C in H_2 atmosphere)	126
10	GO–SO_3H[h]	Decomposition of glucose	Levulinic acid	30 g glucose, 0.5 g catalyst, 200 mL water, 200 °C, 2 h	89	78	5 (catalyst deactivation, due to char formation during reaction)	132
11	WO_3/r-GO[i]	Dehydration of fructose	HMF	1 mmol fructose, 10 mg catalyst, 2 g ionic liquid, 120 °C, 2 h	100	84.2	5 (negligible decrease in catalytic activity)	133
12	Sulfonated Ru/r-GO	Hydrogenolysis of levulinic acid	γ-Valerolactone	200 mg substrate, 0.5 mg of Ru, 10 mL H_2O, 50 °C, 2 MPa H_2 at 50 °C, 40 min	100	82	8 (significant decrease in product yields, due to sintering of Ru NPs, weight loss of the catalyst, and blockage of active Ru sites)	79
13	SO_3H@GO monolith	Esterification of levulinic acid	Benzyl levulinate	50 mmol substrate, 75 mmol benzyl alcohol, 0.008 g cm^{-3} catalyst loading, toluene, 110 °C, 90 min	97	—	5 (stable catalytic activity for 5 min reaction in each cycle)	137
14	GO	Etherification of HMF	OBMF[j]	63 mg HMF, 20 mg catalyst, 0.5 mL CH_2Cl_2, 100 °C, 8 h	98	86	6 (catalytic activity of GO can be regenerated by treating it under Hummers' conditions)	138
15	Cu–Pd/r-GO	Glycerol hydrogenolysis	Lactic acid	1 : 1 molar ratio of NaOH/glycerol, 15 mL H_2O, 140 °C, 1.4 N_2 MPa at 140 °C, 16 h	56.2	49.5	3 (considerable decrease in product yields from 49.5% to 40%)	139
16	VO_2–polyaniline/CNT[k]	Oxidation of HMF	2,5-Diformylfuran	1 mmol HMF, 100 mg catalyst, 9.5 wt% of vanadium, 2 mL dimethyl sulfoxide, 120 °C, 1 MPa O_2 at RT, 11 h	>99	96	5 (significant decrease in product yields from 96% to 75%)	144
17	Pt/CNT	Oxidation of HMF	FDCA[l]	0.5 mmol HMF, 100 : 1 molar ratio of HMF/Pt, 20 mL H_2O, 95 °C, 0.5 MPa O_2 at RT, 14 h	100	98	7 (stable catalytic activity)	146
18	Mesoporous carbon-based solid acid	Dehydration of fructose	HMF	0.5 g fructose, 0.25 g catalyst, 7 mL isopropyl alcohol, 130 °C, 140 min	97.9	87.8	5 (about 10% decrease in HMF yields)	150
19	Ordered mesoporous carbon (CMK-5)	Methylation of volatile fatty acids (VFA)	Fatty acid methyl esters	0.5 vol ratio of VFA/methanol, 65 mg catalyst, 360 °C, 1 atm O_2	—	98	6 (stable catalytic activity)	152

This journal is © The Royal Society of Chemistry 2018

Open Access Article. Published on 18 September 2018. Downloaded on 21/02/2026 10:11:12 PM.
This article is licensed under a Creative Commons Attribution-NonCommercial 3.0 Unported Licence.

Table 1 (*continued*)

Entry	Catalyst	Reaction	Product	Reaction conditions	Catalytic activity		Recycling results	Ref.
					Conv. %	Yield %		
20	Sulfonated silica/carbon nanocomposite	Hydrolysis of cellulose	Glucose	50 mg catalyst, 5 mL water, 150 °C, 24 h	60.7	50.4	3 (small decrease in catalytic activity, due to leaching of acid groups)	160
21	Sulfonated sucrose-derived carbon	Dehydration of xylose	Furfural	0.4 g xylose, 0.2 g catalyst, 16.5 mL of γ-valerolactone, 170 °C, 30 min	—	78.5	5 (stable catalytic activity)	169
22	Biochar supported SnO_2–Co_3O_4	Hydrolysis of corncob	Furfural	0.3 g catalyst, 120 mL water, 180 °C, 200 min	62.7	30	6 (significant decrease in product yields from 30% to 15%, due to leaching of acidic species)	170
23	Willow-derived carbon solid acid	Cellulose hydrolysis	Glucose	50 mg cellulose, 50 mg catalyst, 5 mL water, 160 °C, 8 h	78	65	3 (small decrease in glucose yields, due to mass loss of the catalyst during recovery/purification	174
24	Sulfonated bamboo-derived carbon	Microwave-assisted hydrolysis of hemicellulose	Xylo-oligosaccharides	1 : 200 mass ratio of catalyst to water, 150 °C, 45 min, microwave reactor	—	54.7	3 (catalyst deactivation, due to leaching of acidic species)	179
25	Biomass-derived carbon cryogel	Esterification of levulinic acid	Ethyl levulinate	15 : 1 molar ratio of ethanol to levulinic acid, 150 °C, 4 h	87.2	86.5	5 (catalyst deactivation, due to leaching of active species)	187
26	CoN_x@N-doped carbon	Hydrodeoxygenation of eugenol	Propylcyclohexanol	1 mmol eugenol, 76 mg catalyst, 10 mL *n*-dodecane, 200 °C, 2 MPa H_2 at RT, 2 h	100	>99.9	4 (catalyst deactivation, due to leaching of active sites)	193
27	Co@N-doped carbon	Hydrodeoxygenation of vanillin	2-Methoxy-4-methylphenol	0.5 mmol vanillin, 10 mL water, 180 °C, 0.5 MPa N_2 at RT, 4 h, formic acid (0.2 g) as hydrogen source	95.7	95.7	5 (stable catalytic activity)	72
28	SO_3Na-functionalised glycerol-derived carbon	Transesterification of oil	Biodiesel	1 : 5 (wt/vol) ratio of oil to methanol, catalyst amount (20 wt% of oil), 65 °C, 2 h	100	99	8 (stable catalytic activity)	85

[a] Delignification efficiency. [b] RT – room temperature. [c] HMF – 5-hydroxymethylfurfural. [d] DMF – 2,5-dimethylfuran. [e] DMTHF – 2,5-dimethyltetrahydrofuran. [f] 30 min reaction time. [g] 200 min reaction time. [h] GO – graphene oxide. [i] r-GO – reduced graphene oxide. [j] OBMF – 5,5′-oxy(bis-methylene)-2-furaldehyde. [k] CNT – carbon nanotube. [l] FDCA – 2,5-furandicarboxylic acid.

Open Access Article. Published on 18 September 2018. Downloaded on 21/02/2026 10:11:12 PM.
This article is licensed under a Creative Commons Attribution-NonCommercial 3.0 Unported Licence.

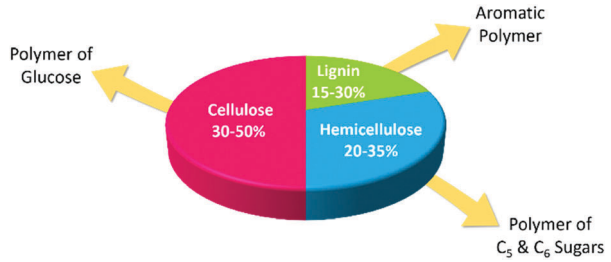

Fig. 6 Composition of lignocellulosic biomass with major constituents: cellulose, hemicellulose, and lignin.

of lignocellulose using similar type of Pd/C catalyst. Results revealed that H_3PO_4 addition promotes both delignification and alcoholysis of hemicellulose, giving a cellulose-rich pulp. In contrast, NaOH addition showed various negative effects, such as lignin repolymerisation, cellulose loss, and no formation of hemicellulose carbohydrates. In another work, the variation in selectivity of phenolic monomers obtained from RCF process of birch wood was examined using Ru/C and Pd/C catalysts.[95] Interestingly, both catalysts gave about 50% of phenolic monomers, but the OH-content of phenolic products drastically increased when changing the catalyst from Ru/C to Pd/C. Recently, Anderson *et al.*[96] developed a flow-through RCF process for fractionation of poplar wood using a 15% Ni/C catalyst mixed with SiO_2. Various spectroscopy and microscopy analysis techniques are used to understand catalyst deactivation and its poisoning. The results revealed several advantages of a flow-through setup for the RCF process of lignocellulose biomass over traditional batch reactors that paving the way for future research of lignocellulose valorisation. Kumaniaev *et al.*[97] also developed a flow-through RCF process for the fractionation of birch wood using a Pd/C catalyst coupled with a liquid acid. About 37 wt% yield of lignin-derived phenolic monomers was obtained at optimized conditions, while solid carbohydrates pulp generated in the RCF process was enzymatically hydrolyzed to glucose without applying prior purification step.

2.2.2 Upgrading of carbohydrates and their derived compounds. The Sels group has developed an efficient one-pot catalytic route to transform cellulose into straight chain alkanes using a modified Ru/C catalyst.[98] About 82% yield of *n*-decane-soluble products, mainly *n*-hexane, was obtained from microcrystalline cellulose at optimal conditions (6 h and 200 °C). The use of a hydrothermal modification strategy played a favorable role in tailoring chemoselectivity of Ru/C catalyst towards furan hydrogenation (rather than glucose-to-sorbitol transformation), one of the key steps for the production of straight-chain alkanes from cellulose. Similar type of a modified Ru/C catalyst is also found to be effective in a liquid phase cellulose-to-naphtha process.[99] The effect of cellulose characteristics, such as purity, crystallinity, degree of polymerisation, and particle size (surface area) was also studied towards production of light naphtha. The direct conversion of hemicellulose in *pubescens* to γ-valerolactone was successfully carried out without using external hydrogen over a Pt/C catalyst, coupled with $AlCl_3$–H_2O and $AlCl_3$–SiO_2–THF/H_2O systems.[100] About 20% yield of γ-valerolactone with a high selectivity of 90.5% was obtained based on the weight of *pubescens* and the amount of carbohydrates converted, respectively. Results suggested the versatile role of Pt/C catalyst in the direct conversion of hemicellulose to γ-valerolactone. A one-pot transformation of cassava waste to 5-hydroxymethylfurfural (HMF) and furfural was studied using a sulfonated carbon-based solid acid catalyst.[101] The catalyst exhibited a favorable role in the hydrolysis of cellulose and hemicellulose, while also promoting dehydration of sugars to HMF and furfural. In addition, the catalyst showed a highly stable activity, thus serving as a promising alternative for hazardous liquid acids (H_2SO_4). The hydrolysis of cellulose into glucose was also studied over a sulfonated carbon-based solid acid, prepared using a phenolic residue precursor.[102] Aliphatic side chains present in the catalyst played a crucial role in improving its catalytic efficiency. An activated carbon supported Ru catalyst was found to be active for the catalytic transfer hydrogenation of cellulose-based oligomers using 2-propanol as a hydrogen source.[103] A 83.4% yield of C_6 sugar alcohols was obtained in a batch reactor. The catalyst is also active in continuous-flow conversion of cellulose oligomers to C_6 sugar alcohols (36.4% yield) and showed a stable catalytic activity during 12 h time-on-stream study (entry 2, Table 1).

Carbon encapsulated Fe NPs were prepared using an ultrasonic method (Fig. 7).[104] The effect of the annealing temperature on textural and phase properties was studied. Results revealed a superior catalytic efficiency of carbon-encapsulated Fe NPs for the hydrogenation of levulinic acid to γ-valerolactone (99% yield). The shell structure of carbon prevents leaching of active Fe sites during reaction, resulting in excellent reusability for at least five times (entry 3, Table 1). Carbon-supported bimetallic Ru–Sn catalysts containing different amounts of Sn were studied for the hydrogenation of levulinic acid to γ-valerolactone.[105] The catalyst containing equal amounts of Ru and Sn showed a stable activity with a 100% selectivity to γ-valerolactone, while the activity of monometallic Ru/C catalyst was progressively decreased with reaction time. In contrast, the Ru_1Sn_4/C catalyst

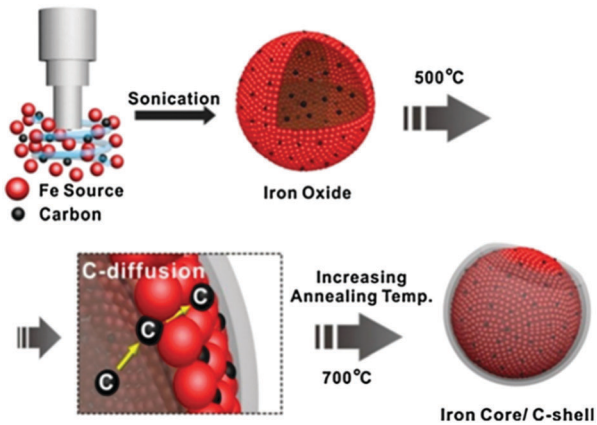

Fig. 7 Schematic illustration for the preparation of carbon-encapsulated Fe NPs. Reproduced with permission from ref. 104. Copyright (2014) Springer Nature.

 This journal is © The Royal Society of Chemistry 2018

Open Access Article. Published on 18 September 2018. Downloaded on 21/02/2026 10:11:12 PM.
This article is licensed under a Creative Commons Attribution-NonCommercial 3.0 Unported Licence.

was found to be inactive due to the formation of an additional phase (β-Sn), which leaches and sinters during reaction. In another work, γ-valerolactone is produced *via* hydrogenation of ethyl levulinate using a series of activated carbon supported bimetallic Ni–Fe (Ni–Fe/AC) catalysts.[106] Among them, the Ni–$Fe_{0.5}$/AC catalyst exhibited the highest activity and achieved 99.3% conversion of ethyl levulinate with 99% yield of γ-valerolactone at optimised reaction conditions (entry 4, Table 1). The existence of uniform dispersed Ni–Fe alloy structure in combination with FeO_x NPs is essential for high catalytic hydrogenation activity. However, significant catalyst deactivation (around 20% loss in γ-valerolactone yield) was observed after four recycles, due to leaching of active species. A simple calcination step was used to regenerate the catalytic activity of Ni–$Fe_{0.5}$/AC towards γ-valerolactone production.

Dehydration of various carbohydrates, such as xylose, glucose, and fructose was studied using a commercial activated carbon (Norit, ROX 0.8).[107] This carbon contains several types of functional groups, including carboxylic acids, $-SO_3H$, carbonyls, phenols, thiophenols, quinones, and anhydride sites, which can act as acidic or basic sites. Results reveal that this activated carbon is a highly suitable catalyst for the dehydration of sugars due to its strong hydrophobic character. In addition, the carbon catalyst efficiently suppresses side reactions that produce acids and humins. Several activated carbon supported monometallic Ru and bimetallic RuRe catalysts were studied for sorbitol hydrogenolysis reaction.[108] Among them, bimetallic catalysts in combination with $Ca(OH)_2$ as a base promoter exhibited higher activity and selectivity towards 1,2-propanediol, lactic acid, ethylene glycol, and linear alcohols. The aqueous-phase hydrodeoxygenation of sorbitol was also investigated using a Pt–ReO_x/C catalyst in a continuous-flow reactor.[109] The Pt–ReO_x/C catalyst exhibited a 34 times higher activity compared to Pt/Zr–P catalyst (based on a Pt mass), which was attributed to a higher hydrothermal stability of Pt–ReO_x/C catalyst related to the carbon support. A catalytic transfer hydrogenolysis of HMF was successfully performed to produce 2,5-dimethylfuran (DMF) and 2,5-dimethyltetrahydrofuran (DMTHF) biofuels using a N-doped carbon-decorated Cu/MgAlO catalyst with cyclohexanol as the hydrogen source.[110] About 96% and 94.6% yields of DMF and DMTHF, respectively, were obtained at optimised reaction conditions (entry 5, Table 1). Moreover, the catalyst exhibited a stable activity for at least five cycles without any considerable loss in catalytic performance. The existence of suitable basic sites on the catalyst surface plays a beneficial role in the activation of alcohol hydroxyl moieties in cyclohexanol to release active hydrogen species. Highly dispersed Cu^0 NPs and electrophilic Cu^+ species catalyse the hydrogen transfer and the subsequent hydrogenolysis of HMF, respectively. Nitrogen-doped carbon supported iron catalysts were found to show a good performance in catalytic transfer hydrogenation of furfural to furfuryl alcohol.[111] The effects of the metal center, nitrogen source, pyrolysis temperature, and the support were studied. A 91.6% conversion of furfural with about 76% yield to furfuryl alcohol were achieved, attributed to the coordination of iron cations by pyridinic nitrogen functionalities on the carbon support. A considerable decrease in catalytic efficiency was noticed after five recycles of the catalyst, due to changes in structure of active phases and blockage of the catalyst pores (entry 6, Table 1).

The effect of solvent mixtures in the hydrogenolysis of xylitol to glycols and glycerol was investigated using an activated carbon supported bifunctional Ru–MnO catalyst.[112] The product distribution obtained in the case of 90 : 10 vol% water/1,4-dioxane and water/2-PrOH solutions is very similar to the one obtained in pure water. Interestingly, the overall selectivity to glycols and glycerol is greatly enhanced (up to 70%) in the case of 90 : 10 vol% water/ROH mixtures (ROH with R = Me, Et, *n*-Pr, and *n*-Bu). Hydrodeoxygenation of α-angelica lactone-derived di/trimers to gasoline was studied using carbon supported Pd and Pt catalysts.[113] α-Angelica lactone can be produced from levulinic acid. The effect of H_2 pressure, reaction temperature, and reaction time on the product selectivities were thoroughly investigated. Considerable amounts of bio-liquids suitable for gasoline application were obtained in this work.

2.2.3 Upgrading of non-carbohydrate compounds. Lignin comprises 15–30% of lignocellulosic biomass and is the only scalable renewable resource, consisting of abundant aromatic chemicals derived from *p*-coumaryl, coniferyl, and sinapyl alcohols.[4] Hence, lignin valorisation is a promising route towards useful aromatic compounds, which are key building blocks for the chemical industry. Phenolic units in lignin are connected with various readily cleavable C–O–C ether bonds (β-O-4, α-O-4, and 4-O-5), next to more stable C–C bonds (Fig. 8). Hence, the efficient cleavage of these bonds is vital to reach a maximum degree of lignin depolymerisation. To achieve this target, chemocatalytic hydrogenolysis of lignin has received tremendous attention in recent times. For example, various bimetallic Ni–Fe catalysts supported on activated carbon (AC) were studied for the hydrogenolysis of lignin.[114] About 23.2 wt% total yield of monomers (mainly propylguaiacol and propylsyringol) was obtained when processing organosolv birch lignin with a Ni_1–Fe_1/AC (the ratio of Ni and Fe was 1 : 1) catalyst. In the case of birch wood sawdust, the total yield of monomers even reached up to 39.5 wt% (88% selectivity to propylguaiacol and propylsyringol) over the Ni_1–Fe_1/AC catalyst, attributed to the synergistic effect of Ni–Fe alloys. A series of bimetallic

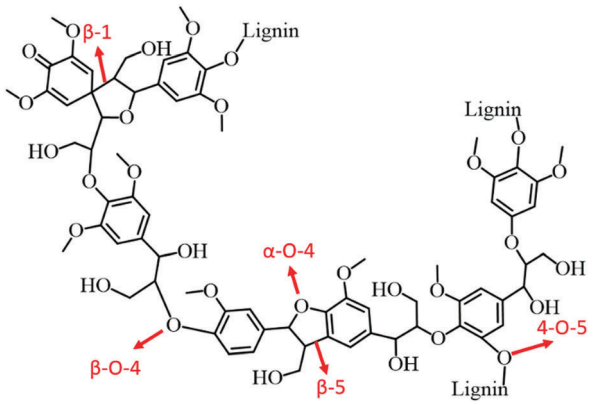

Fig. 8 Various important C–C and C–O–C linkages in lignin polymer.

Open Access Article. Published on 18 September 2018. Downloaded on 21/02/2026 10:11:12 PM.
This article is licensed under a Creative Commons Attribution-NonCommercial 3.0 Unported Licence.

M–W/AC (M = Ru, Pt, and Pd) catalysts were also studied for hydrogenolysis of lignin and its model compounds.[115] Electronic effects of bimetallic catalysts play a pivotal role in stabilising the reaction intermediates. The nature of solvent is also imperative in hydrogenolysis of lignin: higher yields of desired aromatics were obtained with dipolar aprotic solvents, such as *n*-hexane. Bimetallic catalysts not only cleaved the α-O-4 bonds, but also catalysed hydrogenolysis of other major linkages in lignin, consequently resulting in high yields of liquid oil. Zeng *et al.*[116] developed an efficient $Pd(OH)_2/C$ catalyst for cross-coupling of lignin 4-O-5 linkage models with amines *via* an *in situ* generated phenol intermediate. The obtained amine derivatives are valuable chemicals for the production of fine chemicals, pharmaceuticals, and electronic materials. Based on the experimental results, a probable mechanism for the production of amine derivatives from lignin model compounds is proposed.

A multi-functional cobalt NP-embedded carbon catalyst (Co@C) was developed *via* carbonisation of a three-dimensional cobalt coordination polymer.[117] This Co@C catalyst showed excellent efficiency in the oxidation of vanillyl alcohol (a lignin model compound) to vanillin with 99% and 100% selectivities using H_2O_2 and air as oxidants, respectively (Fig. 9). The Co@C catalyst also showed a significantly improved performance compared to other cobalt catalysts and was efficiently re-used without significant loss in catalytic activity. Thorough kinetics and mechanistic studies were performed for the catalytic hydrodeoxygenation and hydrogenation of eugenol, a lignin model compound, using a Ru/C catalyst.[118] Results reveal that hydrogenation of the allyl group and benzene ring of eugenol were favored over dehydroxylation and demethoxylation of oxygen groups present on the aromatic ring of eugenol. The mechanism of ketone group formation as well as the factors responsible for cyclohexane-ring transformation to substituted 5-membered ring compounds were also proposed in this work. A detrimental effect of water is observed in the hydrodeoxygenation of phenol in the presence of MoC_x NPs supported on hollow carbon spheres (HCS).[119] About 87% conversion of phenol with a 74% yield to benzene was obtained over MoC_x/HCS catalyst at optimised reaction conditions. A negligible decrease in product yields was noticed after a recycling test (entry 7, Table 1).

Biodiesel (fatty acid methyl esters) is a biodegradable and nontoxic fuel, and hence, considered as a promising alternative

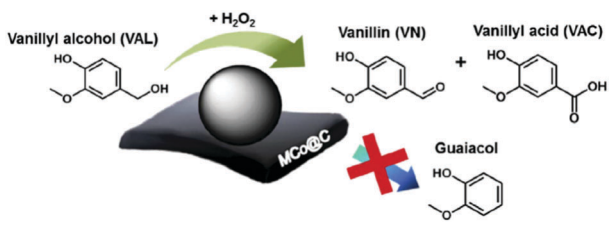

Fig. 9 Oxidation of vanillyl alcohol using Co NP-embedded carbon nanocomposite (Co@C) catalyst. Reproduced with permission from ref. 117. Copyright (2018) Elsevier.

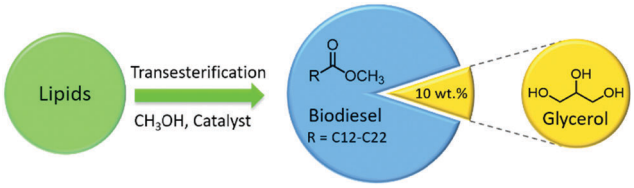

Fig. 10 Transesterification of lipids (oils & fats) with alcohols (*e.g.*, methanol) to produce biodiesel with glycerol as a by-product.

to petro-diesel fuel.[15,120,121] Several carbon-based catalysts have shown good to excellent efficiencies in the production of biodiesel *via* transesterification of oils and fats (Fig. 10). An incomplete hydrothermal carbonisation of β-cyclodextrin into polycyclic aromatic carbon sheets, followed by its sulfonation using H_2SO_4 was performed to develop a novel carbon-based solid acid catalyst.[122] The resulting solid acid simultaneously catalysed esterification and transesterification reactions to produce biodiesel from high free fatty acid containing oils, hereby outperforming a conventional solid acid (Amberlyst-15). In another work, an incomplete carbonization of naphthalene in H_2SO_4 was performed to obtain a carbon-based solid acid catalyst for the production of biodiesel *via* transesterification of purified palm oil.[123] About 95% yield of biodiesel was obtained, which however decreases to 45% after three recycles of the catalyst, due to leaching of acidic species (entry 8, Table 1). Glycerol, an interesting platform chemical, can be largely obtained as a by-product during biodiesel synthesis (Fig. 10).[124,125] A series of bimetallic PtM/C (M = Mn, Fe, Co, Ni, Cu, Zn, and Au) catalysts were developed for the oxidation of glycerol.[126] Among them, Pt_9Sn_1/C catalyst showed the highest activity with a 91% of glycerol conversion and a 50% yield of glyceric acid. Modified Pt NPs after the addition of Sn significantly activate oxygen molecules and/or deprotonation of hydroxyl group in glycerol, resulting in improved catalytic performance of Pt_9Sn_1/C material as well as stable catalytic activity for at least four recycles after treating the catalyst at 400 °C in H_2 atmosphere (entry 9, Table 1).

2.3 Graphene based catalysts

Graphene and its related materials, such as graphene oxide and reduced graphene oxide represents a fascinating class of materials and continues to provide a fertile ground for various applications including catalysis. Graphene-based materials are ideal supports for anchoring a variety of metal NPs and acid–base functionalities. For the first time, in 2004, Geim *et al.* developed single layer graphene nanosheets.[127,128] Afterwards, several promising synthesis procedures, including graphitisation, physical exfoliation, chemical vapour deposition, and chemical oxidative cleavage have been developed to synthesise well-defined graphene-based materials.[129] Graphene oxide (GO) is obtained by the oxidation of graphite, followed by the exfoliation of monolayer sheets in solution. Reduced graphene oxide (r-GO) is simply produced by reduction of graphene oxide and the resulting material partially regains the aromaticity of pristine graphene. The defects and residual O-containing

Open Access Article. Published on 18 September 2018. Downloaded on 21/02/2026 10:11:12 PM.
This article is licensed under a Creative Commons Attribution-NonCommercial 3.0 Unported Licence.

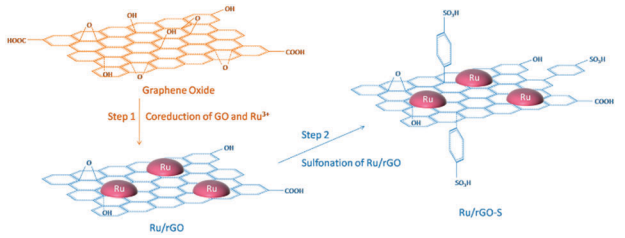

Fig. 11 Schematic illustration of the preparation strategy for a bi-functionalised graphene oxide based catalyst. Reproduced with permission from ref. 79. Copyright (2017) American Chemical Society.

groups present in graphene play an essential role in the synthesis of highly stable and active catalyst systems.[128,130,131]

2.3.1 Upgrading of carbohydrate-containing and -derived compounds. An efficient acid functionalised graphene oxide (GO–SO_3H) was developed for one-pot conversion of hexose sugars, such as glucose and fructose to levulinic acid.[132] About 78% yield of levulinic acid was obtained from glucose at optimised reaction conditions, due to high concentration of Brønsted acid sites on the GO–SO_3H catalyst surface. Reusability studies reveal that char formed during reaction is responsible for catalyst deactivation (entry 10, Table 1). A facile, one-step hydrothermal method was used for the synthesis of r-GO supported WO_3 solid acid.[133] This catalyst showed a complete conversion of fructose with a 84.2% yield of HMF, which was maintained even after five recycles of the catalyst (entry 11, Table 1). In addition, this catalyst was found to be effective in the conversion of cellulose, glucose, and sucrose to HMF. The selective anchoring of TiO_2 NPs (8–9 nm) on r-GO was successfully achieved by a microwave-assisted synthesis method.[134] The resulting TiO_2/r-GO catalyst showed a good efficiency in the aqueous-phase dehydration of D-xylose, comparable with that of TiO_2/carbon black catalyst. Moreover, the catalyst showed higher hydrothermal stability and strong coke resistance in comparison to several solid acid catalysts reported in literature.

In an efficient two-step strategy, Ru NPs were first supported on r-GO after which a subsequent functionalisation with benzenesulfonic acid groups was carried out (Fig. 11).[79] The obtained catalyst showed high performance in the hydrogenation–dehydration of levulinic acid with a 82% yield of γ-valerolactone. In contrast, 4-hydroxyvaleric acid was the major product over a non-functionalised Ru/r-GO catalyst. The combination of strong acid sites and ample amounts of active metal centers in the sulfonated Ru/r-GO catalyst is the key reason for achieving higher yields of γ-valerolactone. Sintering of Ru NPs, weight loss of the catalyst, and blockage of active Ru sites were noticed after eight recycles of the catalyst, hence a significant decrease in product yields from 82% to 53% (entry 12, Table 1). A few-layer graphene (FLG) supported Ru NPs catalyst was also studied for the conversion of levulinic acid to γ-valerolactone.[135] The activity of Ru/FLG is 2–4 times higher than that of Ru particles deposited on activated carbon and other traditional support materials. This was attributed to the higher abundancy of stabilised metallic Ru species in Ru/FLG catalyst. Alternatively, maximal yields of γ-valerolactone (99%) can also be produced from ethyl levulinate in the presence of a r-GO supported polymeric Ru porphyrin catalyst.[136] Various graphene oxide-based catalysts were studied for the esterification of levulinic acid with benzyl alcohol as well as the etherification of benzyl alcohol with butanol.[137] Among them, a graphene oxide monolith functionalised with chlorosulfonic acid showed excellent catalytic performance in both reactions. This catalyst exhibited a stable activity up to five recycles for 5 min reaction times in esterification of levulinic acid (entry 13, Table 1). Graphene oxide, prepared by a modified Hummers' method, was proven to be an efficient catalyst for the etherification of HMF to produce a polymer building block, 5,5′-oxy(bis-methylene)-2-furaldehyde.[138] The solvent plays an important role in this reaction, whereas *in situ* generated water showed a negative effect on the catalytic performance of graphene oxide. About 86% product yield was obtained, attributed to the presence of abundant oxygen containing functional groups on the graphene oxide catalyst. Reusability studies revealed that the catalytic activity of GO can be regenerated by treating it under Hummers' conditions (entry 14, Table 1).

2.3.2 Upgrading of non-carbohydrate compounds. A family of r-GO supported bimetallic CuPd catalysts were developed for upgrading various biomass model compounds, including glycerol.[139] The r-GO support acts as a template that controls the selective growth of Cu nanocrystals with dominant reactive surface facets due to the most proximal lattice match. The incorporation of Pd into the Cu–rGO system led to the formation of a synergistic catalyst system, hence improved reaction rates in the upgrading of biomass-derived polyols (*e.g.*, glycerol, xylitol, and sorbitol). A considerable decrease in product yields from 49.5% to 40% was observed after three recycles of Cu–Pd/r-GO catalyst in glycerol upgrading (entry 15, Table 1). Probable reaction pathways are reported for glycerol hydrogenolysis to lactic acid over Cu–Pd/r-GO catalyst (Fig. 12).[139] The production of biodiesel from lipids in wet microalgae was studied using graphene oxide, sulfonated graphene oxide, sulfonated graphene, and sulfonated active carbon catalyst.[140] Among them, the sulfonated graphene oxide showed the highest conversion of lipids to fatty acid methyl esters, due to the presence of high concentration of hydrophilic hydroxyl groups on the catalyst surface.

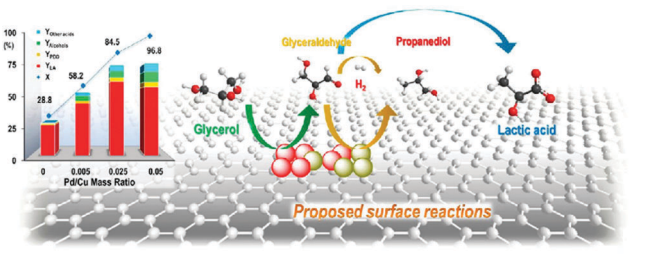

Fig. 12 Glycerol conversion and product yields as well as the proposed reaction pathways in glycerol hydrogenolysis over Cu–Pd/r-GO catalysts. Reproduced with permission from ref. 139. Copyright (2013) American Chemical Society.

Open Access Article. Published on 18 September 2018. Downloaded on 21/02/2026 10:11:12 PM.
This article is licensed under a Creative Commons Attribution-NonCommercial 3.0 Unported Licence.

2.4 Carbon nanotubes based catalysts

Carbon nanotubes (CNTs) offer potential possibilities for stabilising metal NPs, metal oxides, acid–base functional molecules, and even complex hierarchical hybrids. CNTs exhibit defective sp^2 carbon surfaces and improved electron transport, which facilitates the interaction of active phases with the CNTs.[61,141–143] In addition to preventing particle aggregation, the nanoscale confinement within CNTs can also control the diffusion of reactive species and their interactions with the active phases. These fascinating characteristics have been exploited in the field of biomass upgrading, in order to achieve improved conversion rates with high yields of desired products. Arc discharge, laser vaporisation and recently, chemical vapor deposition have been widely used techniques for the preparation of CNTs.[142]

2.4.1 Upgrading of carbohydrate-containing and -derived compounds. Ethylene glycol and 1,2-propanediol are important chemicals used in the production of polymers, resins, perfumes, cosmetics, and functional fluids.[141] They are currently produced from petroleum-derived ethylene and propylene, respectively, *via* cracking, epoxidation, and hydration. Hence, the production of glycols from renewable biomass or its derived molecules has gained a great deal of attention, as a more straightforward alternative to the three-step petrochemical route. Guo *et al.*[141] studied hydrogenolysis of sorbitol to produce ethylene glycol and 1,2-propanediol using Ru/CNTs catalysts. These catalysts showed higher activity than Ru/activated carbon, attributed to enhanced electron conductivity and higher graphitisation degree of CNTs. Ru NPs dispersed on the outer side surfaces of CNTs are catalytically more active than the CNTs-confined Ru NPs. Moreover, the addition of WO_x to Ru/CNTs results in an improved catalytic efficiency, attributed to synergistic Ru–WO_x interactions, which inhibit aggregation of active phase Ru NPs. Vanadium dioxide (VO_2) immobilised on polyaniline-functionalised CNTs (VO_2–PANI/CNT) was investigated for the oxidation of HMF to 2,5-diformylfuran (DFF) (Fig. 13).[144] A spontaneous redox process between VO^{3-} anions and polyaniline moieties on the CNTs surface occurred during reaction, which led to the generation of homogeneously dispersed active VO_2 NPs. Interestingly, the PANI/CNT support showed a preferential adsorption of HMF over DFF, hence limiting further oxidation of DFF. As a result, excellent yields (96%) of DFF were obtained over the VO_2–PANI/CNT catalyst. However, a significant decrease in DFF yields was observed (from 96% to 75%) after five recycles of the catalyst (entry 16, Table 1). Interestingly, leaching of soluble vanadium species is not responsible for catalyst deactivation as evidenced by a hot filtration test. The selective oxidation of HMF to DFF using molecular oxygen as the oxidant was also studied in the presence of Ru complex immobilised on poly(4-vinylpyridine)-functionalised CNTs.[145] About 94% yield of DFF was obtained over the developed catalyst. In contrast, 2,5-furandicarboxylic acid (FDCA) is obtained *via* a similar aerobic oxidation of HMF over functionalised CNTs supported Pt NPs.[146] FDCA is a promising alternative to petroleum-derived terephthalic acid for the production of polyesters, polyamides, and polyurethanes. The existence of various oxygen-based functional groups (carbonyl, quinone, and phenol) in functionalised CNTs enhanced the adsorption of HMF as well as the reaction intermediates and facilitated the hydrogen transfer, thus achieving higher yields of FDCA. The catalyst showed a remarkable stable activity towards HMF oxidation even after seven recycles (entry 17, Table 1). Polymeric Ru porphyrin-functionalised CNTs (Ru-PP/CNTs) were prepared, consisting of a bilayered structure with an amorphous polymeric ruthenium porphyrin outer surface and an internal CNT core.[136] The resulting Ru-PP/CNTs catalyst demonstrated an exceptional performance in the hydrogenation of ethyl levulinate to γ-valerolactone. In addition, the catalyst was found to be effective in the reductive amination of ethyl levulinate with various amines to obtain valuable pyrrolidone derivatives.

2.4.2 Upgrading of non-carbohydrate compounds. A facile, one-pot method was developed for the preparation of NEt_3-functionalised multiwalled CNTs (NEt_3-MWCNT) as single-site basic heterogeneous catalyst for biomass valorisation (Fig. 14).[77] This synthesis route produces a homogeneous distribution of ample, easily accessible basic sites. As a result, the NEt_3-MWCNT catalyst showed remarkable performance in the transesterification of glyceryl tributyrate with methanol, achieving a 77% conversion after 8 hours, whereas only 51% conversion was obtained over a conventional hydrotalcite catalyst. A series of acid functionalised polymer–CNT materials (CNTs–P–SO_3H) were prepared by covalent grafting of multiwalled CNTs with

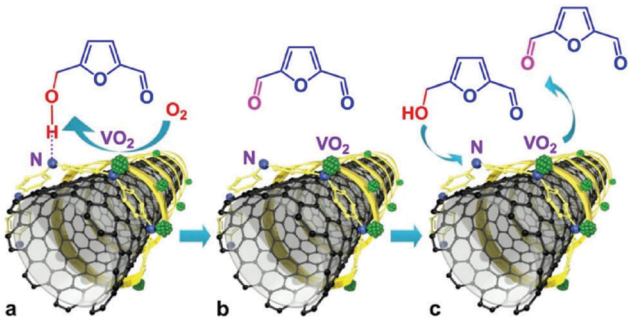

Fig. 13 Selective aerobic oxidation of HMF to 2,5-diformylfuran over VO_2–PANI/CNT catalyst. Reproduced with permission from ref. 144. Copyright (2015) John Wiley and Sons.

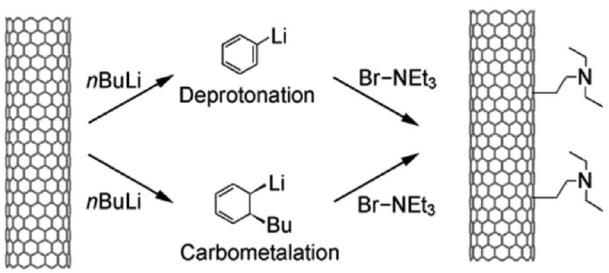

Fig. 14 Functionalisation of multi-walled CNTs by deprotonation–carbometalation and subsequent electrophilic attack of bromotriethylamine. Reproduced with permission from ref. 77. Copyright (2009) John Wiley and Sons.

This journal is © The Royal Society of Chemistry 2018

Open Access Article. Published on 18 September 2018. Downloaded on 21/02/2026 10:11:12 PM.
This article is licensed under a Creative Commons Attribution-NonCommercial 3.0 Unported Licence.

sulfonic acid-functionalised polymers.[78] The catalysts showed excellent activities for the production of biodiesel through transesterification of triglycerides as well as esterification of oleic acid. The combination of a mesoporous structure together with a high dispersion of active sites are the key factors for an improved acidity and consequently higher performance of CNT–P–SO_3H catalysts.

2.5 Mesoporous carbon-based catalysts

Mesoporous carbon materials have gained paramount attention for applications in biomass conversion due to their controllable porous properties, therefore significantly differing from traditional carbon materials.[147–149] In addition, they exhibit high specific surface areas and tunable pore channels, fascinating interfacial features, unprecedented control over their morphology and a rich composition. Template-assisted carbonisation methods are widely used for the synthesis of mesoporous carbons as they provide an efficient control over pore arrangement, structure, and mesoporosity. Another potential benefit of mesoporous carbons in biomass conversions is the enhanced interaction between reactive species and the catalytic active phases. For example, cellulose is not soluble in polar solvents. It is therefore difficult to convert completely the lignocellulose to value-added chemicals or biofuels. Owing to large sized uniform pores and abundant functional groups, mesoporous carbons can enhance the affinity between the non-soluble biomass molecules including cellulose and the catalyst, and consequently improved conversion rates in biomass valorisation.[147]

2.5.1 Upgrading of carbohydrate-containing and -derived compounds. A novel Pt catalyst supported on 3D mesoporous carbon was tested for the hydrolytic hydrogenation of cellulose.[147] Fig. 15 shows high-resolution TEM and SEM images of silica template and the synthesised 3D mesoporous carbon. As mentioned in the previous paragraph, the interaction between the catalyst and cellulose molecules is enhanced in the presence of mesoporous carbon, and hence, facilitated the access of cellulose molecules to the catalytic surface. In addition, the open pore structure of mesoporous carbon permits bulky cello-oligomers to effectively diffuse towards the active sites inside the pores. As a result, high yields of hexitol up to 80% from cellulose were obtained. The catalyst also showed a good performance in the direct conversion of hardwood lignocellulose towards sugar alcohols. A series of functionalised mesoporous carbon-based catalysts were prepared using tannic acid and SBA-15 as carbon source and silica template, respectively.[148] Phenolic hydroxyl groups with weak acidity present in the mesoporous carbon catalyst are the key active sites for the hydrolysis of cellulose to glucose. About 31.4% glucose yield and 53.8% cellulose conversion were obtained at optimised reaction conditions.

A combined catalytic and biotechnological process was developed for the production of HMF and bioethanol from cellulose.[149] In the first step, hydrolysis/dehydration of mechanically activated microcrystalline cellulose was carried out using a mesoporous carbon-based catalyst. Moderate yields of glucose and HMF were obtained. The extracted HMF from the reaction mixture was then subjected to ethanol fermentation. Acid-functionalised periodic mesoporous carbons (CMK-3 and CMK-5) were tested for the continuous production of HMF from fructose in the presence of water.[75] Both CMK-3 and CMK-5 showed good catalytic stability compared with acid-functionalised SBA-15 and commercial Nafion SAC-13 catalysts. Zhang *et al.*[150] developed an efficient mesoporous carbon-based solid acid using ethylene tar and concentrated H_2SO_4 with magnesium acetate as the template. A 87.8% yield of HMF was obtained *via* fructose dehydration, attributed to superior specific surface area and higher concentration of sulfonic acid groups in the developed mesoporous carbon catalyst. Reusability studies revealed a 10% decrease in HMF yields after five recycles of the catalyst (entry 18, Table 1). Hollow mesoporous carbon spheres (Fig. 16) were used as a support for anchoring ArSO_3H groups with controlled loadings (1.8 and 3.2 wt%).[151] Owing to strong Brønsted acidity and hollow nanospherical morphology with thin mesoporous shell, the developed catalysts showed excellent activity and stability for the synthesis of ethyl levulinate from levulinic acid or furfuryl alcohol. Tentative reaction mechanisms were proposed in this study (Fig. 16).

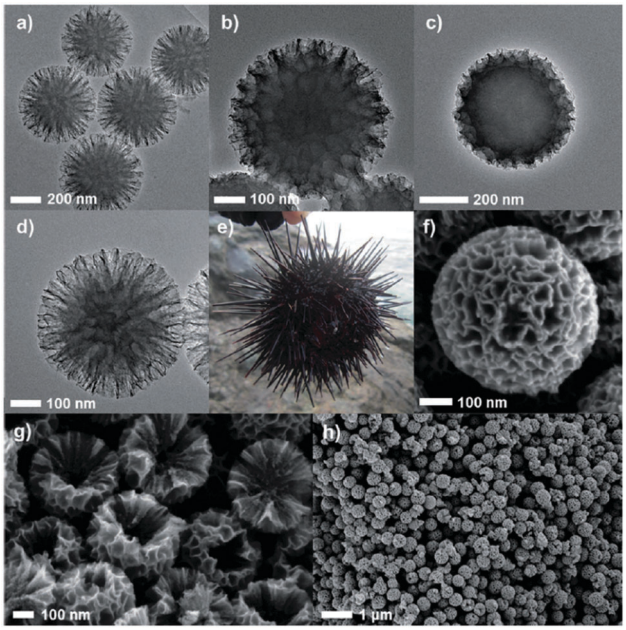

Fig. 15 High resolution TEM images of (a) Echinometra mathae-shaped silica (ESS) template, (b) ESS–carbon composite after drying, (c) ESS–carbon composite after aging, (d) carbon nano-Echinometra mathae (CNE), and (e) image of actual Echinometra mathae. SEM images of (f) a particle of CNE, (g) cross-section of CNE, and (h) prepared CNE particles in a large-scale view. Reproduced with permission from ref. 147. Copyright (2013) John Wiley and Sons.

2.5.2 Upgrading of non-carbohydrate compounds. The conversion of volatile fatty acids to fatty acid methyl esters (FAMEs) was studied using a series of ordered mesoporous carbons (OMCs).[152] Four types of OMCs were prepared, namely interconnected rod structured (i) CMK-3 and (ii) CMK-5 using Al-SBA-15 hard template, and cubic *la3d* (iii) CMK-8 and (iv) CMK-9 using Al-KIT-6 hard template. Among them,

Open Access Article. Published on 18 September 2018. Downloaded on 21/02/2026 10:11:12 PM.
This article is licensed under a Creative Commons Attribution-NonCommercial 3.0 Unported Licence.

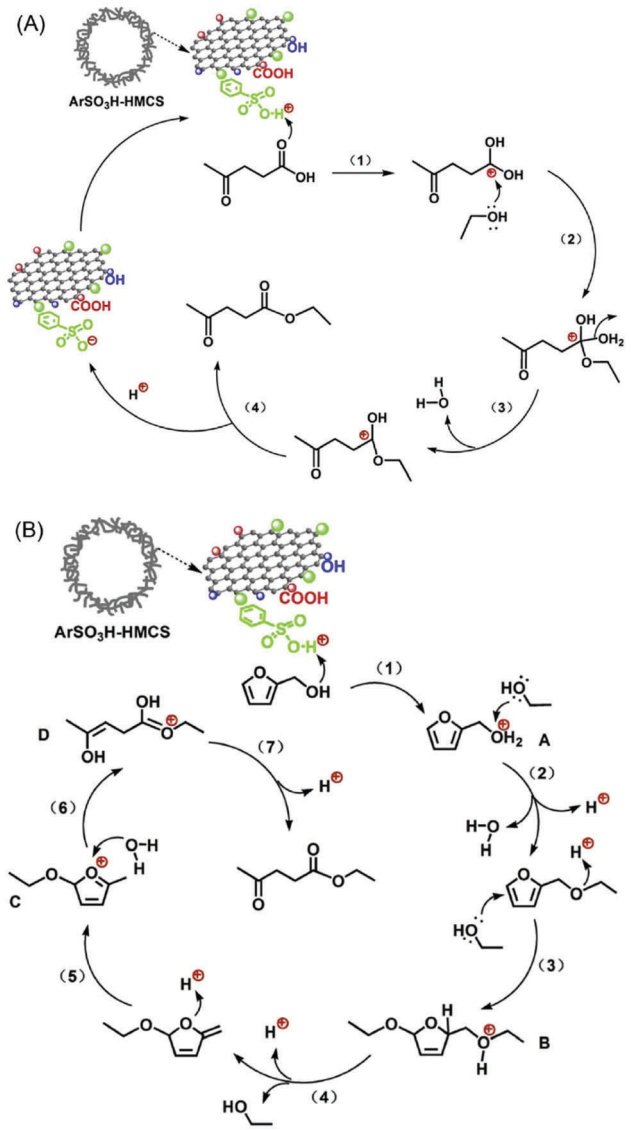

Fig. 16 Possible mechanisms for the synthesis of ethyl levulinate (A) from esterification of levulinic acid and (B) from ethanolysis of furfuryl alcohol over $ArSO_3H$-functionalised hollow mesoporous carbon spheres (HMCSs). Reproduced with permission from ref. 151. Copyright (2015) Elsevier.

CMK-5 showed the highest catalytic activity in the production of FAMEs as well as stable activity even after six recycles (entry 19, Table 1), which was ascribed to its unique interconnected rod structure with hollow rod-type carbon framework. Peng *et al.*[153] developed a facile, cost-effective route to synthesise various sulfonic acid-functionalised mesoporous carbon catalysts. Owing to a more hydrophobic surface and a larger pore size, the optimised catalyst showed a good performance in the esterification of oleic acid with methanol and a stable catalytic activity even after four recycles.

2.6 Mesostructured carbon-containing composites

The development of mesostructured composites, wherein carbon phase is well-dispersed, is of high research interest, not only for the reason of stabilising catalytically active carbon phase, but also to achieve synergistic properties in the resulting catalysts.[80] Over the last few years, a lot of research has been performed towards the design of various mesostructured carbon based composites. In particular, periodic mesoporous organosilicas (PMOs) have attracted significant attention because of their versatile properties towards promising biomass valorisation.[80,154] Post-synthetic grafting and co-condensation of organosilanes with silica precursors are often used for the synthesis of PMOs. Nevertheless, the utilization of organosilane precursors is practically unfavorable because of their high expensive nature. Tremendous research efforts have therefore been made to develop PMOs-based analogies, starting with relatively cheap carbon precursors, such as phenolic resin,[155,156] 2,3-dihydroxynaphthalene,[157] *p*-toluenesulfonic acid,[158] furfuryl alcohol,[81,159] sucrose,[160–163] and followed by incorporation of carbon precursors into preformed mesoporous hard templates (*e.g.*, ordered mesoporous silica),[81,157–159,163] or one-pot formation of mesostructured nanocomposites in the presence of soft template (*e.g.*, tri-block pluronic co-polymer).[155,156,160–162] The advantages of mesostructured carbon-containing composites for catalytic biomass valorisation are comparable or superior, depending on the reaction conditions used, to those of mesoporous carbon-based catalysts as discussed in Section 2.5. Interestingly, the presence of robust silica framework in mesoporous silica–carbon composites provides value-added benefits, such as strong thermal stability against elevated temperature/pressure reaction conditions as well as high hydrophilicity for the immobilization of relative functional groups on the catalyst surface.[160]

2.6.1 Upgrading of carbohydrate-containing and -derived compounds. The Sels group has made significant advances towards developing efficient mesoporous structured carbon-based composites for biomass valorisation. They developed a facile one-pot evaporation-induced self-assembly (EISA) procedure for the synthesis of mesoporous silica–carbon nanocomposites using sucrose, TEOS, and F127 as carbon precursor, silica precursor, and structure-directing template, respectively.[160–162] The synthesis process typically involves evaporation of sucrose/silica/F127 solution, followed by carbonization in N_2 atmosphere at 400 or 550 °C. This leads to transformation of F127 into columnar micelles, which were hexagonally arrayed into mesostructure, while sucrose moieties are transformed into carbon residues, forming nanocomposites containing hydrophobic carbon in close contact with the stabilizing hydrophilic silica framework.[161] The resulting hybrid materials were finally treated with H_2SO_4 to obtain sulfonated silica–carbon nanocomposites.[161,162] Silica–carbon nanocomposite (initial weight ratio SiO_2 : C = 33 : 66) carbonized at 550 °C exhibited high catalytic performance in hydrolysis of cellulose to glucose (up to 50.4% glucose yield).[160] This catalytic performance was attributed to the presence of strong and accessible Brønsted acid sites as well as to the hybrid surface structure, which promotes adsorption of reaction substrates on the catalyst surface. A small decrease in catalytic activity of sulfonated silica–carbon nanocomposite was found for cellulose hydrolysis after three recycles, due to leaching of acidic species (entry 20, Table 1). These catalysts were also active for the ethanolysis

 This journal is © The Royal Society of Chemistry 2018

Open Access Article. Published on 18 September 2018. Downloaded on 21/02/2026 10:11:12 PM.
This article is licensed under a Creative Commons Attribution-NonCommercial 3.0 Unported Licence.

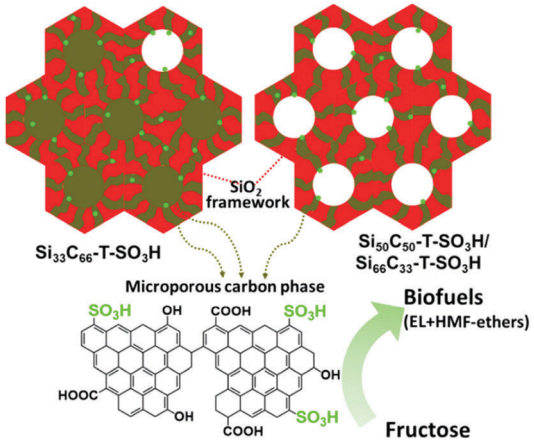

Fig. 17 Structural scheme of sulfonated silica–carbon nanocomposites. Red color entity represents silica framework, brown color entity represents microporous carbon phase, green color dots represent SO_3H groups, and EL represents ethyl levulinate. Reproduced with permission from ref. 162. Copyright (2017) Elsevier.

of fructose to levulinic esters and furanic ethers with the optimized combined yields of *ca.* 80%, as shown in Fig. 17.[162] The developed composites contain a hierarchical pore architecture, of which mesoporosity facilitates fast mass transport, whereas microporosity is beneficial to attain fast sugar catalysis. The observed catalyst deactivation was due to fouling of the acid sites instead of leaching, however, the catalytic activity could be fully regenerated using a simple re-sulfonation step. A modified EISA method was developed for scalable synthesis of acidic mesostructured silica–carbon nanocomposite catalysts.[164] The resultant sulfonated nanocomposites displayed good catalytic activity in fructose ethanolysis and in condensation of 2-methylfuran with furfural. This catalytic performance was attributed to several parameters, such as well-ordered mesostructure, tunable hydrophilicity/hydrophobicity and high concentration of strong acidic SO_3H sites.

EISA method is also applied for the synthesis of ordered mesoporous carbon–alumina nanocomposites, which was then used as a support for loading Pt NPs.[156] The resulting nanocomposites showed high catalytic performance in one-pot transformation of cellulose into hexitols, which was attributed to tunable hydrophobicity/hydrophilicity, adjustable metal–support interaction, and strong hydrothermal stability. Mesoporous silica–carbon solid acid catalysts obtained by a hard-template synthesis method were also tested in conversion of fructose, HMF, and furfuryl alcohol with ethanol into HMF ethers and levulinic esters.[158] Results reveal that higher yields of desirable bio-products were obtained over the silica–carbon catalysts, containing higher acid sites (1.9–2.3 mmol g^{-1}) and acid strengths.

2.6.2 Upgrading of non-carbohydrate compounds. Various sulfonated mesoporous silica–carbon nanocomposites were synthesized using a hard templating method *via* three types of silicas (KIT-6, SBA-15, and mesocellular silica).[157] The resulting composites contain a high density of acidic groups (SO_3H, COOH, and OH), attached to the deposited carbon layer. Hence, their catalytic performance was tested for the acid-catalysed esterification of maleic anhydride, succinic acid, and oleic acid with ethanol. Results revealed that all composites show a high intrinsic catalytic activity (TOF), outperforming a commercial solid acid, *i.e.* Amberlyst-15. This high catalytic performance was attributed to abundant strong SO_3H acid sites located inside wide and accessible mesopores and high water-tolerant nature of the carbon layer. A sulfonated mesoporous silica–carbon nanocomposite obtained by a controlled carbonization of sucrose, impregnated in SBA-15 and its subsequent sulfonation, was tested for both the esterification of palmitic acid and the transesterification of soybean oil with methanol.[163] The composite with a 35 wt% carbon showed high catalytic performance towards biodiesel production, which was attributed to high density of accessible Brønsted acid sites.

2.7 Carbon nanofiber based catalysts

Carbon nanofibers (CNFs) have emerged as an interesting class of one-dimensional nanostructured carbon materials, which can exhibit comparable or superior properties to other carbonaceous materials in terms of thermal stability, mechanical strength, and exposed active sites on the outer surface of CNFs.[165] In addition, CNFs exhibit strong hydrothermal stability, and thus, often preferred as efficient catalyst supporting materials over metal oxide supports.

2.7.1 Upgrading of carbohydrate-containing and -derived compounds. Sels *et al.*[70] developed an attractive catalyst, consisting of pear-shaped Ni particles at the tip of CNFs, for the conversion of cellulose into polyols (Fig. 18). Results revealed that CNFs grown on Ni/γ-Al_2O_3 allow the promising conversion of cellulose with a 50.3% yield of sorbitol. A minor loss in

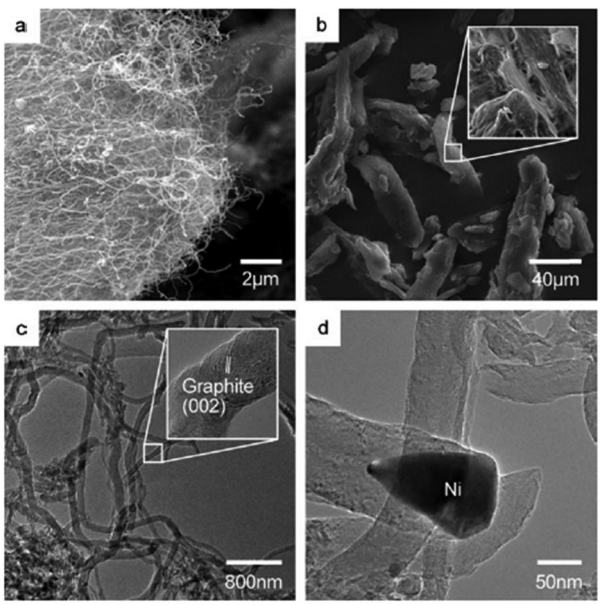

Fig. 18 SEM images of (a) carbon nanofibers grown over Ni/γ-Al_2O_3 catalyst and (b) microcrystalline cellulose. TEM images of (c) carbon nanofibers and (d) a pear-shaped Ni particle at the tip of a carbon nanofiber. Reproduced with permission from ref. 70. Copyright (2010) John Wiley and Sons.

Open Access Article. Published on 18 September 2018. Downloaded on 21/02/2026 10:11:12 PM.
This article is licensed under a Creative Commons Attribution-NonCommercial 3.0 Unported Licence.

sorbitol yield at similar conversions of cellulose was noticed after three recycles of the catalyst, which was attributed to catalyst weight loss during recovery/purification steps. In another work, the acid–metal balance of CNFs-supported Ni catalysts was tuned for selective hydrogenation of cellulose to C_6 sugar alcohols.[166] Effects of oxidising agent, Ni activation process, and Ni loading were investigated, resulting in 76% yield of hexitols with 69% selectivity of sorbitol at 93% conversion of cellulose. Song *et al.*[165] developed a series of La-modified Ru/CNFs catalysts for hydrogenation of levulinic acid into γ-valerolactone. Owing to a high concentration of metallic Ru active sites and a synergistic Ru–La interaction, improved reaction rates were obtained over the $Ru_1La_{0.5}$/CNFs catalyst. Interestingly, a considerable decrease in catalytic activity of RuLa/CNFs was noticed with the further increase of La amount (La/Ru > 0.5), due to blockage of Ru active sites by surplus La dopant.

2.7.2 Upgrading of non-carbohydrate compounds. van Haasterecht *et al.*[167] examined the hydrothermal stability and the catalytic efficiency of Ni/CNFs materials for aqueous phase reforming of ethylene glycol to produce H_2. Results revealed the deactivation of the catalysts at standard reaction conditions, due to aggregation of active phase metallic Ni particles. Several strategies were therefore demonstrated to limit Ni particles growth, such as introducing additional H_2 into the reactor, increasing the concentration of reactant, and addition of a base (KOH) to the reaction mixture. Among those, base addition was found to be the most effective route in stabilizing Ni NPs, resulting in a stable H_2 production rate with a high selectivity (99%) during 50 h time-on-stream. In another work, several Ni/CNFs catalysts, prepared by a homogeneous impregnation method, were used to produce H_2 *via* low-temperature steam reforming of bio-oil.[168] Best catalytic results (94.7% and 92.1% of carbon conversion and H_2 yield, respectively) were obtained over 22% Ni/CNFs catalyst. Results indicated that reaction temperature, molar ratio of steam to carbon, and Ni loading play a crucial role on the performance of the Ni/CNFs catalyst.

2.8 Biomass-derived carbon catalysts

Many types of biomass substrates have been evaluated to prepare carbon-based catalysts (*e.g.* wood, bamboo, oilseed cake, oil palm trunk, sugarcane bagasse, vegetable oil asphalt, and carbohydrates). For this, carbonisation methods are normally used, including pyrolysis, gasification, hydrothermal, and flash carbonisation as these strategies allow to obtain well-controlled micro-/nanostructures of carbon materials with tunable surface chemistries and abundant functional sites.[78,82–84] Moreover, applying renewable organic substrates instead of inorganic substrates for catalyst synthesis also contributes to an improved process sustainability.

2.8.1 Upgrading of carbohydrate-containing and -derived compounds. Furfural is a highly promising biomass-derived platform molecules and can be used to produce a myriad of valuable chemicals, such as furfuryl alcohol, tetrahydrofuran, 2-methylfuran, γ-valerolactone and cyclopentanone.[169] Several attempts have been made to directly produce this chemical from lignocellulosic biomass. For example, Zhang *et al.*[169] developed an efficient catalytic protocol for the production of furfural from either raw corn stalk or xylose using a novel carbon solid acid, which was synthesised through carbonisation of sucrose followed by a sulfonation treatment. The catalyst exhibited excellent Brønsted acidity, resulting in 78.5% and 60.6% yields of furfural from xylose and corn stalk, respectively. The catalyst showed a remarkable stable activity even after five recycles in xylose dehydration (entry 21, Table 1). In another work, corncob is used to produce furfural over a biochar supported SnO_2–Co_3O_4 Lewis acid catalyst.[170] About 30% yield of furfural was achieved, due to an efficient xylose isomerisation in aqueous medium. However, only a 15% yield of furfural was obtained after six recycles of the catalyst, attributed to leaching of acidic species (entry 22, Table 1). A sulfonated biochar catalyst, synthesised using *Miscanthus x giganteus* grass and H_2SO_4, also afforded 60 and 42% yields of furfural from dehydration of xylose and xylan, respectively.[171]

The optimisation of hydrothermal carbonisation conditions, such as temperature and time, was undertaken to prepare a glucose-derived carbon, which was then functionalised with $–SO_3H$ species.[172] The resulting catalyst showed good activity in cellulose hydrolysis and fructose dehydration reactions with glucose and HMF yields of 44 wt% and 20 wt%, respectively. A one-pot synthesis of $–SO_3H$ and COOH-functionalised carbon solid acids was successfully performed by hydrothermal carbonisation of glucose in the presence of sulfosalicylic acid and acrylic acid, respectively.[173] The functionalisation led to a change in the particles shape and resulted in good catalytic activity for the hydrolysis of cellulose. Importantly, the HSO_3-functionalised carbon solid acid showed excellent stability up to five recycles without leaching of $–SO_3H$ species. A sulfonated willow-derived carbon catalyst was successfully prepared through sulfonation of a pencil refill.[174] This catalyst, containing $–SO_3H$, –COOH, and –OH groups, is highly suitable for the transformation of cellulose into glucose, reaching 78% conversion and 65% glucose yield, due to its strong acidic strength and well-defined macroporous structure. A minor loss in glucose yields was found after three recycles of the catalyst, due to catalyst mass loss during recovery/purification steps (entry 23, Table 1). Numerous carbon-based solid acids were prepared using different biomass sources, such as glucose, cellulose, bamboo, and rice husk.[175] The developed solid acids, containing $–SO_3H$ and –COOH groups, showed good catalytic performances for the hydrolysis of cellulose with a maximum 81.8% yield of total reducing sugar for the glucose-derived acid catalyst. An amorphous carbon-based acid catalyst, prepared by sulfonation of bio-char obtained from fast pyrolysis of biomass, was also studied for the hydrolysis of cellulose.[176] The complete conversion of cellulose with about 90% yields of α,β-methyl glucosides in methanol was obtained. Sulfonation of carbonised de-oiled seed waste cake, a solid waste from biodiesel production, was carried out to obtain multifunctional carbon-based solid acids.[177] The catalysts contain various –OH, –COOH, and $–SO_3H$ groups as well as several nitrogen species (pyridinic, pyrrolic, *etc.*). Improved structure–activity properties were

Open Access Article. Published on 18 September 2018. Downloaded on 21/02/2026 10:11:12 PM.
This article is licensed under a Creative Commons Attribution-NonCommercial 3.0 Unported Licence.

obtained with 4-benzenediazoniumsulfonate as the sulfonating agent, compared to H_2SO_4. The catalysts showed good activity in cellulose saccharification (glucose yield is in the range of 35–53%) as well as in fatty acid esterification (conversion up to 97%), hereby outperforming a conventional liquid acid (H_2SO_4) and other solid acids (zeolites, ion-exchange resins, *etc.*). A biomass residue obtained from the extraction of palm oil was used for the synthesis of a sulfonated carbon solid acid catalyst.[178] A positive correlation between the concentration of sulfonic acid groups and the catalytic activity was noticed in the hydrolysis of cellobiose. Moreover, the sulfonated carbon showed higher catalytic activity than commercial acid resins. A sulfonated bamboo-derived carbon catalyst was studied for microwave-assisted conversion of bamboo-derived hemicellulose to xylo-oligosaccharides.[179] The catalyst contains various acid groups, such as $-SO_3H$, –COOH, and phenolic –OH. A 54.7 wt% yield of xylo-oligosaccharides based on xylan content was obtained at optimised reaction conditions. Reusability studies revealed a significant decrease in catalytic activity of sulfonated bamboo-derived carbon after three recycles, due to severe leaching of acidic species (entry 24, Table 1).

A novel sulfonated polymer impregnated carbon solid acid catalyst was studied for the dehydration of xylose to furfural. The detailed synthesis procedure is shown in Fig. 19.[180] The catalyst exhibited excellent activity and provided almost quantitative conversion of xylose with selective synthesis of furfural. A carbon-based solid acid, prepared using glucose and an aqueous solution of H_2SO_4 as carbon and sulfonation agent, respectively, was studied for fructose dehydration.[181] About 90% yield of HMF was achieved with dimethylsulfoxide as the solvent. The catalyst can be reused for several times without significant loss in catalytic activity. The selective dehydration of fructose to HMF was also investigated over various sulfonated carbon solid acids prepared using fructose as the carbon source.[182] About 87% yield of HMF at nearly complete conversion of fructose was achieved. The advantage of microwave-assisted heating over conventional heating was demonstrated, allowing shorter reaction times for the dehydration of fructose.[182] Hydrothermal carbonisation of various biomass substrates, such as lignin, cellulose, wood meal, and xylose, followed by sulfonation, was attempted to prepare amorphous carbon-based solid acid catalysts.[183] All catalysts possess aromatic structures, as well as hydroxyl and carboxyl functional groups. The catalysts exhibited a good activity in the production of HMF (yields of 47–65%) from inulin, hereby outperforming various traditional solid acid catalysts. A series of metal chloride-modified sulfonated carbon catalysts, synthesised from cellulose, were tested for the selective conversion of carbohydrates to ethyl levulinate in an ethanol medium.[183] Various metal chlorides, such as NaCl, KCl, $MgCl_2$, $AlCl_3$, $FeCl_3$, $CrCl_3$, and $SnCl_4$ were used in this study. Among them, the $FeCl_3$ modified carbon catalyst showed the highest performance in the conversion of fructose with a 58 mol% yield of ethyl levulinate. On the other hand, small amounts of water in the reaction mixture favoured the formation of HMF and levulinic acid.

A porous carbon material obtained from bamboo shoots was used as an efficient support for depositing Pt NPs.[184] The resulting catalysts possessed a high specific surface area, hierarchical porous structure, uniform dispersion of Pt NPs, large amounts of functional nitrogen and oxygen groups, and excellent water dispersibility. As a result, the carbon-supported Pt catalysts showed good activity for furfural hydrogenation with a controlled selectivity to furfuryl alcohol and cyclopentanone in water. Cyclopentanone is a promising building block for the production of low cost fragrances, fungicides, and perfume ingredients.[185] The effect of carbonisation temperature of support, reaction temperature, and reaction pressure were also studied on the products distribution.[184] A tandem aldol condensation–hydrogenation of furfural with acetone was carried out using a bi-functional catalyst composed of ultrafine dispersed Pd NPs on a CN@MgO hybrid support (CN = nitrogen doped carbon).[186] The hydrophilic N-doped carbon enhanced the water dispersibility, catalyst stability, and the dispersion of Pd NPs (2.2 nm in average size) in the Pd/CN@MgO catalyst. Almost 99% furfural conversion with 95% selectivity to saturated ketones were obtained over the Pd/CN@MgO catalyst. Effects of carbonisation and calcination conditions on the textural and acid properties of carbon cryogel, obtained from a facile sol–gel polycondensation of acidic lignin-furfural mixtures, were studied.[187] Calcination of the carbon cryogel led to higher thermal stability and stronger acid sites, and consequently superior catalytic performance in the esterification of levulinic acid, as shown by the 87.2% conversion and 86.5% ethyl levulinate yield at optimised reaction conditions (entry 25, Table 1). Reusability studies revealed that levulinic acid conversion decreases from 87.2% to 70.6% after third cycle, and then, a stable catalytic activity up to 5th cycle. Leaching of active sites is a key reason for the observed catalyst deactivation. Various functionalised carbon based catalysts, prepared by the chemical activation of olive stone waste, were tested for isopropanol decomposition.[188] Among the catalysts tested, the H_3PO_4-activated carbon showed a steady state conversion with propylene as the major product in the absence of oxygen. In the case of base-activated carbon catalysts, variable amounts of acetone and propylene were obtained.

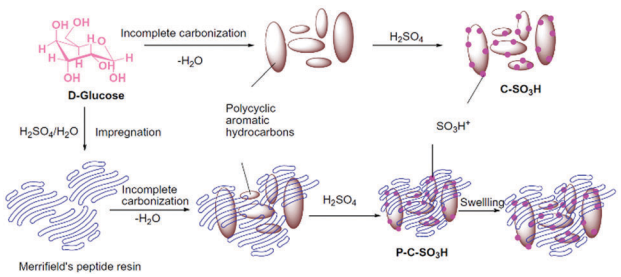

Fig. 19 Synthesis procedure for sulfonated polymer impregnated carbon solid acid catalyst. Reproduced with permission from ref. 180. Copyright (2015) Elsevier.

2.8.2 Upgrading of non-carbohydrate compounds. Catalytic hydrodeoxygenation (HDO) of lignin oil is a promising strategy to reduce the amount of oxygen, resulting into a high-quality

Open Access Article. Published on 18 September 2018. Downloaded on 21/02/2026 10:11:12 PM.
This article is licensed under a Creative Commons Attribution-NonCommercial 3.0 Unported Licence.

bio-oil that can be efficiently upgraded to compatible transportation fuels.[189–192] Co-Pyrolysis of cellulose and cobalt nitrate under NH_3 atmosphere was performed to prepare novel magnetic N-doped carbon supported cobalt nitride catalysts (CoN_x@NC).[193] Their catalytic efficiency for HDO of lignin-derived phenols was subsequently tested. The CoN_x@NC catalyst pyrolysed at 650 °C exhibited the best HDO activity, reaching a >99.9% yield of propylcyclohexanol from eugenol. This catalyst selectively cleaves the C_{aryl}–OCH_3 bond to form 4-propylphenol, prior to hydrogenation of the aromatic ring, hence improved eugenol conversions and higher yields of propylcyclohexanol under mild reaction conditions. However, a drastic decrease (about 25%) in product yields was observed after four recycles of the catalyst, due to leaching of active sites (entry 26, Table 1). A one-pot carbonisation of glucose with melamine and $CoCl_2$ as C, N and Co sources, respectively, was carried out to prepare a novel N-doped Co@C catalyst (Co@NC).[72] During catalyst synthesis, the coordinated Co^{2+} ions are reduced to Co NPs, followed by incorporation into N-doped graphitic carbon (Fig. 20). The Co@NC catalyst, pyrolysed at 700 °C, exhibited the highest activity for HDO of vanillin using formic acid as a hydrogen donor as well as a stable catalytic activity even after five recycles (entry 27, Table 1). Noticeably, the Co@NC-700 catalyst showed a 15.4 times higher activity compared to a carbon supported cobalt catalyst. The existence of N-derived defective sites in Co@NC is the key reason for the superior performance of Co@NC-700, due to a dual function as a base additive in formic acid dehydrogenation as well as a metal-like active phase in vanillin HDO.

Esterification of plant oil with methanol to produce biodiesel was investigated over a series of bagasse-derived carbon solid acids.[194] The catalyst, prepared with a dilute acid hydrothermal treatment, showed the best performance towards biodiesel production. This catalyst also demonstrates a more durable activity compared to conventional homogeneous catalysts. Sulfonation of biochar and wood-derived carbon was carried out using H_2SO_4 and SO_3 for the esterification of free fatty acids with methanol.[195] Wood-derived carbon solid acids showed higher activity compared to biochar-derived catalysts, which was attributed to the highest density of acid (SO_3H) species present in wood-derived carbon solid acids. The catalyst reusability is thoroughly studied and appropriate strategies were suggested to regenerate the catalyst activity after reaction. A facile one-step hydrothermal carbonisation of water hyacinth was performed in the presence of *p*-toluenesulfonic acid to obtain promising carbon-based solid acids with variable acid density.[84] Catalysts with higher amounts of acid sites showed better performance in oleic acid methanolysis as well as in xylose dehydration. Higher hydrothermal carbonisation temperatures (220–240 °C) enhanced the catalyst reusability due to improved graphitisation and hydrophobicity of the carbon surface. Esterification of free fatty acids in waste cooking oil with methanol was studied to produce biodiesel using a carbonaceous solid acid prepared by a one-step mild hydrothermal carbonisation of glucose, followed by sulfonation using hydroxyethylsulfonic acid.[196] Catalytic results revealed a strong

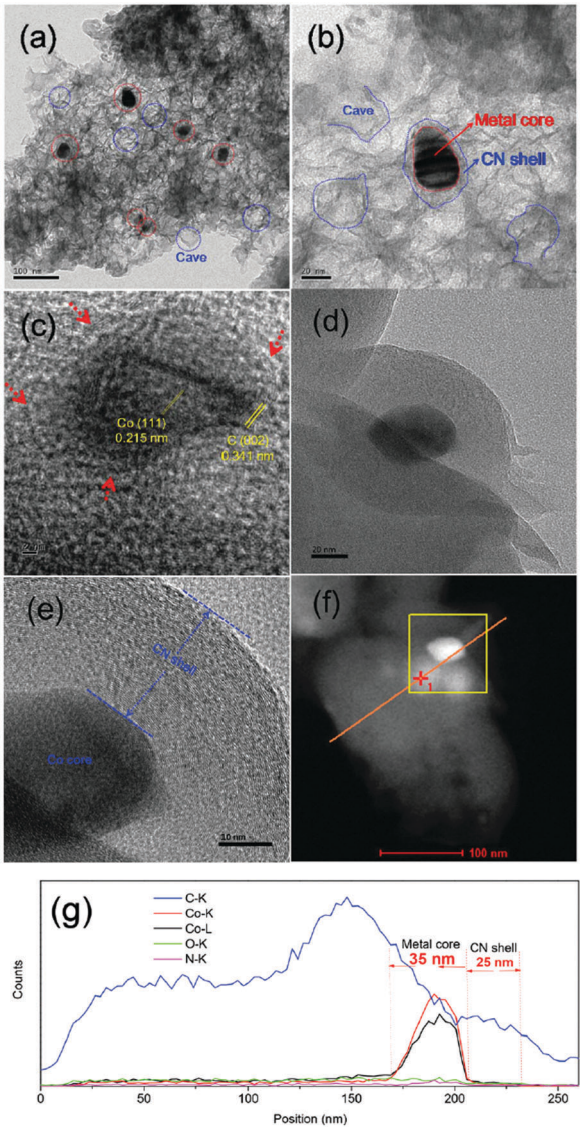

Fig. 20 TEM images (a–e), STEM image (f) and line scanning EDS elemental analysis (g) of Co@NC-700 catalyst. Reproduced with permission from ref. 72. Copyright (2017) Royal Society of Chemistry.

decrease in the content of free fatty acids (up to 93.4%) in waste cooking oil. Catalyst stability was demonstrated with only a 7% decrease in free fatty acids conversion after five recycles. A bagasse-derived carbon solid acid showed excellent catalytic activity with a 95% yield of methyl oleate from esterification of oleic acid with methanol, hereby outperforming both niobic acid and Amberlyst-15 catalysts.[197] The obtained results are comparable or superior to those of starch- and glucose-derived carbon catalysts, respectively. Furthermore, the bagasse-derived carbon solid acid efficiently catalysed the conversion of waste cooking oils (39 wt% free fatty acid content), obtaining a 93.8% biodiesel yield. An incomplete carbonisation of coffee residue followed by sulfonation was carried out to prepare sulfonated carbon catalysts for the esterification of caprylic acid.[198] The sulfonation temperature played a crucial role in optimising the –SO_3H density on the catalytic surface. The catalyst carbonised

 This journal is © The Royal Society of Chemistry 2018

Open Access Article. Published on 18 September 2018. Downloaded on 21/02/2026 10:11:12 PM.
This article is licensed under a Creative Commons Attribution-NonCommercial 3.0 Unported Licence.

at 600 °C and sulfonated at 200 °C showed the highest caprylic acid conversion (71.5%). A robust sulfonated carbon catalyst derived from oil-cake waste was tested for biodiesel production.[199] The catalyst exhibited superior acid density, large porosity, high specific surface area, and remarkable thermal stability. As a result, the catalyst showed excellent activity and good reusability in the esterification of free fatty acids into corresponding methyl esters, thus outperforming a homogeneous H_2SO_4 catalyst. A sulfonated carbon solid acid, obtained after a one-pot carbonisation–sulfonation of cellulose using concentrated H_2SO_4, was investigated for the esterification of rapeseed oil fatty acids.[200] The activity of the carbon solid acid was similar to Amberlyst-15 and led to a 96.5% esterification activity.

Zhang *et al.*[201] investigated the production of Jatropha biodiesel and hydrogen using carbonaceous acid and base catalysts. Two carbon supports were prepared from Jatropha-hull hydrolysate (JHC) and hydrolysis residue (JRC), followed by the deposition of active species to obtain carbonaceous solid acid (C-SO_3H@Fe/JHC) and solid base (Na_2SiO_3@Ni/JRC) catalysts, respectively. The C-SO_3H@Fe/JHC catalyst was used for the esterification of free fatty acids in crude Jatropha oil. Subsequent transesterification of remaining triglycerides catalysed by Na_2SiO_3@Ni/JRC ultimately afforded a high biodiesel yield of 96.7%. Interestingly, the solid base catalyst obtained after three recycles showed a high performance in the hydrothermal gasification of glycerol with 81% yield of H_2. In another work, de-oiled Jatropha curcas seed cake waste was used to prepare a carbon-based solid acid catalyst, which was then tested in the esterification of Jatropha curcas in order to reduce free fatty acid content for biodiesel production.[202] The conversion of free fatty acids reached 99% under optimised reaction conditions, due to an improved porosity of the carbon framework. Moreover, the biomass-derived catalyst outperformed a conventional sulfuric acid catalyst. A carbon-based solid base catalyst was prepared by treating a SO_3H–carbon catalyst obtained from glycerol with an aqueous alkali solution.[85] The solid base catalyst contains polycyclic aromatic carbon sheets attached with versatile –SO_3Na, –COONa, and –ONa functionalities. The resulting catalyst showed a remarkable catalytic activity in transesterification of sunflower oil with high yields of biodiesel (99%) at atmospheric pressure. In addition, no considerable loss in biodiesel yield was found even after eight recycles of the catalyst (entry 28, Table 1).

The production of biodiesel from oil, obtained by solvent extraction of *Calophyllum inophyllum* seeds, was studied over a biomass-derived carbon catalyst.[203] The catalyst is itself synthesised *via* carbonisation of the residual cake of *Calophyllum inophyllum*, followed by sulfonation in concentrated H_2SO_4. The resulting solid acid efficiently catalysed simultaneous esterification and transesterification of free fatty acids and triglycerides present in *Calophyllum inophyllum* oil, respectively. Sulfonated carbon-based solid acid catalysts, prepared using a simultaneous carbonisation and sulfonation of glucose with conc. H_2SO_4, were tested for two reactions, namely transesterification of tributyrin with methanol and dehydration of fructose to HMF.[204] The catalyst prepared at 150 °C showed excellent activity in both reactions with 97.2% and 93% yields of methyl butyrate and HMF, respectively, which was attributed to its high density of –SO_3H sites.

Glycerol esterification with acetic acid or acetic anhydride is an important reaction that gives three valuable products, namely monoacetin, diacetin, and triacetin.[124,205–207] These acetins have great commercial significance as transportation fuel additives and antiknock additives. Moreover, the addition of small amounts of triacetin improves the properties of biodiesel. Hence, this reaction acts as a key driving force to enhance the profitability of biodiesel production. Several sulfonated carbon catalysts were developed from biomass waste at different synthesis conditions.[208] Due to their strong acidity and higher thermal stability, excellent activities were obtained for glycerol esterification to a mixture of monoacetin, diacetin, and triacetin. In addition, the strong hydrophobic character of these catalysts resulted in an excellent reusability for glycerol esterification. Sulfonated glucose-derived carbon catalysts showed higher activity for the hydrolysis of alginate, a major constituent of algal biomass, compared with that of H_2SO_4 and other commercial solid acid catalysts, such as carbon black, activated carbon, Amberlyst-15, and zeolites.[209] This performance was ascribed to the high concentration of strong Brønsted acid sites (–SO_3H) in the glucose-derived carbon catalysts. Biochar, obtained after fast pyrolysis of pinewood, was used for the encapsulation of Fe NPs.[210] The catalyst has a core–shell structure resulting from *in situ* encapsulation of iron within a graphitic shell. Catalytic experiments demonstrated an efficient conversion of bio-syngas with a good selectivity to liquid hydrocarbons. The catalytic dehydration of 2-butanol was studied using a carbon-based solid acid prepared by chemical activation of olive stone with H_3PO_4.[76] The catalyst shows high surface acidity due to the presence of residual phosphorous species on the catalyst surface, resulting in improved catalytic activities. *cis*-2-Butene and *trans*-2-butene are the major products with lower amounts of 1-butene *via* E2-mechanism (one-step mechanism) of 2-butanol dehydration, which is a rate-determining step.

2.9 Conclusions of carbon-based catalysts

Based on the examples discussed in this chapter, it is clear that the large specific surface area and strong hydrothermal stability of carbon-based catalysts play a favorable role in biomass upgrading. On one hand, immobilization/dispersion of functional species (SO_3H, metals, *etc.*) is facilitated on high surface area carbon supports. This leads to a higher number of surface-exposed active sites available for biomass valorisation. On the other hand, the strong hydrophobic nature of carbon materials prevents leaching of active species during biomass processing reactions, allowing a more efficient catalyst reusability, as evidenced by Table 1. In addition, the unique properties of nanostructured carbon materials, especially graphene, not only play a key role in stabilising acid–base and/or redox functional species (entries 10–13, Table 1), but also enable them to perform as metal-free catalysts in biomass upgrading (entry 14, Table 1).

Open Access Article. Published on 18 September 2018. Downloaded on 21/02/2026 10:11:12 PM.
This article is licensed under a Creative Commons Attribution-NonCommercial 3.0 Unported Licence.

Unfortunately, despite all of these attractive characteristics and potential catalytic applications, carbon materials, especially graphene and CNTs, still suffer from several drawbacks, such as lack of large-scale synthesis methods, high production costs, low bulk density, and mass diffusion constraints, limiting their catalytic applications at the industrial scale.[211,212] In this framework, using biomass substrates (Section 2.8) for one-pot synthesis of functionalised carbon-based catalysts would be a promising solution in terms of catalyst costs, functionalisation, and scalability. In parallel, the application of mesostructured carbon catalysts (Sections 5 and 6) in biomass upgrading would be an ideal strategy to overcome the current mass transfer limitations of microporous carbon materials. However, more efforts are still needed to optimise structure–activity features of biomass-derived carbon and mesoporous carbon catalysts to obtain breakthrough catalytic results in biomass valorisation.

3. Metal–organic frameworks

Metal–organic frameworks (MOFs) belong to an extraordinary family of crystalline porous materials with unique characteristics and versatile functionalities.[36,213,214] They have found plentiful applications in various fields, including catalysis, sensing, luminescence, separation, gas adsorption, H_2 storage, and optical devices. MOFs contain two key building blocks: (i) metal ions or metal–oxo clusters and (ii) multidentate organic moieties. The unique nature of metal ions or clusters as lattice nodes and organic moieties as linkers allow the formation of robust metal–ligand coordination frameworks with well-defined porous structures quite similar to those found in zeolites. The capacity to fine-tune pore geometries up to a mesoporous size range is a notable advantage of MOFs over microporous zeolites.[36] This pore modification is feasible by selecting a suitable combination of metal ions and organic linkers as well as by tailoring MOFs synthesis parameters. Mesoporous structures can facilitate efficient diffusion of (bulky) biomass substrates towards unsaturated active metal centres in MOFs, thus overcoming mass transport limitations often encountered with microporous zeolites. To meet the requirements of a specific target application, properties of MOFs can be further tuned by anchoring desired active phases. Overall, MOFs are highly tunable materials, which led to more than 20 000 synthesised MOFs, described in literature up to date.[36] In addition, the high crystallinity of MOFs assists to carry out thorough structure–activity relationship investigations as well as molecular simulations that can provide valuable implications for the rational design of new, high performing MOF materials.

3.1 Factors affecting the catalytic activity of MOFs in biomass upgrading

Over the past few years, MOFs have been in the forefront of research in catalytic biomass valorisation. The diversity of both metal nodes and organic ligands as well as their synergistic interactions enables MOFs to perform as active phase catalysts, catalyst supports or even catalyst synthesis precursors. Owing to durable metal–ligand coordination networks, MOFs can exhibit large pore volumes and superior specific surface areas. Therefore, the individual properties of inorganic and organic components are usually well accessible and uniformly distributed throughout the MOFs, a fundamental advantage over conventional heterogeneous solid catalysts.[215] The broad spectrum of starting materials as well as efficient synthesis strategies offer unlimited options for fine-tuning textural properties of MOFs. This is indispensable because biomass feedstocks usually contain larger molecules, hence their diffusion towards catalytic active sites can be improved by carefully adjusting pore dimensions and morphologies. For instance, Li *et al.*[216] reported that the morphology of Fe-MIL-101-NH_2 could be modified by simply varying the synthesis times of MOF, without effecting its crystal structure. The resulting MOFs showed good catalytic performances in glycerol oxidation reaction.

The individual attributes of metal nodes and organic ligands can offer abundant acid–base properties.[215,217] The unsaturated metal sites in MOFs obviously exhibit Lewis acidity. They also show adequate redox and basic properties, depending on the nature of metal–oxygen connection modes of MOFs. Owing to higher Lewis acidity, MOFs can be used as solid acid catalysts for isomerisation of glucose to fructose.[218] Notice that Brønsted acid sites are essential in many biomass-upgrading reactions. Nevertheless, MOFs exhibit negligible Brønsted acidity. Therefore, several viable strategies have been developed to attach Brønsted acidic groups onto a particular site of the MOFs.[216,219] Organic ligands provide facile approaches to introduce such acid functionalities.[220] Mainly, sulfonated-functionalised MOFs have received paramount attention in catalysis because of their superacidity, which is stronger than 100% H_2SO_4.[221] Since functionalised MOFs can combine the advantages of both MOFs and incorporated acid–base functional sites, they are particularly suitable to catalyse cascade chemical reactions for efficient biomass upgrading. For instance, the SO_3H-functionalised UiO-66 MOF showed an exceptional catalytic activity in the conversion of levulinic acid and its esters to produce γ-valerolactone (Fig. 21).[222] Results indicated that Zr^{4+}–O^{2-} acid–base pair sites, uniformly imbedded in the UiO-66 framework, enhance catalytic transfer hydrogenation

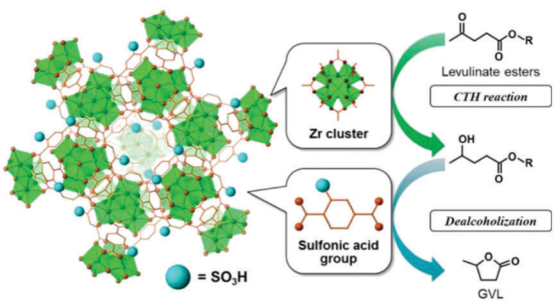

Fig. 21 SO_3H-Functionalised UiO-66 MOF for catalytic transfer hydrogenation (CTH) of levulinate esters to γ-valerolactone. Note: Zr and O atoms are shown in green and brown, respectively. Reproduced with permission from ref. 222. Copyright (2017) American Chemical Society.

Open Access Article. Published on 18 September 2018. Downloaded on 21/02/2026 10:11:12 PM.
This article is licensed under a Creative Commons Attribution-NonCommercial 3.0 Unported Licence.

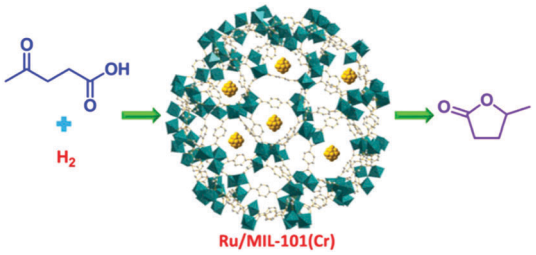

Fig. 22 Selective hydrogenation of levulinic acid into γ-valerolactone over Ru/MIL-101(Cr) catalyst. Reproduced with permission from ref. 225. Copyright (2016) Springer Nature.

of levulinate esters, while $-SO_3H$ groups attached to organic linkers catalyse successive intramolecular dealcoholisation to produce high yields of γ-valerolactone.[222]

The confinement properties of MOFs stimulated by the existence of rigid coordination frameworks is a key driving force for their application as catalyst supports, but concurrently as protective agents for the development of highly stable heterogeneous catalysts. Metal NPs are likely to undergo sintering at elevated temperature conditions, leading to the formation of larger sized particles with lower specific surface areas, resulting in decreased catalytic activities. The versatile and tailorable porous channels of MOFs offer potential approaches for the encapsulation of active phase metal NPs in order to prevent their agglomeration, hence improving their catalytic performance.[223,224] Guo *et al.*[225] demonstrated a beneficial effect of MIL-101(Cr) MOF in stabilising highly dispersed Ru nanoclusters (2.4 nm) (Fig. 22). The resulting Ru/MIL-101(Cr) catalyst showed good activity in the conversion of levulinic acid to γ-valerolactone, hereby outperforming a zeolite supported Ru catalyst.

MOFs have also been employed as practicable catalyst precursors as well as the sacrificial templates for the preparation of carbon supported metal catalysts.[226–228] Pyrolysis of MOFs at suitable temperatures gives porous carbon materials derived from the organic ligands. The formed carbon matrix in turn serves as a high surface area support, which stabilises the *in situ* generated metal NPs, originating from the metal nodes. In this manner, highly stable catalyst systems, consisting of uniformly dispersed metallic NPs on a porous carbon matrix, with multifunctional properties can be obtained. Carbon-supported bimetallic catalysts can also be synthesised by tailoring the MOF-templated strategy as reported by Guomin Xiao and his co-workers (Fig. 23).[227] They developed an efficient

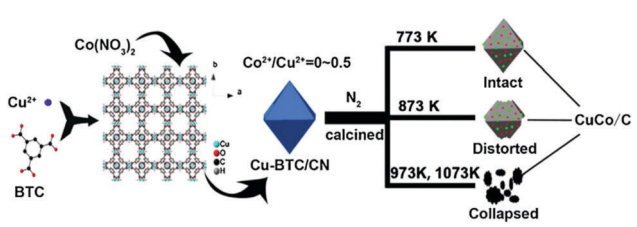

Fig. 23 Schematic illustration for the synthesis of CuCo/C catalyst. Reproduced with permission from ref. 227. Copyright (2017) Elsevier.

bimetallic CuCo catalyst supported on a porous carbon matrix *via* thermolysis of a Co-doped Cu–BTC MOF under N_2 atmosphere. The effect of pyrolysis temperature from 500 to 800 °C was studied on the size and shape properties of CuCo/C catalysts. The catalytic efficiency of various MOFs-based materials in biomass valorisation are discussed in the following paragraphs. In addition, an overview of the most vital catalytic results obtained in MOFs catalysed biomass upgrading is presented in Table 2.

3.2 Pristine MOFs and their composites

In the 1990s, the first catalytic application of MOFs was reported for the cyanosilylation of aldehydes.[229] With the development of more advanced MOFs, their catalytic applications in biomass valorisation have been dramatically increased in recent years.

3.2.1 Upgrading of carbohydrates-containing and -derived compounds. Čelič *et al.*[226] studied deoxygenation of liquefied biomass using a Ni-containing MOF, named MIL-77. Surprisingly, a ten-fold higher catalytic activity was found for MIL-77 compared to a commercial $Ni/SiO_2–Al_2O_3$ catalyst. The *in situ* generated Ni NPs are the key catalytic active sites for hydrotreatment of bio-oil. Hydrolysis of carboxymethyl cellulose was studied using an aluminium-based MIL-53 MOF.[230] About 40.3% and 54.2% molar yields of HMF and total reducing sugar were obtained at 200 °C for 4 h, respectively. This MOF catalyst can be reused for at least three times with a minor loss in HMF yield from 40.3% to 38.4%, which was attributed to catalyst mass loss during recovery/purification steps and/or blockage of active sites by humins products (entry 1, Table 2). Huang *et al.*[231] developed a novel MOF nanocomposite by *in situ* growth of zeolitic imidazolate framework NPs inside the pores of a 3-dimensional reduced graphene oxide hydrogel. The resulting MOF catalyst contains both micropores and mesopores with large specific surface area and abundant acidic sites. A maximum 94% yield of formic acid from cellulose was obtained at optimised reaction conditions.

Two types of zeolitic imidazolate frameworks (ZIFs), such as Zn-ZIF-8 and Co-ZIF-67 (Fig. 24) were tested for the catalytic conversion of sugars (sucrose, glucose and fructose) to methyl lactate.[232] ZIFs are a subclass of MOFs with zeolite-type topology, characterised by a 3D-porous isotropic framework. About 42% yield of methyl lactate was achieved over Zn-ZIF-8 due to its catalytically favourable properties, such as smaller crystal size and higher amounts of acid sites, especially Lewis acid sites. Reusability studies revealed a considerable decrease in product yields from 34.8% to 27.2% after four recycles of ZIF-8 (160 mg catalyst), due to blockage of active sites and structural changes in the catalyst (entry 2, Table 2). The synthesis of lactic acid from carbohydrates is an important step in biomass upgrading.[233] Lactic acid is a valuable chemical for the bioplastic industry and functions as a platform molecule towards production of various attractive chemicals, such as acetaldehyde, pyruvic acid, acrylic acid, propylene glycol, 2,3-pentanedione, 1,2-propanediol, and lactic acid esters. Huang *et al.*[233] developed an efficient one-pot transformation

Open Access Article. Published on 18 September 2018. Downloaded on 21/02/2026 10:11:12 PM.
This article is licensed under a Creative Commons Attribution-NonCommercial 3.0 Unported Licence.

Table 2 Catalytic applications of the most significant MOF-based materials in biomass valorisation

Entry	Catalyst	Reaction	Product	Reaction conditions	Catalytic efficiency		Recycling results	Ref.
					Conv. %	Yield %		
1	MIL-53(Al)	Hydrolysis of carboxymethyl cellulose	HMF[a] TRS[b]	100 mg substrate, 75 mg catalyst, 80 mL H_2O, 200 °C, 4 h	—	40.3 54.2	3 (small decrease in product yields, due to catalyst mass loss during recovery/purification and blockage of active sites by humins products)	230
2	Zn-ZIF-8	Sucrose upgrading	Methyl lactate	225 mg sucrose, 500 mg catalyst, 8 g methanol, 160 °C, 24 h	>99	42	4 (catalyst deactivation, due to blockage of active sites and structural changes in the catalyst)	232
3	MIL-100(Fe)	Fructose upgrading	Lactic acid	50 mg fructose, 50 mg catalyst, 10 mL water, 190 °C, 2 h	87	32	4 (catalyst deactivation, due to blockage of pores/active sites and leaching of active species. A simple method was used for the regeneration of the catalytic activity)	233
4	Composite of MIL-101(Cr) and activated fly ash	Dehydration of xylose	Furfural	300 mg xylose, mixture of water and toluene, 150 °C, 3 h	88.8	71	10 (stable catalytic activity)	235
5	1 wt% Pt@MOF-5	Oxidative condensation of furfural	Furan-2-acrolein	1 mmol furfural, 25 mg catalyst, 25 mg K_2CO_3, 15 mL EtOH, 150 °C, 4 h, 0.3 MPa O_2 at RT[c]	84	75.7	5 (stable catalytic activity)	224
6	Ru/UiO-66	Hydrogenation of furfural	Furfuryl alcohol	0.1 mL furfural in 9.9 mL H_2O, 100 mg catalyst, 20 °C, 5 bar H_2 at 20 °C, 4 h	—	94.9	5 (negligible decrease in catalytic activity)	243
7	5 wt% Ru/MIL-101(Cr)	Hydrogenation of levulinic acid	γ-Valerolactone	1 mmol substrate, 6 mg catalyst, 10 mL H_2O, 5 h 70 °C, 1 MPa H_2 at RT	100	99	4 (catalyst deactivation, due to leaching of active Ru species)	225
8	MIL-101(Cr)–SO_3H	Dehydration of glucose	HMF	1.24 mmol glucose, 5.22×10^{-5} mol catalyst, THF & H_2O, 130 °C, 24 h	—	29	4 (catalyst deactivation, due to fouling of the catalyst by humins)	37
9	MIL-101(Cr)–SO_3H	Dehydration of fructose	HMF	500 mg fructose, 300 mg catalyst, 5 mL DMSO, 120 °C, 1 h	>99	90	5 (small decrease in HMF yields from 90% to 85%, due to accumulation of oligomeric products on the catalyst surface)	220
10	MIL-101(Cr)–SO_3H	Ethanolysis of furfuryl alcohol	Ethyl levulinate	1.15 mmol substrate, 100 mg catalyst, 4 mL ethanol, 140 °C, 2 h	100	79.2	5 (small decrease in product yields, due to accumulation of oligomeric products on the catalyst surface)	249
11	2.4 wt% Ru/PTA-HKUST-1	Hydrogenolysis of cellulose[d]	Ethylene glycol	50 mg substrate, 50 mg catalyst, 8 mL H_2O, 245 °C, 4 MPa H_2 at RT, 4 h	96.2	50.2	Catalyst deactivation was found after a recycling test, due to partial decomposition of MOF composite	253
12	5 wt% Ru/SO_3H–UiO-66	Hydrogenation–cyclisation of methyl levulinate	γ-Valerolactone	500 mg substrate, 50 mg catalyst, 80 °C, 0.5 MPa H_2 at 80 °C, 15 mL H_2O, 4 h	100	81	5 (stable catalytic activity)	254
13	5 wt% Pd/MIL-101(Cr)–SO_3H	γ-Valerolactone hydrogenation	Ethyl valerate	10 mmol substrate, 100 mg catalyst, 5.8 mL ethanol, 250 °C, 3 MPa H_2 at RT, 10 h	98	83	3 (drastic catalyst deactivation, due to aggregation of Pd NPs at elevated reaction temperatures in acidic solution)	255
14	3 wt% Pd/MIL-101(Al)–NH_2	Hydrogenation of HMF	DHMTHF[e]	1 mmol HMF, 20 mg catalyst, 8 mL H_2O, 30 °C, 1 MPa H_2 at 30 °C	100	96	5 (stable catalytic activity was found for 1 h reactions, but product selectivity was significantly decreased from 96% to 80% for 12 h reactions, due to changes in structural and textural properties of the catalyst)	257
15	2 wt% Pd/MIL-101(Cr)–SO_3H	HDO of vanillin[f]	2-Methoxy-4-methylphenol	2 mmol vanillin, 50 mg catalyst, 1 h, 20 mL H_2O, 90 °C, 1 MPa H_2 at 90 °C	100	98.4	7 (stable catalytic activity)	258
16	Fe/C–S	Dehydration-oxidation of fructose	DFF[g]	1.2 mmol substrate, catalyst (20 mol% metal), 2 mL EtOH, 100 °C, N_2 (1 bar) for 2 h and then O_2 (1 bar) for 3 h at RT, 3 h	>99	>99	6 (stable catalytic activity)	263

This journal is © The Royal Society of Chemistry 2018

Open Access Article. Published on 18 September 2018. Downloaded on 21/02/2026 10:11:12 PM.
This article is licensed under a Creative Commons Attribution-NonCommercial 3.0 Unported Licence.

Table 2 (*continued*)

Entry	Catalyst	Reaction	Product	Reaction conditions	Catalytic efficiency		Recycling results	Ref.
					Conv. %	Yield %		
17	FeCo/C	Oxidation of HMF	DFF	1 mmol HMF, catalyst (20 mol% metal), 100 °C, 1 MPa O_2 at RT, 1 mmol Na_2CO_3, 2 mL toluene, 6 h	> 99	> 99	6 (stable catalytic activity)	264
18	Ni/C	Hydrogenation of furfural	THFOL[h]	30 mg furfural, 30 mg catalyst, 5 mL of 2-propanol, 120 °C, 1 MPa H_2 at RT, 2 h	100	100	5 (stable catalytic activity)	266
19	$CuNi_{0.5}$@C	Hydrogenation of furfural	Cyclopentanone	5 g furfural, 2 wt% of catalyst based on substrate, 95 mL H_2O, 130 °C, 5 MPa H_2 at RT, 5 h	99.3	97	4 (very small decrease in product yields, due to blockage of active sites by coke formed during reaction)	228

[a] HMF – 5-hydroxymethylfurfural. [b] TRS – total reducing sugar. [c] RT – room temperature. [d] Untreated cellulose with mean particle diameter of 25 μm. [e] DHMTHF – 2,5-dihydroxymethyltetrahydrofuran. [f] HDO – hydrodeoxygenation. [g] DFF – 2,5-diformylfuran. [h] THFOL – tetrahydrofurfuryl alcohol.

Fig. 24 (i) Structures of (a) ZIF-8 and (b) ZIF-67 frameworks and (ii) SEM images of (a) ZIF-8 and (b) ZIF-67. Reproduced with permission from ref. 232. Copyright (2016) Elsevier.

of hexose sugars to lactic acid over a Fe-based MIL-100 catalyst. About 32% yield of lactic acid was obtained from fructose, attributed to the unique morphology and textural properties of MIL-100(Fe) MOF. In contrast, only 18% and 20% yields of lactic acid were obtained over Cu–BTC and Cr-based MIL-100, respectively. The MIL-100(Fe) MOF was also found to be effective for the production of lactic acid from glucose, sucrose, inulin, and cellobiose. Owing to blockage of pores/active sites by the reaction substrates and leaching of active species, the catalytic activity of MIL-100(Fe) is significantly decreased after four recycles (entry 3, Table 2). A potential procedure for regeneration of the catalytic activity was used after four recycles, giving about 28% yield of lactic acid from fructose. This regeneration method involves the dissolution of recovered catalyst in HF/HNO_3 solution and the subsequent addition of H_3BTC ligand. The obtained mixture was oven dried at 150 °C for 12 h, followed by washing with water–ethanol and again dried overnight in air to obtain a regenerated MOF catalyst. In another work, the effect of the metal node on the performance of M-MOF-74 (M = Co, Ni, Mg, and Zn) catalysts was studied for the conversion of sugars to methyl lactate.[234] Among them, Mg-MOF-74 exhibited the best catalytic activity with 35% and 47% yields of methyl lactate from glucose and sucrose, respectively. A probable mechanism for the production of methyl lactate from glucose was reported. A composite of MIL-101(Cr) and activated fly ash was found to be effective for the dehydration of xylose to furfural.[235] About 71% yield of furfural is obtained at optimised reaction conditions, which is maintained even after ten recycles of the catalyst (entry 4, Table 2). These results were attributed to a remarkable hydrothermal stability and the synergistic effect between Cr species (Lewis acid sites) in MIL-101(Cr) and hydroxyl groups (Brønsted acid sites) on activated fly ash.

The oxidation of HMF gives a set of highly valuable building blocks for polymer and fine chemicals industries. These include

Open Access Article. Published on 18 September 2018. Downloaded on 21/02/2026 10:11:12 PM.
This article is licensed under a Creative Commons Attribution-NonCommercial 3.0 Unported Licence.

2,5-diformylfuran, 5-hydroxymethylfuran-2-carboxylic acid, 5-formyl-2-carboxylic acid, and 2,5-furandicarboxylic acid.[236] The selectivity of these chemicals can be tuned by varying catalyst compositions and reaction parameters. Lucarelli *et al.*[236] developed a feasible base-free oxidation of HMF to DFF using three types of square planar Ni-based MOFs, *i.e.* Ni(BDP), Ni(BPEB) and $Ni_3(BTP)_2$. Among them, $Ni_3(BTP)_2$ showed the best catalytic performance, giving a 27% yield of DFF under mild reaction conditions. The catalytic difference between these three Ni-based MOFs relates to a variable accessibility of the metal centres. An efficient MOF catalysed one-pot process was developed to produce furilydenepropanenitrile derivatives, which are key polymer building blocks.[237] The first step *i.e.* oxidation of HMF was studied using Fe-containing MOFs (MIL-100IJFe and Fe(BTC)) and a Cu containing MOF (Cu_3IJBTC)$_2$). MIL-100IJFe post-treated with NH_4F showed an exceptional catalytic performance, affording a 100% yield of 2,5-diformylfuran (DFF) from HMF, which was attributed to the presence of abundant MOF-stabilised Fe(III) active species. The second step *i.e.*, Knoevenagel condensation of DFF with malononitrile or ethyl cyanoacetate was performed by exploiting the basicity of the reaction medium. Kikhtyanin *et al.*[238] compared the catalytic efficiency of several MOFs for aldol condensation of furfural with acetone. Results indicated that aldol condensation occurs on the acidic sites of MOFs rather than on basic sites. Particularly, catalysts possessing ample amounts of Brønsted acid sites, which are generated by the interaction of metal cations with surrounding water molecules, showed the best performance. Aerobic oxidative condensation of furfural with alcohols was also studied over various Co-based MOF catalysts.[239] Two different strategies were applied for the generation of catalytic active species in these MOFs: (1) removal of coordinated water molecules at 300 °C, resulting in preferentially exposed metal active centres and (2) pyrolysis at 700 °C, generating multi-element carbon–matrix nanocomposites. Interestingly, both MOFs showed good catalytic performances (84.9% conversion and 99% selectivity) in the condensation of furfural with alcohols. Zr-Containing MOFs with terephthalate (UiO-66) or 2-aminoterephthalate ligands (UiO-66-NH_2), were studied for the esterification of levulinic acid with simple alcohols as well as biomass-derived complex alcohols.[240] The obtained catalytic activities are comparable (and in some cases higher) to those of previously reported solid acid catalysts. Results reveal that the active sites are located at the defect sites associated with ligand deficiencies in these MOFs.

3.2.2 Upgrading of non-carbohydrate compounds. Larasati *et al.*[241] studied the effect of the synthesis method (reflux and solvothermal) on the catalytic performance of MOFs, based on Zr^{4+} and a benzene 1,3,5-tricarboxylate linker, for the esterification of palmitic acid to produce biodiesel. The solvothermal synthesised MOF gave the best catalytic results with a 69% conversion of palmitic acid. Zr-MOFs, such as UiO-66 and UiO-66-NH_2 are also investigated as solid acid catalysts for the esterification of saturated and unsaturated fatty acids with methanol and ethanol.[242] Very good yields of fatty acid alkyl esters (94–99%) were obtained at mild reaction conditions, which was attributed to optimum amount of acidic sites.

3.3 MOF-supported metal NPs

Transition-metal NPs with small sized particles (usually below 5 nm) show distinctive physicochemical and redox properties as well as unusual catalytic activities that differ considerably from their bulk analogues.[216] Owing to strong, well-defined porous frameworks, MOFs can be used as efficient catalyst supports for the stabilisation of metal NPs with controlled size distributions. Compared to conventional porous inorganic materials, such as zeolites and mesoporous silica, MOFs can exhibit synergetic interactions, depending on their nature and composition, with the metal NPs *via* coordination and π–π forces.[243]

3.3.1 Upgrading of carbohydrates-containing and -derived compounds. Aerobic oxidative condensation of furfural with alcohols is one of the promising strategies for stabilising furanics as well as for obtaining desirable chemicals for gasoline applications. Various MOFs-supported Pt catalysts, such as Pt@MOF-5, Pt@UIO-66, and Pt@UIO-66-NH_2 were synthesised using an impregnation method followed by a gas-phase reduction step.[224] Their catalytic efficiency was tested for the oxidative condensation of furfural with ethanol to furan-2-acrolein using molecular oxygen. Among them, 1 wt% Pt@MOF-5 catalyst showed the best performance with 84% conversion of furfural and 75.7% yield to furan-2-acrolein. This catalyst showed a remarkable stable activity even after five recycles, without any considerable loss in product yields (entry 5, Table 2). The synergetic effect of well-dispersed Pt NPs with the MOF-5 channel is the key reason for superior performance of the Pt@MOF-5 catalyst. Selective hydrogenation of furfural to furfuryl alcohol was studied over Ru NPs supported on a series of Zr-based MOFs.[243] Among the catalysts tested, Ru/UiO-66 catalyst showed the highest performance with 94.9% yield of furfuryl alcohol, which slightly decreased after five recycles (entry 6, Table 2). Interestingly, the Ru NPs in Ru/UiO-66 catalyst were initially found to oxidise in contact with air, but the resulting RuO_x species were reduced again under reaction conditions, which are key active sites for hydrogenation of furfural. Hester *et al.*[229] developed a thermally stable catalyst composed of Pt NPs encapsulated in a Zr-based UiO-67 MOF using a linker design method. The H_2-chemisorption ability of UiO-67 was improved after the incorporation of Pt NPs, thus promoting Pt@UiO-67 MOF as a new appealing catalyst for hydrogenation reactions and hydrogen storage applications. The Pt@UiO-67 catalyst was found to be effective in the hydrogenation as well as in the oxidation of HMF. 5 wt% Ru/MIL-101(Cr) catalyst showed higher performance in the hydrogenation of levulinic acid to γ-valerolactone compared to a Ru/zeolite catalyst.[225] More than 99% levulinic acid conversion and γ-valerolactone selectivity were obtained at optimised reaction conditions. The synergistic effect between the strong acidity of the MIL-101(Cr) support and the fine dispersion of metallic Ru sites is a key reason for high performance of Ru/MIL-101(Cr) catalyst. However, about 40% decrease in product yields was observed after four recycles of the catalyst, due to leaching of active Ru species (entry 7, Table 2).

3.3.2 Upgrading of non-carbohydrate compounds. The oxidation of glycerol gives numerous value-added products, such as

Open Access Article. Published on 18 September 2018. Downloaded on 21/02/2026 10:11:12 PM.
This article is licensed under a Creative Commons Attribution-NonCommercial 3.0 Unported Licence.

dihydroxyacetone, glyoxalic acid, and glyceric acid.[244] Li *et al.*[216] found that by controlling the catalyst synthesis time, the structure–activity properties of bimetallic Pd–Ce catalysts supported on various Fe-MIL-101-NH_2 MOFs can be tuned for the oxidation of glycerol to dihydroxyacetone. Interestingly, although the morphology of Fe-MIL-101-NH_2 is highly dependent on catalyst synthesis time, its crystal structure is unaffected. The resulting MOF-supported bimetallic catalysts were found to attain higher yields of dihydroxyacetone in comparison with the corresponding monometallic Pd-based MOF and Pt-Bi/C catalyst. A hybrid catalyst support consisting of Ce-based MOF crystals and partially reduced graphene oxide nanosheets (PRGO) was developed for the dispersion of Pd NPs.[38] Results revealed that the MOF-based hybrid support assists in generating highly dispersed Pd NPs, while also creating abundant acid sites. Hence, the developed catalyst exhibited superior efficiency in the hydrogenolysis of a lignin model compound, vanillin towards 2-methoxy-4-methyl phenol.

3.4 Acid functionalised MOFs

The catalytic Lewis acidity strength of the MOFs (originating from isolated metal sites in their structure) was investigated, first time, for the cyanosilylation of aldehydes.[245] In contrast to the Lewis acidity, understanding the Brønsted acidity of MOFs is challenging and remains less explored. Many biomass conversion reactions, including dehydration, hydrolysis, depolymerisation, hydrodeoxygenation, and esterification/transesterification require abundant Brønsted acid sites. Several practicable strategies have therefore been developed to introduce Brønsted acid functionalities (sulphate, phosphate, nitric acid, *etc.*) into MOFs. These include encapsulation of Brønsted acid molecules into the framework cavities of MOFs (Fig. 25),[219] (post)synthetic functionalisation of organic linkers with acidic groups, or ligation of Brønsted acid moieties to isolated metal nodes.[37] Hence, a handful of studies dealing with the conversion of biomass using acid functionalised MOFs have been reported in recent years.

3.4.1 Upgrading of carbohydrates-containing and -derived compounds. The conversion of glucose to HMF proceeds through two steps *i.e.* Lewis acid catalysed isomerisation of glucose to fructose and the subsequent Brønsted acid catalysed dehydration to HMF (Fig. 26).[246] Considering catalyst reusability and process costs, the use of a single versatile catalyst having both Brønsted and Lewis acid properties would be preferable over the application of two separate catalysts. Since large quantities of water are generated during fructose dehydration, the developed catalysts must also exhibit a high tolerance to water. In view of these challenges, a remarkable hydrothermally stable and strong acidic MOF based catalyst was developed by partially replacing the organic linker of Zr-based MOF (UiO-66) with 2-monosulfo-benzene-1,4-dicarboxylate.[246] The resulting catalyst, consisting of both Lewis (Zr^{4+}) and Brønsted ($-SO_3H$) acid sites, exhibited a high catalytic performance for the one-pot conversion of glucose into HMF in aqueous solution (Fig. 26). The catalyst could also be reused for at least three times, with a minor loss in catalytic activity. Yabushita *et al.*[218]

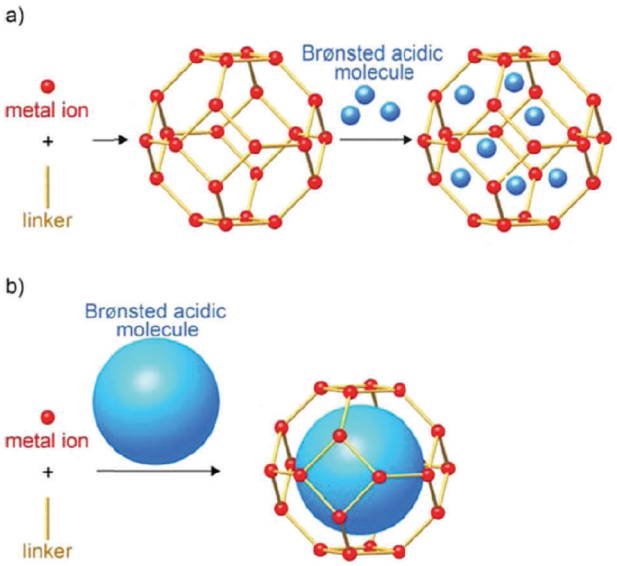

Fig. 25 Schematic representation of encapsulation of Brønsted acidic molecules within MOF: (a) two-step method and (b) one-step method. Reproduced with permission from ref. 219. Copyright (2015) American Chemical Society.

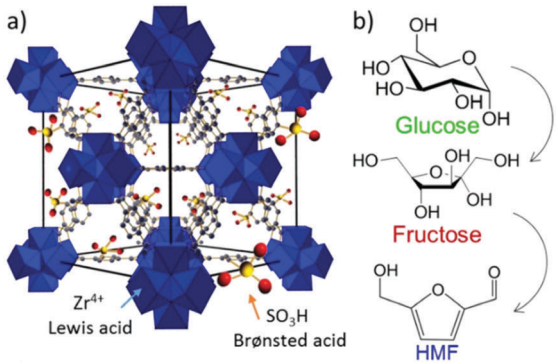

Fig. 26 (a) Schematic representation of an acidic UiO-66 framework. (b) Conversion of glucose to HMF *via* fructose isomerisation. Reproduced with permission from ref. 246. Copyright (2018) John Wiley and Sons.

performed a partial phosphate modification of Zr-cluster nodes in a NU-1000 MOF to generate selective acid sites for glucose-to-HMF transformation. The presence of reduced Lewis acidity as well as Brønsted acidity is beneficial for the isomerisation of glucose to fructose and the subsequent dehydration to HMF, respectively. Moreover, the partial phosphate modification strategy also inhibited side reactions in glucose isomerisation. Selective conversion of glucose to HMF was also studied using different nitro- and sulfo-modified MIL-101(Cr) catalysts.[37] Among them, the MIL-101(Cr)–SO_3H catalyst showed the highest yield (29%) of HMF after 24 h reaction. The porous structure and crystalline nature of MIL-101(Cr)–SO_3H catalyst are unaffected after four recycles, but the activity is decreased due to humins, adsorbed on the catalytic surface (entry 8, Table 4). Although the formation of insoluble humins could be prevented by performing the reaction in ethanol, yields of desired products,

Open Access Article. Published on 18 September 2018. Downloaded on 21/02/2026 10:11:12 PM.
This article is licensed under a Creative Commons Attribution-NonCommercial 3.0 Unported Licence.

such as HMF and 5-ethyl-HMF were decreased. A similar type of SO_3H-functionalised MIL-101(Cr) MOF, containing both Lewis and Brønsted acid sites, was examined for dehydration of glucose to HMF under both batch and flow reaction conditions.[247] A 44.9% yield of HMF at full conversion was obtained in batch scale. Interestingly, the catalyst is stable and provides a steady HMF yield (35–45%) under continuous-flow for 56 h time-on-stream.

Fructose, bearing a five-membered ring, is the preferred precursor for the production of HMF. Glucose, on the other hand, has a more stable six-membered ring. Hence, several studies have been undertaken for fructose-to-HMF transformation using MOFs based acid catalysts. For instance, a series of SO_3H-functionalised MOFs, synthesised by post-synthetic modification of organic linkers with chlorosulfonic acid, were studied for the dehydration of fructose to HMF.[220] The grafting rate of $-SO_3H$ determines the Brønsted acid concentration and its strength in the MOF. About 90% HMF yield was achieved at nearly complete conversion of fructose over an optimised MIL-101(Cr)–SO_3H catalyst. A minor loss in product yields (from 90% to 85%) was observed after five recycles of the catalyst, due to accumulation of oligomeric products on the catalyst surface (entry 9, Table 2). Hu *et al.*[245] developed two types of hydrothermally stable, sulfonated NUS-6 MOFs, composed of Zr and Hf with high BET surface areas of 550 and 530 $m^2\ g^{-1}$, respectively. Both MOFs possess a hierarchical porous structure of coexisting micropores ($\sim$0.5, $\sim$0.7, and $\sim$1.4 nm) and mesopores ($\sim$4.0 nm) with strongly connected $-SO_3H$ groups. The NUS-6(Hf) MOF showed a higher catalytic performance in the dehydration of fructose with a 98% yield of HMF, which was attributed to its strong Brønsted acidity as well as its more suitable pore size that inhibited side reactions. A multicomponent MOF-based solid acid catalyst, composed of polyvinylpyrrolidone modified halloysite nanotubes encapsulated in a SO_3H functionalised UiO-66 MOF, showed good performance for fructose dehydration with a 92.4% HMF yield.[248] The concentration of acid sites in the functionalised MOF can be adjusted by simply varying the ratio of support and SO_3H species. This MOF catalyst can be efficiently recycled for at least five times without much decrease in its activity and selectivity.

Kuwahara *et al.*[222] synthesised a SO_3H-functionalised Zr-MOF (UiO-66) for catalytic transfer hydrogenation of levulinic acid and its esters to γ-valerolactone. Results revealed the formation of strongly connected $-SO_3H$ groups in the UiO-66 framework, without affecting the structure of Zr lattice nodes. However, functionalisation resulted in a decreased crystallinity and BET surface area. The optimised MOF, containing a 60 mol% fraction of $-SO_3H$ while retaining a high BET surface area, exhibited the best catalytic performance, attributed to synergistic effect of Lewis basic $Zr_6O_4(OH)_4$ and Brønsted acidic ($-SO_3H$) centers. The transformation of furfuryl alcohol to ethyl levulinate in ethanol was examined using a SO_3H functionalised MIL-101(Cr) MOF.[249] The as-prepared catalyst showed higher BET surface area, excellent hydrothermal/chemical stability, and enhanced accessibility of Brønsted acid sites. Owing to these fascinating properties, the MIL-101(Cr)–SO_3H catalyst showed good activity with a 79.2% yield of ethyl levulinate at full conversion of furfuryl alcohol. Reusability test revealed a minor loss in product yields after five recycles of the catalyst, attributed to adsorption of oligomeric products on the catalyst surface (entry 10, Table 2).

3.4.2 Upgrading of non-carbohydrates. Thermal gradient effects and non-consistent reaction conditions are the major challenges in conventional thermal organic transformations.[250] Alternatively, microwave heating could benefit organic reactions by improving process efficiency and energy conservation. To compare both heating technologies, the esterification of oleic acid with methanol to produce bio-diesel esters was studied over a porous MIL-101(Cr)–SO_3H.[250] Noticeably, a maximum 93% yield of methyl oleate was obtained after just 20 min of microwave heating, while longer reaction times of up to 10 h were required to achieve similar product yields under conventional heating. A facile solvothermal method was used for the encapsulation of Keggin-type $Cs_{2.5}H_{0.5}PW_{12}O_{40}$ heteropolyacid into a UiO-66 MOF, leading to an improved Lewis acidity.[251] As a result, this functionalised MOF showed a good catalytic performance in the acidolysis of soybean oil, containing medium-chain fatty acids, towards low-calorie structured lipids.

3.5 Bifunctionalised MOFs

Bifunctionality is a synergistic concept stimulated for developing versatile materials that can facilitate catalytic cascade chemical reactions in biomass valorisation. The properties and activities of bifunctional catalysts could be significantly different from the corresponding mono-functional catalysts. Especially, acid and redox properties are vital for efficient biomass valorisation. On the one hand, acid sites (*e.g.*, $-SO_3H$) can fractionate/depolymerise the complex biomass molecules into the model compounds. On the other hand, redox active sites (*e.g.*, metal NPs) can catalyse the subsequent upgrading of model compounds to value-added chemicals. MOFs have the ability to accommodate both acid–base and metal active sites. Tailoring these bifunctional properties is essential for achieving improved catalytic results in biomass upgrading.

3.5.1 Upgrading of carbohydrates-containing and -derived compounds. Chen *et al.*[252] investigated the effect of the acid/metal balance in water-tolerant bifunctional Ru–PTA/MIL-100(Cr) (PTA – phosphotungstic acid) catalysts for the transformation of cellulose and cellobiose into sugar alcohols. By controlling the loading of encapsulated PTA in MIL-100(Cr), the amount and strength of acid sites are optimised (Fig. 27). The Ru–PTA/MIL-100(Cr) catalyst with loadings of 3.2 wt% Ru and 16.7 wt% PTA showed a 63.2% yield of hexitols with a 57.9% selectivity to sorbitol at complete conversion of cellulose as well as 97.1% yield of hexitols with a 95.1% selectivity to sorbitol at complete conversion of cellobiose. Highly dispersed metallic Ru NPs (1.4 nm) played a favorable role in the hydrogenation activity, while acid sites of PTA/MIL-100(Cr) are responsible for hydrolysis reaction. In another work, metallic Ru NPs deposited on a PTA functionalised HKUST-1 MOF was tested for cellulose conversion to ethylene glycol.[253] A maximum 50.2% yield of ethylene glycol was obtained over the developed catalyst, consisting of 2.4 wt% Ru and 34.8 wt% PTA. The acid sites

Open Access Article. Published on 18 September 2018. Downloaded on 21/02/2026 10:11:12 PM.
This article is licensed under a Creative Commons Attribution-NonCommercial 3.0 Unported Licence.

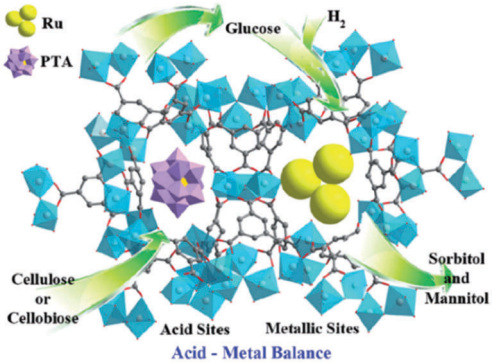

Fig. 27 Metal–acid bi-functional Ru–PTA/MIL-100(Cr) catalyst for transformation of cellulose or cellobiose into sugar alcohols. Reproduced with permission from ref. 252. Copyright (2013) John Wiley and Sons.

of PTA promote both hydrolysis of cellulose and subsequent C–C bond cleavage of cellulose-derived sugars, while the smaller sized metallic Ru particles (average particle size of 2 nm) catalyse glycolaldehyde hydrogenation to form ethylene glycol. Catalyst recycling led to leaching of active species, due to partial decomposition of MOF composite (PTA functionalised HKUST-1), and hence, a considerable decrease in product yields (entry 11, Table 2). A one-pot catalytic hydrogenation strategy for converting methyl levulinate into γ-valerolactone was developed using a bifunctional catalyst composed of metallic Ru NPs deposited on a SO_3H-functionalised UiO-66.[254] The resulting catalyst showed a 81% yield of γ-valerolactone under mild reaction conditions, which was maintained even after five recycles of the catalyst (entry 12, Table 2). The catalytic performance of Ru/SO_3H–UiO-66 was attributed to synergistic effect of imbedded tiny metallic Ru NPs (2–4 nm diameter) and abundant Brønsted acidic sites of SO_3H–UiO-66 support, hereby outperforming a Ru/C catalyst. The activity and selectivity of Ru/SO_3H–UiO-66 were significantly decreased upon neutralisation of its acid sites, confirming the indispensable role of sulfonic acid groups. The above studies[252–254] demonstrate that metallic Ru NPs with an average size of below 4 nm could exhibit good catalytic performance in the hydrogenation of biomass model compounds. A ligand-based solid solution method was used for the incorporation of $–SO_3H$ functional groups into the framework of a Cr-MIL-101 MOF, followed by loading of Pd NPs.[255] The $–SO_3H$ density played a critical role in the ring opening of γ-valerolactone. Subsequent HDO afforded ethyl pentenoate, which was then hydrogenated to ethyl valerate (83% yield) over the Pd NPs. Reusability studies revealed a drastic decrease in product yields from 83% to below 10% after three recycles of the catalyst, which was attributed to aggregation of Pd NPs at elevated reaction temperatures in acidic solution (entry 13, Table 2). A multicomponent Pd/UiO-66@SGO (SGO – sulfonated graphene oxide) catalyst was investigated for one-pot conversions of glucose and fructose into 2,5-dimethylfuran.[256] Brønsted acid sites present in UiO-66@SGO promote the dehydration of carbohydrates to HMF, whereas the subsequent hydrogenolysis and hydrogenation to form 2,5-dimethylfuran were catalysed by Pd NPs. The 4.8 wt% Pd/UiO-66@SGO catalyst can be reused up to five times without significant loss in catalytic activity. A direct anionic exchange method followed by a reduction step was employed for the synthesis of Pd NPs supported on a NH_2 functionalised MOF (Pd/MIL-101(Al)–NH_2).[257] Isolated amine moieties present in the framework of the MOF assist the formation of uniform dispersed Pd NPs. Its catalytic efficiency in HMF upgrading was then demonstrated, reaching a 96% yield of 2,5-dihydroxymethyl-tetrahydrofuran with a full conversion of HMF. In the case of the reusability tests (five cycles) carried out at 1 h reaction time, a stable catalytic activity was found (entry 14, Table 2). In contrast, product selectivity was significantly decreased from 96% to 80% (after five recycles) for 12 h reaction time. This was attributed to changes in the structural and textural properties of the catalyst.

3.5.2 Upgrading of non-carbohydrates. A bifunctional catalyst consisting of Pd NPs immobilised on a mesoporous sulfonic acid-functionalised MOF, MIL-101(Cr)–SO_3H was studied for the hydrodeoxygenation (HDO) of vanillin.[258] Brønsted acid coordination sites of sulfonic acid groups attached to the MOF induce the activation of reactants. Hence, the 2 wt% Pd/MIL-101(Cr)–SO_3H catalyst exhibited high performance in the HDO of vanillin towards 2-methoxy-4-methylphenol product. This catalyst can be reused for at least seven times with no loss of catalytic activity and selectivity (entry 15, Table 2). Pd NPs immobilised on a SO_3H-functionalised MIL-101(Cr) was also found to be an effective catalyst in the hydrodeoxygenation of vanillin under mild reaction conditions.[259] In another work, hydrodeoxygenation of vanillin was studied using ultra-small Pd NPs (1.5–2.5 nm) encapsulated in an amine-functionalised MOF (NH_2-UiO-66).[260] Almost 100% conversion of vanillin with a high selectivity to 2-methoxy-4-methylphenol was achieved over 2 wt% Pd@NH_2-UiO-66. The synergy between well-dispersed metallic Pd sites and the amine-functionalised MOF support is the key reason for high hydrogenation activity of Pd@NH_2-UiO-66 catalyst. Hence, both acid- and base-functional sites are necessary for the efficient hydrodeoxygenation of vanillin. Phenol hydrogenation was studied using Pd/UiO-66 and NH_2-functionalised Pd/UiO-66 catalysts.[261] Interestingly, the incorporation of NH_2 groups induced a decreased crystallinity in UiO-66, resulting in weak interaction between Zr and Pd in Pd-UiO-66-NH_2. Hence, the NH_2-free Pd-UiO-66 catalyst showed better catalytic activities in phenol hydrogenation.

Although algae-derived bio-oil is regarded as an efficient renewable source of transportation fuel, the existence of large concentrations of oxygen-containing C16–C18 fatty acids leads to several problems, such as polymerisation, strong corrosion, poor stability, and low calorific value. Hence, algae bio-oil cannot be used as transportation fuel without removing these fatty acids. For this, Fang *et al.*[262] developed a facile one-pot strategy to convert palmitic acid into hexadecane over a bifunctional MOF catalyst, consisting of encapsulated phosphotungstic acid inside the MOF structure of PdCu@Fe^{III}-MOF-5. The developed catalyst shows an improved acidity and completely converts palmitic acid with a high selectivity to hexadecane. This superior catalytic performance was attributed to its unique yolk–shell

Open Access Article. Published on 18 September 2018. Downloaded on 21/02/2026 10:11:12 PM.
This article is licensed under a Creative Commons Attribution-NonCommercial 3.0 Unported Licence.

MOF nanostructure, enhanced acidity, and the supercritical fluid medium.

3.6 MOFs-derived catalysts

Highly stable carbon-based metal or metal oxide catalysts can be developed using MOFs as sacrificial templates. A typical concern of MOFs, regarding their relatively low hydrothermal/chemical stability, can thus be turned into an advantage, by employing thermolysis under inert conditions for *in situ* generation of homogenously dispersed metal NPs on the carbon support.[226] The resulting composite catalysts can contain ample amounts of functional sites, hence achieving notable catalytic activities in biomass conversion reactions.[227,228]

3.6.1 Upgrading of carbohydrates-containing and -derived compounds. A sulfur doped Fe/C catalyst was synthesised using a MOF-templated strategy and tested its catalytic efficiency for one-pot conversion of fructose into 2,5-diformylfuran (DFF).[263] Pyrolytic disintegration of the MOF template led to the formation of octahedral Fe_3O_4 NPs with preferentially exposed (111) crystal facets on sulfur doped carbon (Fig. 28). About 99% yield of DFF was obtained at optimised reaction conditions, which can be maintained even after six recycles of the catalyst (entry 16, Table 2). The formation of higher product yields was ascribed to low adsorption energy of DFF on the support as well as the existence of non-oxidised sulfur that makes the catalyst system less oxidised. In another work, DFF is produced from HMF using a carbon supported Fe–Co catalyst obtained after thermolysis of MIL-45b MOF.[264] The unique hollow structure of the Fe–Co/C catalyst promotes the adsorption of HMF as well as the rapid desorption of formed DFF, leading to a higher product yield, comparable to that obtained with noble metal catalysts. The Fe–Co/C catalyst was also efficiently reused for six times without any significant loss in its activity and selectivity (entry 17, Table 2). MOF-5 derived carbonaceous solid acids bearing $-SO_3H$ functional species were studied for the dehydration of fructose into HMF.[265] Better catalytic results were obtained when the reaction was performed in a dimethyl sulfoxide–isopropanol solvent mixture, with a high concentration of isopropanol. Selective hydrogenation of furfural to tetrahydrofurfuryl alcohol was studied over carbon-embedded Ni (Ni/C) catalysts synthesised by the direct thermal decomposition of Ni-based MOFs.[266] The performance of Ni/C greatly depends on the applied MOF precursors, calcination conditions (temperature and time), and reaction parameters. Complete conversion of furfural towards tetrahydrofurfuryl alcohol (100% yield) was obtained over Ni/C-500 catalyst synthesised by the pyrolysis of Ni-MOF at 500 °C for 120 min. This catalyst showed a remarkable stable activity even after five recycles (entry 18, Table 2). The high performance of Ni/C catalyst is attributed to the uniform dispersion of Ni NPs (an average particle size of ~14 nm) and relatively high BET surface area (~92 $m^2\ g^{-1}$). Selective hydrogenation of furfural was also studied using a CuCo bimetallic catalyst dispersed on a porous carbon matrix, synthesised by the pyrolysis of a Co-doped Cu–BTC MOF at different temperatures ranging from 500 to 800 °C.[227] Best catalytic results (98.7% furfural conversion and 97.7% furfuryl alcohol selectivity) were achieved with a Co : Cu molar ratio of 0.4 and a precursor calcination at 600 °C. Results revealed that doping with Co improved the metal dispersion, while the pyrolysis temperature significantly influences the particle size and chemical state. A one-pot cascade conversion of furfural to cyclopentanone was successfully carried out using bimetallic CuNi NPs embedded in a carbon matrix (CuNi@C).[228] Compared with conventional precipitation methods, the MOF-templated procedure gave a higher specific surface area (91.6 $m^2\ g^{-1}$) and well-dispersed CuNi NPs (about 15 nm) with a Ni : Cu molar ratio of 0.5. As a result, the $CuNi_{0.5}$@C catalyst showed the best performance with a 97% yield of cyclopentanone at optimised reaction conditions. Reusability studies revealed a minor loss in product yields after four recycles of the catalyst, due to blockage of active sites by coke formed during reaction (entry 19, Table 2).

3.6.2 Upgrading of non-carbohydrates. Hydrogenolysis of glycerol is an important reaction for the production of 1,2-propanediol, which has significant industrial applications (*e.g.*, cosmetics, polymers, pharmaceuticals, and antifreeze additives).[267] For this reaction, a novel Cu/ZnO catalyst with nanoscale ZnO particles scattered on metallic Cu was tested. The catalyst was prepared *via* facile pyrolysis of the Cu(Zn)-based HKUST-1 MOF followed by a reduction step (Fig. 29).[268]

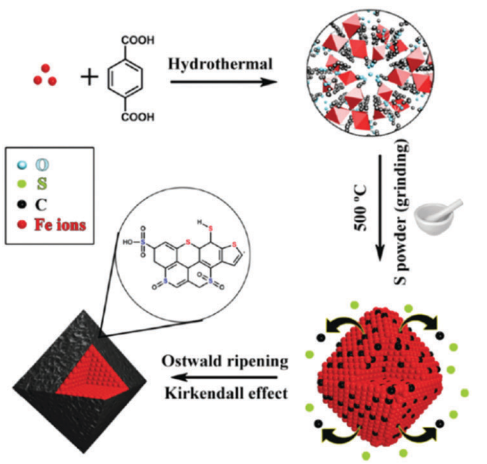

Fig. 28 MOF-templated strategy for the design of Fe/C–S catalysts. Reproduced with permission from ref. 263. Copyright (2017) Royal Society of Chemistry.

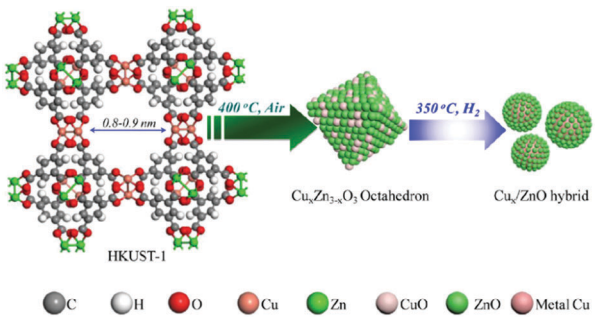

Fig. 29 Preparation of a Cu/ZnO catalyst from Cu(Zn)-HKUST-1. Reproduced with permission from ref. 268. Copyright (2017) Elsevier.

This journal is © The Royal Society of Chemistry 2018

Open Access Article. Published on 18 September 2018. Downloaded on 21/02/2026 10:11:12 PM.
This article is licensed under a Creative Commons Attribution-NonCommercial 3.0 Unported Licence.

The MOF-templated $Cu_{1.1}$/ZnO catalyst showed higher activity and superior stability for the hydrogenolysis of glycerol in a fixed-bed reactor compared with conventional Cu/ZnO catalysts prepared by co-precipitation and solvent-free grinding methods. The synergistic interface of Cu–ZnO played a beneficial role on the performance of $Cu_{1.1}$/ZnO catalyst for 1,2-propanediol synthesis. A bimetallic Ni–Co nanoalloy catalyst encapsulated in an N-doped carbon matrix (NC), synthesised using a MOF-templated strategy, was tested for the selective hydrogenation of phenol, a lignin model compound.[269] Both the pyrolysis temperature and the composition of nanoalloy played a crucial role on the performance of CoNi@NC catalyst. The 1Co–1Ni@NC catalyst showed a 2.8- and 4.3-fold higher activity than Co@NC and Ni@NC, respectively, which was attributed to synergistic Ni–Co interaction in the bimetallic catalyst. Mechanistic studies revealed a one-step hydrogenation of phenol to cyclohexanol.

3.7 Conclusions of MOFs-based catalysts

In conclusion, a large number of research articles have reported on the topic of MOFs-catalysed biomass valorisation. This interest has been mainly stimulated by the unique porosity properties of MOFs compared to various other catalytic materials, such as microporous zeolites, mesoporous silica, and microporous carbon materials. Overall, the tunable porous channels of MOFs seem to play three important roles: (i) minimising mass diffusion limitation, (ii) improving surface area, and (iii) allowing a more efficient immobilisation of functional species. In addition, the building blocks of MOFs, namely metal ions or metal-oxo clusters and organic ligands, exhibit adequate amounts of acid–base and redox properties, which can be tailored in function of specific biomass upgrading reactions. However, several challenges still exist towards fertile catalytic applications of MOF-based materials in biomass valorisation. (1) Developing viable routes for the synthesis of cost-effective MOF-based materials. For this, more efforts should be directed towards one-pot synthesis of functionalised MOFs using relatively cheap precursors. (2) Improving the hydrothermal stability of MOFs and minimizing the leaching of active species,[270] for which both strong coordination between ligands and metal centers[233] as well as MOFs composites (*e.g.*, with activated fly ash)[235] could play a crucial role. (3) In-depth analysis of structure–activity relationships of MOFs during biomass conversions, thus providing useful implications to tune their catalytic activity and selectivity.

4. Solid phase ionic liquids based catalysts

Ionic liquids (ILs) have recently emerged as novel clean solvents as well as promising functional catalysts for the development of new frontier catalytic technologies. ILs, popularly known as low temperature or room temperature molten salts, are composed of organic cations and (in)organic anions.[271] ILs typically contain bulky and asymmetric ions that will limit their crystallisation, resulting in melting points below 100 °C and occasionally even below room temperature.[40] Ethylammonium nitrate with a melting point of 12 °C was the first representative low temperature molten salt, and was synthesised in 1914.[272] The development of moisture-stable ILs in 1992 has boosted the applicability of ILs in many fields, including catalysis. The extraordinary properties of ILs mark them as highly appealing ''green'' alternative to traditional organic solvents for various catalytic processes. Interesting properties include low vapor pressure, non-flammability, wide range of working temperatures, and high ionic conductivity.[271,273] Theory estimates a total of 10^{18} types of ILs can be developed by tailoring the nature and the composition of cation/anion components. However, only about 1000 types of ILs have been synthesised up to date.[40,274]

4.1 Factors affecting the catalytic activity of solid phase ILs in biomass upgrading

ILs have found versatile applications in catalytic biomass processing due to the presence of abundant amounts of both Lewis and Brønsted acid sites.[275,276] Important examples are depolymerisation of lignocellulose biomass and its components (cellulose, hemicellulose, and lignin), dehydration of biomass-derived carbohydrates and biodiesel synthesis. As both the anionic and the cationic parts of ILs are easily varied, the properties of ILs can be tuned to fulfil a specific catalytic purpose. This extreme flexibility provides fertile opportunities to design or optimise the most suitable IL systems for achieving enhanced reaction rates in biomass conversions. Owing to the combination of polar and non-polar properties, ILs may also induce a nano-segregation of solvents and substrates, which could potentially improve the chemical reactivity.[277] However, several challenges need yet to be solved in order to improve the catalytic applicability of ILs at the industrial scale. For instance, many catalytic processes require significant amounts of ILs, which is economically undesirable because of the high cost of ILs.[39–41] The handling of ILs can also be difficult because of their high viscosity, in turn imposing mass transport limitations in catalytic reactions. Moreover, severe leaching of ILs into the reaction mixture, associated with the concerns of their separation and recycling, strongly limits their practical applications in biomass refinery processes.[41,278] To overcome these issues, an appealing strategy *i.e.* combining the advantages of both ILs and solid materials has received great attention that has led to development of a new class of functionalised heterogeneous catalysts, namely 'solid state ILs'.[39–42] Immobilisation of ILs on solid materials by either covalent or non-covalent bonds can be achieved using various feasible synthesis methods, including physisorption, self-assembly, grafting, sol–gel, ionic exchange, or polymerisation. As an example, Fig. 30 illustrates of supported-mono-ILs.[39]

Supported ionic liquids (SILs) offer several advantages for catalytic biomass conversions over the corresponding pristine ILs.[40,41,279,280] SILs not only combine the original properties of ILs and supports, but also endows new functional sites and robust stabilisation, due to synergistic IL-support interactions. It is also possible that deposition of ILs on a high specific surface area material can provide increased number of accessible active

Open Access Article. Published on 18 September 2018. Downloaded on 21/02/2026 10:11:12 PM.
This article is licensed under a Creative Commons Attribution-NonCommercial 3.0 Unported Licence.

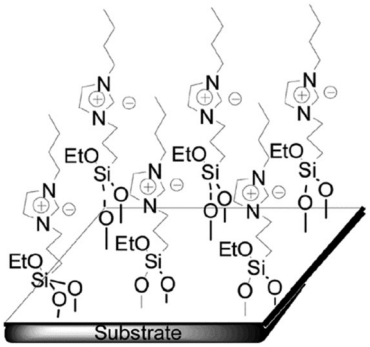

Fig. 30 Representation of supported-mono-ILs. Reproduced with permission from ref. 39. Copyright (2014) Royal Society of Chemistry.

sites at the catalyst surface, while consuming small amounts of ILs. More importantly, the IL film formed on the support surface provides a homogeneous environment for catalytic reactions, while appearing as a dry solid, allowing facile separation of SILs from the reaction mixture. Overall, these advantageous features of SILs can assist the development of practicable, sustainable catalytic routes for large-scale bio-refinery processes.

The catalytic properties of SILs depend on many factors. Surely, the choice of the anionic and cationic parts will be a dominant factor that governs the catalytic strength of SILs.[40] Each IL has a unique set of anionic and cationic parts, resulting in a very specific interaction. As an example, the different types of interactions in a typical imidazolium-based IL are illustrated in Fig. 31.[280] Tailorable SILs with desired functional sites can be developed by simply varying the nature and the composition of anionic and cationic parts. The nature of the support is another key factor influencing the catalytic efficiency of SILs. For example, compared with traditional porous silica and polymer supports, the use of oxidised multi-walled carbon nanotubes as a supporting material was found to significantly improve the catalytic performance of SILs.[281] Moreover, the particle size of the support as well as the synthesis routes of the SILs can also affect the catalytic activity.[279] Particularly, grafting of ILs, a widely used method, can considerably alter the activity of SILs in various ways.[282] The advantages of grafting compared to impregnation are confirmed by CO_2 diffusivity measurements. Grafted silica exhibits faster CO_2 diffusion than impregnated silica, indicating that ILs incorporated into the inner pores of solid materials during impregnation hamper the diffusion of reactive species. In addition, grafting of ILs shows a negligible effect on the blockage of porous structure of solid materials, hence grafted solid surface allows for strong immobilisation of functional groups compared to impregnated surface. Finally, the IL loading can also exert a significant role in tuning the surface properties of SILs to achieve better catalytic activity.[279] The loading of ILs can be adjusted by controlling the particle size of the support and the preparation method.

Both acid and base functionalised SILs can be developed by simply immobilising acid or base functionalised ILs on the surface of solid supports, respectively.[40,41,280,283] ILs with protic ammonium, pyrrolidinium, or imidazolium ions exhibit adequate amounts of acid sites. Strong Brønsted acidic ILs can also be prepared by anchoring $-SO_3H$, carboxylic acids or alkane sulfonic acids as side chains on the cations (Fig. 32).[284] On the other hand, a number of ILs with considerable amounts of basic sites exist, including ILs with lactate, formate, acetate, dicyanamide, *etc.* Interestingly, strong interactions between functionalised ILs and a solid support can prevent leaching of functional sites during biomass transformation reactions. Furthermore, incorporation of metal NPs into functionalised SILs can provide novel, bifunctionalised heterogeneous catalysts (Fig. 32).[284] These bifunctionalised SILs possess abundant acid or base and redox properties, which could enable efficient catalysis of cascade biomass conversions in a one-pot way. The existence of various kinds of interactions may play an essential role in stabilising these functional sites and active metal centers (Fig. 31).

Solid polymeric ILs (PILs), a new class of recyclable IL based catalysts, are also perceived as fascinating catalytic alternatives for efficient biomass upgrading.[285,286] The incorporation of IL moieties into a polymer chain can combine some of the unique properties of ILs with the common features of polymers. High thermal stability, tunable shaping, and corrosion resistance are some of the added benefits of PILs. PILs can be used as catalyst support or as catalytic active phase, depending on their nature and composition. However, conventional PILs typically exhibit low specific surface areas, resulting in negligible amounts of

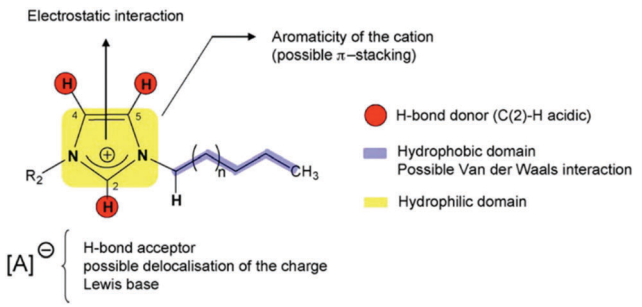

Fig. 31 Schematic representation of different types of interactions present in a typical imidazolium-based ionic liquid. Reproduced with permission from ref. 280. Copyright (2010) Elsevier.

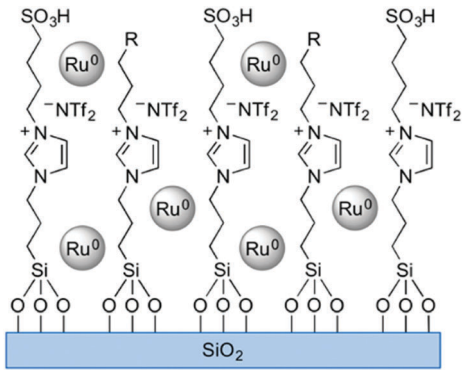

Fig. 32 Schematic representation of a bifunctional catalyst composed of an acid-functionalised SIL and Ru NPs. Reproduced with permission from ref. 284. Copyright (2016) American Chemical Society.

This journal is © The Royal Society of Chemistry 2018

Open Access Article. Published on 18 September 2018. Downloaded on 21/02/2026 10:11:12 PM.
This article is licensed under a Creative Commons Attribution-NonCommercial 3.0 Unported Licence.

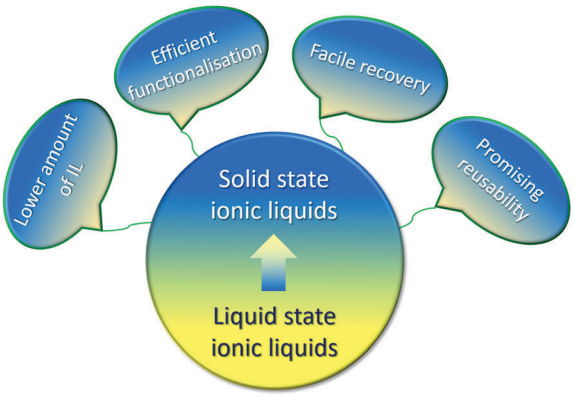

Fig. 33 Key advantages of solid phase ionic liquids.

surface active sites available for catalytic reactions. To overcome this problem, novel porous PILs with well-defined structures and controlled geometries have been developed using appropriate synthesis methods.[42,286] In addition to an increased active surface area, porous PILs may also improve mass transport due to tunable porous dimensions. Hence, higher reaction rates in biomass upgrading could be expected. Furthermore, the surface wettability of porous PILs can be efficiently tuned at a molecular level by carefully selecting the synthesis precursors.[42] This is vital because surface wettability plays an essential role in tuning the interaction of solid catalysts with reaction substrates. For instance, hydrophobic solid surface favour the adsorption of hydrophobic reactant species. Therefore, an improved hydrophobicity of the catalyst surface can lead to higher activities and excellent selectivities in related reactions. In conclusion, Fig. 33 summarises the key advantages of solid phase ionic liquids. In the following sections, various catalytic biomass conversions were reviewed, partitioned in two categories: (1) supported ILs based catalysts and (2) polymerised ILs based catalysts. In addition, a summary of the most important catalytic results obtained in solid-state ILs catalysed biomass upgrading is presented in Table 3.

4.2 Supported ILs based catalysts

Supported IL catalysts as a concept was initially introduced in the 1990s.[287] Depending on the composition and configuration of ILs immobilised on solid supports, SILs can be classified as supported IL phase, supported IL catalyst, and solid catalyst with an IL layer.[288–290] Many solid supports, such as mixed oxides (Mg–Al–O), bio-char, mesoporous silica (SBA-15 and MCM-41), carbon nanotubes, MOFs, and polystyrene have been used for the immobilisation of ILs.

4.2.1 Upgrading of carbohydrates-containing and -derived compounds. The efficient hydrolysis of lignocellulose biomass and its model compounds is a foremost challenge in bio-refining and for instance a major hurdle for large-scale cellulosic ethanol production. For this, SILs can offer a homogeneous environment to dissolve cellulose as well as abundant acid properties for the cleavage of cellulose to reducing sugar molecules (*e.g.*, glucose). A silica-immobilised imidazolium-type acidic SIL was found to be highly effective in the hydrolysis of untreated cellulose in water, hereby outperforming *n*-propylsulfonic acid on silica ($PrSO_3H$–SiO_2) and sulfonic acid on silica (SO_3H–SiO_2) catalysts.[291] About 48% yield of total reducing sugars (TRS) was obtained over the SIL acid catalyst, with a small decrease in TRS yields after four recycles (entry 1, Table 3). In contrast, only 19.9% and 13.2% TRS yields were obtained with $PrSO_3H$–SiO_2 and SO_3H–SiO_2 catalysts, respectively. A chlorozincate IL immobilised on a sulfonic acid functionalised bio-char was also tested for the hydrolysis of cellulose in aqueous solution, obtaining a reasonably good yield of TRS (58.7%).[292] Compared to the OH groups of IL-SO_3H, the IL-Zn groups act as more efficient cellulose-binding sites, resulting in a stable catalytic activity even after three recycles of the catalyst (entry 2, Table 3). A series of acid functionalised ILs covalently grafted on SiO_2 (IL-SO_3H/SiO_2, IL-HSO_4/SiO_2, and IL-SO_3H-HSO_4/SiO_2), as well as a IL/SiO_2 were tested for the dehydration of various carbohydrates (cellulose, cellobiose, sucrose, glucose, xylose, and fructose) towards furan derivatives.[293] The dual acidic functionalised SIL (IL-SO_3H–HSO_4/SiO_2) was found to be highly active with 99, 96, 94, 76, and 99% conversions of fructose, glucose, xylose, sucrose, and cellobiose, respectively. Reusability studies revealed a small decrease in HMF yields from 97.5% to 92.7% after five recycles of the catalyst in fructose dehydration (entry 3, Table 3). Sphere-shaped SILs with particle sizes ranging from 293 to 610 nm have been prepared by the immobilisation of an acidic functionalised IL on the surface of SiO_2 particles.[294] The developed SIL catalyst showed excellent performance in the dehydration of fructose with full conversion and 63% yield of HMF, outperforming zeolites and strong acid ion exchange resin catalysts. In addition, the SIL catalyst can be efficiently recycled for at least seven times without any significant loss in catalytic activity (entry 4, Table 3). Dehydration of fructose into HMF was also tested using a novel polypropylene fiber supported IL catalyst, reporting good HMF yields (86.2%) at optimised reaction conditions.[295] Reusability studies showed a stable catalytic activity even after ten recycles of the catalyst, without any considerable loss in HMF yields (entry 5, Table 3). In addition, the fiber supported IL showed higher catalytic performance compared to acid resins and silica supported ILs, which was ascribed to the better accessibility of the substrates in case of the fiber supported IL. A Brønsted acidic IL immobilised on a silica gel was found to be effective for a series of esterification reactions, including esterification of acetic acid with various alcohols.[296] In addition, IL/silica gel exhibited excellent reusability for seven times without considerable loss in catalytic performance.

Eucalyptol, a major component of eucalyptus oil ($\sim$90%), is as an attractive platform molecule for the production of valuable C10-chemicals, such as menthanes, menthenes, menthadienes, and cymene.[284] Several bifunctionalised catalysts consisting of metallic Ru NPs immobilised on acid-functionalised SILs (RuNPs@SILs) were applied in the hydrodeoxygenation of eucalyptol under both batch and continuous-flow conditions.[284] The RuNPs@SILs showed excellent catalytic activity and selectivity towards a deoxygenation product, *p*-menthane, which was attributed to well-balanced acid and metal functionalities.

Open Access Article. Published on 18 September 2018. Downloaded on 21/02/2026 10:11:12 PM.
This article is licensed under a Creative Commons Attribution-NonCommercial 3.0 Unported Licence.

Table 3 Catalytic applications of the most significant solid state ILs in biomass valorisation

Entry	Catalyst	IL	Reaction	Product	Reaction conditions	Conv. % (yield %)	Recycling results	Ref.
1	Acidic IL–SiO_2	1-(1-Butylsulfonic)-3-methylimidazolium chloride	Cellulose hydrolysis	Reducing sugar	30 mg cellulose, 2 mL water, 190 °C, 3 h	— (48)	4 (small decrease in product yields)	291
2	SO_3H-IL–Zn/biochar	1-Trimethoxy-silylpropyl-3-methylimidazolium chloride	Microwave-assisted cellulose hydrolysis	Reducing sugar	200 mg cellulose, 100 mg catalyst, 1.5 mL H_2O, 90 °C, 2 h	— (58.7)	3 (stable catalytic activity)	292
3	SiO_2 supported IL–SO_3H–HSO_4	3-Sulfobutyl-1-(3-propyltriethoxysilane) imidazolium hydrogen sulfate	Fructose dehydration	HMF[a]	4 : 1 mass ratio of fructose to catalyst, 1.8 g DMSO[b], 110 °C, 2 h	>99 (97.5)	5 (small decrease in HMF yield from 97.5% to 92.7%)	293
4	SiO_2 supported IL–HSO_4	1-(Triethoxy-silyl-propyl)-3-methylimidazolium hydrogen sulfate	Fructose dehydration	HMF	50 mg fructose, 40 mg catalyst, 0.5 mL DMSO, 130 °C, 30 min	99.9 (63)	7 (stable catalytic activity)	294
5	Polypropylene fiber–IL	3-Sulfopropylpyridinium hydrogen sulfate	Fructose dehydration	HMF	0.5 g fructose, 7.5 mol% catalyst based on fructose, 10 mL DMSO, 100 °C, 30 min	— (86.2)	10 (stable catalytic activity)	295
6	$Fe_{25}Ru_{75}$@SILP	[1-Butyl-3-(3-triethoxy silyl propyl)-imidazolium]NTf_2	Hydrogenation of furfural-acetone	Aromatic alcohol	0.4 mmol substrate, 40 mg catalyst, 0.5 mL mesitylene, 100 °C, 20 bar H_2 at 100 °C, 18 h	>99 (94)	2 (considerable decrease in product yields from 94% to 83%)	297
7	$CrCl_2$-Im-SBA-15	1-(Tri-ethoxy-silyl)-propyl-3-methylimidazolium chloride	Glucose dehydration	HMF	10 wt% glucose in the aqueous phase, 10 mg catalyst, 150 °C, 3 h	50 (35)	2 (catalyst deactivation, due to leaching of active species)	299
8	Cr(salen)-IM-HSO_4-MCM-41	[CPTES-IM-SO_3H][HSO_4]/[Cl]	Glucose dehydration	HMF	100 mg substrate, 50 mg catalyst, 2 mL DMSO, 140 °C, 4 h	99 (43.5)	5 (minor loss in catalytic activity, due to leaching of active species and adsorption of reaction substrates on the catalyst surface)	278
9	IL/Mg–Al–La	1-Butyl-3-methylimidazolium hydroxide	Transesterification of fatty oil	Biodiesel	12 : 1 molar ratio of methanol to oil, 3 wt% catalyst amount based on oil, 65 °C, 6 h	— (98.7)	6 (considerable decrease in biodiesel yield from 98.7% to 85.4%, due to leaching of active basic species)	304
10	Acidic IL/silica	—	Transesterification of oil	Biodiesel	25 : 1 molar ratio of methanol to oil, 5 wt% catalyst amount based on oil, 60 °C, 20 h	87.6 (87.6)	5 (considerable decrease in biodiesel yield from 87.6% to 70.2%, due to leaching of IL)	305
11	IL-Fe_3O_4@NH_2-MIL-88B(Fe)	1,4-Butanediyl-3,3′-bis(3-sulfopropyl) imidazolium dihydrogensulfate	Esterification of oleic acid	Biodiesel	10.5 : 1 molar ratio of alcohol to acid, 8.5 wt% catalyst based on oleic acid, 90 °C, 4.5 h	93.2 (93.2)	6 (noticeable decrease in biodiesel yields, due to catalyst mass loss during recovery/purification)	306
12	$CrCl_3 \cdot 6H_2O$-FPIL[c]	1-Vinyl-3-propane sulfonate imidazolium	Fructose dehydration	HMF	100 mg substrate, 30 mg catalyst, 1 mL DMSO, 120 °C, 1 h	98.7 (90.6)	5 (stable catalytic activity)	285
13	Poly(IL)–$CrCl_2$	[BVIM]Cl[d]	Glucose dehydration	HMF	40 mg substrate, 10 mol% catalyst based on glucose, 1 mL DMF, 120 °C, 3 h	— (65.8)	Significant loss in HMF yields after six recycles	316
	Poly(IL)–Et_2AlCl	[BVIM]Cl				— (49)	Minor loss in HMF yields after six recycles	
14	Poly(IL)-$H_3PW_{12}O_{40}$	1-Vinyl-3-propane sulfonate imidazolium	Fructose dehydration	HMF	50 mg fructose, 30 mg catalyst, 0.5 mL DMSO, 130 °C, 1 h	97.9 (83)	5 (considerable loss in HMF yields, due to leaching of active species)	317
15	Au_1–Pd_1@MPIL[e]	3-Cyanopropyl-1-vinyl imidazolium chloride	HMF oxidation	FDCA[f]	0.1 mmol HMF, HMF/metal molar ratio (100), 2 mL water, 90 °C, O_2 (10 mL min^{-1}), 12 h	99.7 (99)	5 (stable catalytic activity)	42
16	Acidic poly(IL)	—	Esterification of methacrylic acid	MMA[g]	1 : 1.2 molar ratio of substrate/methanol, 5 wt% catalyst based on substrate, 95 °C, 3 h	100 (100)	5 (stable catalytic activity)	319
17	Macroporous poly(IL)	1-Vinyl-3-(3-sulfopropyl) imidazolium hydrogen sulfate	Esterification of oleic acid	Biodiesel	12 : 1 molar ratio of alcohol/acid, 8.5 wt% catalyst based on oleic acid, 80 °C, 4.5 h	92.6 (92.6)	6 (small decrease in acid conversion from 92.6% to 89.3%, due to catalyst mass loss during recovery/washing steps)	286

This journal is © The Royal Society of Chemistry 2018

Open Access Article. Published on 18 September 2018. Downloaded on 21/02/2026 10:11:12 PM.
This article is licensed under a Creative Commons Attribution-NonCommercial 3.0 Unported Licence.

Table 3 (*continued*)

Entry	Catalyst	IL	Reaction	Product	Reaction conditions	Conv. % (yield %)	Recycling results	Ref.
18	PAL-poly(IL)[h]	1-Butysulfonate-3-vinylimidazole hydrogen sulfate	Esterification of oleic acid	Biodiesel	12 : 1 molar ratio of alcohol/acid, 7 wt% catalyst based on oleic acid, 75 °C, 5 h,	69 (69)	6 (significant decrease in biodiesel yield from 69% to 22%, due to leaching of IL, decreased surface area, and mass loss of the catalyst)	320
19	PW/poly(IL)[i]	1-Butyl-3-vinylimizolium bromide	Isomerisation of α-terpineol	1,8-Cineole	1.16 g of α-terpineol, 1.12 wt% catalyst based on substrate, 50 mL cyclohexane, 50 °C, 8 h	100 (51.7)	7 (stable catalytic activity)	321

[a] HMF – 5-hydroxymethylfurfural. [b] DMSO – dimethyl sulfoxide. [c] FPIL – functional polymeric IL. [d] [BVIM]Cl – 3-butyl-1-vinylimidazolium chloride. [e] MPIL – mesoporous poly(IL). [f] FDCA – 2,5-furandicarboxylic acid. [g] MMA – methyl methacrylate. [h] PAL – nanofiber-like palygorskite. [i] PW – phosphotungstic acid.

Kinetic experiments under continuous-flow conditions identified the acid catalysed deoxygenation of eucalyptol as the rate-limiting step. The partial substitution of Ru by a non-noble metal (Fe) in RuNPs@SIL led to tailored catalytic activities and selectivities in the hydrogenation of various aromatic substrates including furfural and furfuralacetone.[297] A facile organometallic synthesis method was used for the synthesis of FeRuNPs@SIL catalysts. This preparation method allowed a controlled formation of finely dispersed bimetallic FeRu NPs. Among several tested catalysts, bimetallic $Fe_{20}Ru_{80}$NP@SIL and $Fe_{25}Ru_{75}$NP@SIL showed the best performance with more than 94% yield to the aromatic alcohol at nearly complete conversion of furfuralacetone. Reusability studies, carried out under shaken conditions rather than magnetically stirred conditions in order to prevent mechanical degradation of the catalyst, revealed a decrease in product yield (83%) after two recycles of $Fe_{25}Ru_{75}$NP@SIL catalyst (entry 6, Table 3). The effect of the catalyst support, *i.e.* conventional silica, mesoporous SBA-15, and polystyrene on the catalytic performance of acid functionalised SILs was studied.[298] The obtained catalysts were tested for the production of ethylene glycol diacetate *via* esterification of ethylene glycol with acetic acid. Ethylene glycol diacetate is a useful solvent for paints, coatings, plastics, and wood stains. Interestingly, the conventional silica supported IL showed the best catalytic performance for the synthesis of ethylene glycol diacetate and a pseudo-homogeneous second order kinetic model was proposed, based on thorough kinetic experiments.

Compared to conventional solid supports, the confinement of ILs into the porous materials (mesoporous silica, MOFs, porous bio-char, *etc.*) can reduce the extent of IL leaching during catalytic reactions.[40] Interestingly, confinement effects and interactions of ILs with the pore walls may result in physicochemical properties that significantly differ from conventional SILs. Moreover, these properties may be strongly dependent on the configuration of ILs inside the pores, *e.g.*, as grafted monolayers or physically confined multilayers (Fig. 34).[40] A metal chloride ($CrCl_2$) immobilised on a thin layer of IL (1-(triethoxysilyl-propyl)-3-methylimidazolium chloride, $(EtO)_3$–Si–PMImCl) grafted on mesoporous silica (SBA-15) was studied for glucose dehydration in an aqueous medium.[299] The coordination of $CrCl_2$ to $PMIm^+Cl^-$ creates loosely bound, catalytically active Cr^{2+} species. The high mobility of these

Fig. 34 Incorporation of ILs into porous materials by two different strategies: (A) covalent grafting of monolayer IL on the pore wall and (B) physical confinement of multilayers of ILs into the nanopores. Reproduced with permission from ref. 40. Copyright (2017) American Chemical Society.

Open Access Article. Published on 18 September 2018. Downloaded on 21/02/2026 10:11:12 PM.
This article is licensed under a Creative Commons Attribution-NonCommercial 3.0 Unported Licence.

complexes was shown to be beneficial for the selective synthesis of HMF from glucose. However, severe catalyst deactivation was noticed after two recycles of the catalyst, due to leaching of large amounts of active species (entry 7, Table 3). The effect of metal chlorides (*e.g.*, $CrCl_2$, $AlCl_3$, $CuCl_2$, and $FeCl_3$) on the structure–activity properties of an immobilised IL/SBA-15 catalyst was also studied for the dehydration of glucose to HMF.[300] Results revealed that the ordered mesoporous structure is retained after grafting of the IL, though the specific surface area of SBA-15 was slightly decreased. Higher HMF yields were obtained over the developed SILs compared to various homogeneous metal chloride catalysts. Multifunctional catalysts composed of chromium(III) Schiff base complexes and acidic ILs, both immobilised onto the surface of MCM-41 were investigated for the dehydration of various carbohydrates, such as glucose, fructose, and inulin.[278] The reaction temperature, reaction time, and the solvent were optimised for HMF production. About 43.5%, 83.5% and 80.2% yields of HMF were obtained from glucose, fructose, and inulin, respectively. A minor loss in catalytic activity for glucose dehydration was noticed after five recycles of the catalyst, due to leaching of active species and adsorption of reaction substrates on the silica surface (entry 8, Table 3). A series of SBA-15 supported acidic IL catalysts were tested for biphasic alkylation of 2-methylfuran with formalin.[301] The developed SIL catalysts showed higher activities and a superior selectivity (90%) towards bis(5-methylfuran-2-yl)methane, compared to commercial sulfonic acid resin catalysts. In addition, the SBA-15 supported acidic IL catalysts were also found to be active for the alkylation of 2-methylfuran with various biomass-derived substrates, such as furfural, glycolaldehyde, glyceraldehyde, and 3,4-dimethoxybenzaldehyde.

Multifunctional ILs supported on a porous bio-char were prepared by pyrolysis of cellulose and IL and subsequently tested for the production of levoglucosenone (LGO) and dihydrolevoglucosenone (DLGO) *via* catalytic reforming of cellulose pyrolysis volatiles (Fig. 35).[302] DLGO is an attractive bio-based solvent alternative to dipolar aprotic solvents and can be further transformed to 1,6-hexanediol, a commodity chemical with widespread industrial applications. A 31.6% yield of LGO was obtained on a cellulose carbon basis (24.6 wt%). Moreover, the addition of hydrogen gas and a hydrogenation catalyst in the catalytic bed enabled the production of DLGO. Hollow nanosphere structured N-doped carbon supported sulfonic acid-functionalised ILs were developed for the selective conversion of fructose to promising fuel blends, such as 5-ethoxymethylfurfural and ethyl levulinate.[303] Results revealed that strong interactions between functionalised IL groups and the N-doped carbon framework play a favourable role in limiting acid site leaching. Hence, the developed SIL catalyst exhibited large amounts of strong Brønsted acid sites, which efficiently catalyse the ethanolysis of fructose, thus avoiding self-polymerisation of intermediates, leading to higher total yields of 5-ethoxymethylfurfural and ethyl levulinate.

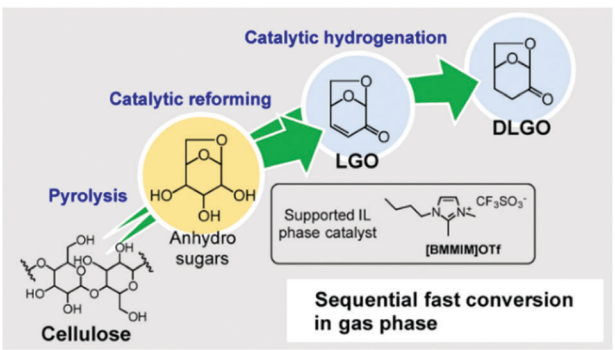

Fig. 35 Production of levoglucosenone (LGO) and dihydrolevoglucosenone (DLGO) by catalytic reforming of volatiles obtained from cellulose pyrolysis using supported IL catalysts. Reproduced with permission from ref. 302. Copyright (2017) American Chemical Society.

4.2.2 Upgrading of non-carbohydrate compounds. The high cost of raw materials (*e.g.*, virgin oil) used for transesterification reactions is a major hurdle for the commercialisation of biodiesel production.[121] Hence, the use of waste cooking oils or non-edible oils has been investigated as a more economical route towards large-scale biodiesel production. IL immobilised on mixed oxides of Mg–Al and Mg–Al–La were tested for the transesterification of waste cooking oil.[304] The Mg–Al–La based SIL showed the best catalytic performance with a 98.7% yield of biodiesel. A noticeable decrease in biodiesel yield from 98.7% to 85.4% was noticed after six recycles of the catalyst, due to leaching of basic sites (entry 9, Table 3). In another work, an acid functionalised IL immobilised on silica gel was also tested for the transesterification of waste cooking oil with methanol.[305] Various reaction parameters, including the ratio of methanol to oil, catalyst loading, reaction temperature, and reaction time were optimised to obtain a maximum yield (87.6%) of biodiesel. Reusability studies revealed a noticeable decrease in the biodiesel yield from 87.6% to 70.2% after five recycles of the catalyst, due to leaching of IL (entry 10, Table 3). A Brønsted acid IL confined within the framework of an amino-functionalised magnetic MOF (Fe_3O_4@NH_2-MIL-88B(Fe)) was prepared.[306] The resulting SIL catalyst showed a good performance in the esterification of oleic acid (93.2% biodiesel yield), which was attributed to abundant acid properties. A considerable decrease in biodiesel yields was found after six recycles of the catalyst, due to mass loss of the catalyst during recovery/purification steps (entry 11, Table 3). As an alternative to waste cooking oils, a non-edible untreated feedstock, *i.e. Koelreuteria integrifoliola* was used as a substrate for the production of biodiesel using an acidic IL immobilised on a magnetic support Fe_3O_4@SiO_2.[307] The SIL catalyst has a well-controlled core–shell structure and showed tremendous performance in catalysing both transesterification and esterification reactions of crude *Koelreuteria integrifoliola* seed oil. Gas-phase dehydration of glycerol to produce acrolein was studied using a series of silica supported Brønsted acidic IL catalysts.[308] Acrolein is a key intermediate for the synthesis of acrylic esters, super absorbers, polymers, and detergents. All catalysts in this study were found to be active in the dehydration of glycerol. Glycerol conversions in the range of 35–90% were obtained with selectivities to acrolein in the range of 29–58%.

Open Access Article. Published on 18 September 2018. Downloaded on 21/02/2026 10:11:12 PM.
This article is licensed under a Creative Commons Attribution-NonCommercial 3.0 Unported Licence.

Various metals incorporated SILs were investigated in the alkylation and acylation of lignin model compounds.[309] Results revealed that the nature of the cation controls both catalytic behaviour and active phase leaching. More specifically, silica-supported Fe- and Sn-ILs showed a drastic leaching compared to the Al-ILs. However, the Fe-based IL was found to be more active, which might be due to the homogeneous catalytic reaction because of the Fe leaching into the reaction medium. Leaching issues were also observed when using other supports, such as metal oxides (Nb_2O_5, TiO_2, Na-Y, and Al_2O_3) or activated charcoal. The formation of highly stable complexes between metal halide anions and aromatic lignin model compounds is the key reason for leaching of active phases. Compared to alkylation, the SILs showed better catalytic results for acylation of lignin model compounds. The effect of metal chlorides (*e.g.*, $SnCl_2$, $FeCl_3$ or $CrCl_3$) immobilised on activated carbon supported IL catalysts was studied for the isomerisation of α-pinene oxide to campholenic aldehyde.[310] α-Pinene oxide can be produced from renewable terpenes. Among them, the $SnCl_2$ immobilised SIL showed the best catalytic performance with a 65% yield of campholenic aldehyde and reasonable good reusability. These results were confirmed by mechanistic kinetic models.[311] In another work, the isomerisation of β-pinene oxide to myrtanal was investigated over similar types of metal chloride immobilised activated carbon supported IL catalysts.[312] Myrtanal is a vital intermediate for fragrance and pharmaceutical industries. The catalytic activity and product distribution were highly dependent on the nature of the ionic liquid. Short reaction times and high reaction temperatures favoured the formation of myrtanal. About 68% yield of myrtanal was obtained over a $ZnCl_2$ immobilised SIL catalyst.

4.3 Polymeric ILs based catalysts

Polymeric ILs (PILs) are solid materials that can be prepared using a variety of strategies, such as incorporation of ILs into the polymeric substrates,[313] homo-polymerisation of ILs, copolymerization of ILs with other monomers, or hard templating methods.[42,286] Acid or base functionalisation and incorporation of metal NPs have also been carried out to obtain multifunctional PILs.[314] In this case, polymerised ILs could fulfil several important roles, like facilitating the stabilisation of metal NPs, controlling the accessibility of reagents/substrates to the active sites, and providing specific environments for an efficient and selective adsorption of the reagents.[315]

4.3.1 Upgrading of carbohydrates-containing and -derived compounds. A series of functionalised PILs, prepared *via* coupling of a SO_3H-functionalised PIL with different counterpart anions containing $CrCl_3{\cdot}6H_2O$, were investigated for the conversion of various carbohydrates into HMF.[285] The resulting PILs showed better catalytic performances for fructose-to-HMF conversion compared with other solid catalysts, such as silica supported ILs, metal oxides, and ion exchange resins. Remarkably, no considerable decrease in HMF yields (90.6%) was observed after five recycles of the catalyst (entry 12, Table 3). In addition, reasonable good yields of HMF were obtained from cellulose and glucose over the developed PIL catalysts. The dehydration of cellulose and glucose into HMF was also studied using PIL-supported metal chloride catalysts.[316] Among several tested PILs, the combination of a poly(3-butyl-1-vinylimidazolium chloride) IL with $CrCl_2$ showed the best catalytic performance with a 65.8% yield of HMF from glucose, which is much higher than that obtained over the respective IL monomer. The PIL–$CrCl_2$ catalyst also showed a considerable activity for cellulose-to-HMF conversion. Although, the analogous PIL–Et_2AlCl catalyst is less effective than the PIL-$CrCl_2$, recyclability tests indicated a higher stability with almost constant HMF yields (49%) even after six recycles of the PIL–Et_2AlCl catalyst in glucose dehydration (entry 13, Table 3). An efficient Brønsted-acidic PIL was obtained after immobilisation with $H_3PW_{12}O_{40}$ and subsequently tested for the dehydration of glucose and fructose to HMF.[317] About 83% and 26% yields of HMF were obtained from fructose and glucose, respectively. However, a considerable loss in HMF yields was noticed after five recycles of the catalyst in fructose dehydration, due to leaching of active species (entry 14, Table 3). Direct synthesis of γ-valerolactone from biomass involves an acid-catalysed transformation of carbohydrates into levulinate or its corresponding esters, followed by a metal catalysed hydrogenation step and thus, requires a bifunctional catalyst. To achieve this, an efficient catalytic system consisting of an acid PIL and a redox Co/TiO_2 phase was developed, showing excellent performance for one-pot conversions of furfuryl alcohol, 5-hydroxymethylfurfural, or fructose into γ-valerolactone *via* ethyl levulinate formation.[318] An aerobic oxidation of HMF to FDCA was investigated using mesoporous PIL-supported Au–Pd nanoalloys.[42] Interestingly, the surface wettability of PIL, which was tuned by varying the cross-linkers with different hydrophilic and hydrophobic properties, plays a central role in the selective transformation of HMF to FDCA (Fig. 36). Results also revealed that PIL-supported Au–Pd nanoalloys exhibit higher activity and stable catalytic performance, even after five recycles, compared to the corresponding monometallic NPs, due to the existence of synergistic Au–Pd nanoalloy effects (entry 15, Table 3).

4.3.2 Upgrading of non-carbohydrate compounds. An acid functionalised PIL catalyst with larger sized particles (0.5–3 mm) was synthesised by a copolymerisation method using an acid IL,

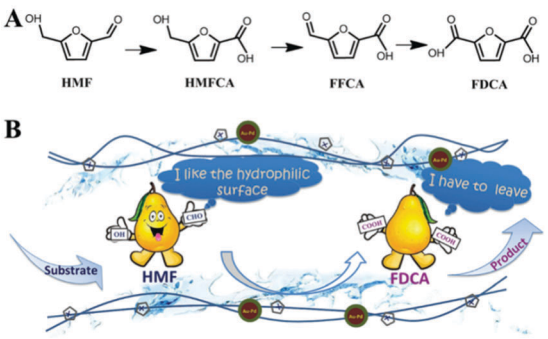

Fig. 36 Proposed reaction pathway for the oxidation of 5-hydroxymethylfurfural (HMF) to 2,5-furandicarboxylic acid (FDCA) catalysed by Au_1–Pd_1@PIL. Reproduced with permission from ref. 42. Copyright (2017) Royal Society of Chemistry.

Open Access Article. Published on 18 September 2018. Downloaded on 21/02/2026 10:11:12 PM.
This article is licensed under a Creative Commons Attribution-NonCommercial 3.0 Unported Licence.

styrene, and ethylene glycol dimethacrylate.[319] The developed PIL catalyst displayed higher thermal stability, excellent mechanical strength as well as better catalytic activity compared to a commercial resin catalyst in the esterification of methacrylic acid with methanol. A remarkable stable catalytic activity was found during five consecutive reactions (entry 16, Table 3). A macroporous PIL, containing a multi-layered structure and repeated units of $-SO_3H$ and $-HSO_4$ with fine separation efficiency, was synthesised using a hard template method.[286] The optimum macroporous structure of PIL played a key role towards improving the mass transport properties during biodiesel production compared with several conventional porous solid acid catalysts, reaching a 92.6% yield of biodiesel over the PIL catalyst. Reusability studies revealed a minor decrease in oleic acid conversion from 92.6% to 89.3%, due to mass loss of the catalyst during recovery/purification steps (entry 17, Table 3). A PIL catalyst supported on nanofiber-like palygorskite was found to be effective for the esterification of oleic acid with methanol, reaching about 69% yield of biodiesel at optimised reaction conditions.[320] However, a significant decrease in biodiesel yield from 69% to 22% was found after six recycles of the catalyst, due to leaching of IL, decreased surface area, and mass loss of the catalyst (entry 18, Table 3). Phosphotungstic acid (PW) was successfully immobilised on an imidazole PIL *via* an ion-exchange method.[321] The obtained catalyst was tested for the isomerisation of α-terpineol to 1,8-cineole. Results revealed a strong correlation between the molar ratio of PW to IL monomer and the acidic strength. A 51.7% selectivity to 1,8-cineole at full conversion of α-terpineol was obtained at optimised reaction conditions and this catalytic performance was maintained for seven consecutive runs (entry 19, Table 3).

4.4 Conclusions of solid-state ILs-based catalysts

As discussed in this section, both supported ILs and polymeric ILs possess numerous advantages over the corresponding pristine ILs in terms of hydrothermal stability, recyclability, and the amount of IL needed for a catalytic reaction (Fig. 33 and Table 3). In addition, SILs exhibit new active sites, generated by synergistic effects between the IL and the supporting material, which are vital for achieving improved reaction rates in biomass valorisation. In order to enhance the applicability of SILs based catalysts in biomass upgrading, particularly at the industrial scale, several problems have yet to be solved.[40,322] (1) Understanding the role of impurities (*e.g.*, water, halides, unreacted organic or inorganic salts), originating during SILs synthesis, in biomass conversions. This is vital because even trace amounts of impurities could dramatically affect the rate and mechanism of a reaction. (2) Developing eco-friendly procedures for the synthesis of ILs because most of the existed methods use large amounts of hazardous precursors and organic solvents. (3) In-depth structural exploration of ILs in SILs, including intrinsic nature (electrostatic field, ionic strength, *etc.*), acid–base strength, and ILs/support interaction, which is key to tailor the catalytic activity/selectivity of SILs for specific biomass conversions.

5. Magnetic iron oxide based catalysts

Nanoscale metals, metal oxides, or combinations of both display excellent catalytic activities for a broad spectrum of chemical reactions.[53,323–325] Tailoring the particle size, morphology, and composition of metallic materials generates changes in their electronic and geometric arrangements, which could result in an improved catalytic activity. Hence, the properties of nanoscale catalysts can be dramatically different from the corresponding macroscopic bulk materials, potentially leading to unusual catalytic results.[326–329] However, the separation and recovery of nanoscale catalysts from liquid-phase reaction mixtures for subsequent recycling remains a great challenge. Although filtration or centrifugation are typically used for the recovery of solid catalysts, these post-reaction steps add cost to the entire production, especially in the case of nano-sized catalysts. A promising solution to tackle this issue is the application of magnetic catalytic nanomaterials.[330,331] Owing to outstanding paramagnetic properties and inherent insolubility, magnetic catalysts can be efficiently separated from complex reaction mixtures using external magnets without affecting their activity and selectivity (Fig. 37).[332] Iron oxide based nanomaterials (mainly Fe_3O_4) are widely used magnetic catalysts in biomass conversions due to their low cost, facile preparation, and strong magnetic properties.[30,50,333] Related magnetic materials, such as γ-Fe_2O_3, spinel ferrites with a general formula $M^{2+}Fe^{3+}{}_2O_4$ (M = Co, Ni or Mn), Fe-based alloys (FeB, FeNiB, *etc.*), and iron oxide supported materials also show potential for catalytic biomass conversions.[309–311] Overall, magnetically recoverable catalysts have demonstrated high efficiency in a wide range of ''one-pot, multi-step'' catalytic reactions, including oxidation, epoxidation, hydrogenation, hydroformylation, olefin metathesis, polymerisation, photocatalysis, and C–C bond formation reactions.[331,334–338] Moreover, novel applications in asymmetric synthesis, organocatalysis, Knoevenagel condensation, or CO_2 cycloaddition reaction have been developed. In this section, the focus lies on the applicability of iron oxide based magnetic catalysts for biomass conversions.

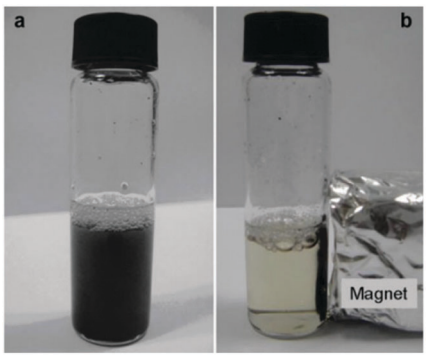

Fig. 37 Magnetic separation of a finely dispersed Fe_3O_4 based catalyst used for cellulose hydrolysis. Reproduced with permission from ref. 332. Copyright (2012) Springer Nature.

 This journal is © The Royal Society of Chemistry 2018

Open Access Article. Published on 18 September 2018. Downloaded on 21/02/2026 10:11:12 PM.
This article is licensed under a Creative Commons Attribution-NonCommercial 3.0 Unported Licence.

5.1 Factors affecting the catalytic activity of iron oxides in biomass valorisation

In some applications, the use of magnetic catalysts is particularly interesting because of the difficulties involved with the use of conventional catalyst separation steps, such as filtration or centrifugation. For example, a solid mixture containing hemi(cellulose) pulp and solid catalyst (*e.g.*, Ru/C) is obtained after reductive catalytic fractionation of lignocellulose (Fig. 38).[91] Another example is related to the formation of humins (carbonaceous, polymeric by-products), obtained as supplementary solid residues during carbohydrate dehydration towards HMF production.[331] These insoluble humins can subsequently hamper the recovery and reusability of the catalyst. Since the separation of a solid catalyst from solid reaction products is highly challenging, the application of catalytic materials having strong magnetic properties could be a valid solution.

Pure iron oxide magnetic NPs suffer from several drawbacks, such as self-interactions which induces particle aggregation, rapid exothermic reactions in the presence of oxygen, and a high sensitivity to air, all resulting in a reduced applicability for magnetic catalytic purposes.[47,339,340] In order to preserve the magnetic properties of iron oxide NPs, while improving their catalytic activity, several encapsulating strategies have been developed. Fig. 39 shows some key benefits of encapsulated iron oxide magnetic catalysts. For instance, protection of the Fe_3O_4 surface with a coating layer has been frequently studied. In this way, highly stable core–shell Fe_3O_4@M catalysts can be obtained, wherein Fe_3O_4 constitutes the core and M (coating layer) is the shell. SiO_2 is commonly used coating material for Fe_3O_4 because it is cheap, inert, non-toxic, and besides, it has a high specific surface area.[46,47,341] An additional benefit of SiO_2 is the promising surface functionality of core–shell Fe_3O_4@SiO_2 magnetic catalysts due to the presence of abundant surface silanol groups (–SiOH). These silanol species offer facile approaches for selective anchoring of acid (–SO_3H) or base (–NH_2) functional species upon Fe_3O_4@SiO_2 materials.

The stabilisation of magnetic iron oxide NPs can also be achieved using various polymers (*e.g.*, polyphenylquinoxaline, polypyridylphenylene, and hyperbranched polyethylenimine)

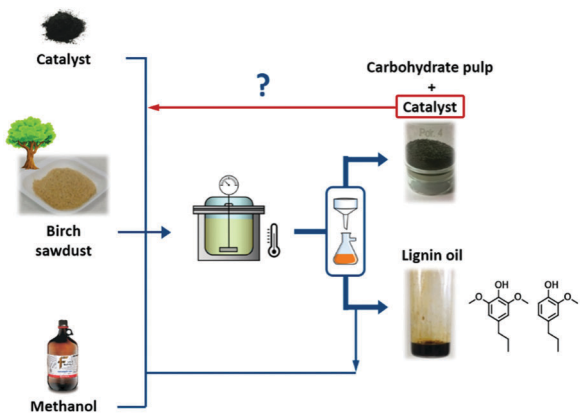

Fig. 38 A schematic representation for the catalytic reductive fractionation of lignocellulose sawdust using Ru/C catalyst in methanol under H_2 pressure.

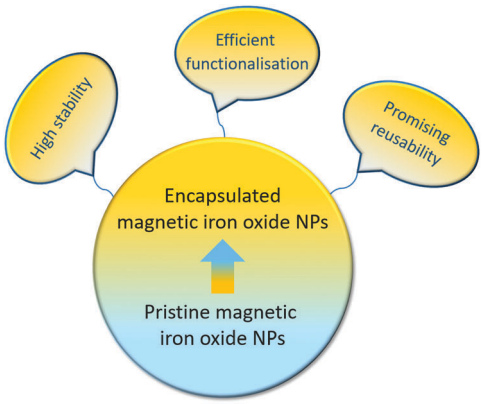

Fig. 39 Key benefits of encapsulated iron oxide magnetic catalysts.

as the protective agents.[342] These polymers are thermally stable up to 400–500 °C, enabling the resulting catalysts for wide-temperature-range reactions in biomass valorisation. The presence of nitrogen-containing species in the repeating units of these polymers offers potential routes for the immobilisation of catalytic active metals (Cu, Co, and Pd) as illustrated in Fig. 40.[342] The encapsulation of iron oxide NPs by hydroxyapatite (HAP) is another promising strategy, which not only limits particle aggregation, but also paves the way for the introduction of new catalytic active sites. For example, Ca^{2+} in the framework of hydroxyapatite can be exchanged with other transition metal cations (Pd^{2+}, Ru^{2+}, *etc.*).[343] Results revealed that a Pd-exchanged HAP encapsulated γ-Fe_2O_3 (γ-Fe_2O_3@HAP-Pd) efficiently catalyses the selective oxidation of HMF to FDCA at mild reaction conditions. The exchanged magnetic catalyst synthesis typically involves the cation exchange of Ca^{2+} in γ-Fe_2O_3@HAP with Pd^{2+}, followed by a reduction step using $NaBH_4$.

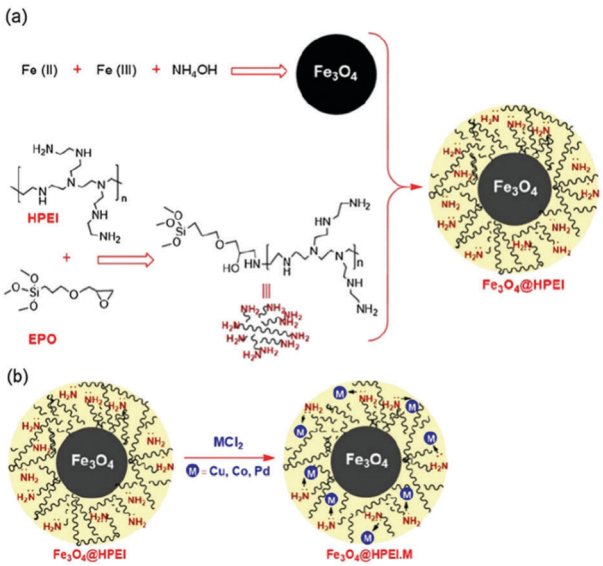

Fig. 40 (a) Preparation of hyperbranched polyethylenimine (HPEI) encapsulated magnetic Fe_3O_4 nanoparticles (Fe_3O_4@HPEI) and (b) chelation of metal species (Pd, Co and Cu) with nitrogenous ligands in Fe_3O_4@HPEI. Reproduced with permission from ref. 342. Copyright (2017) John Wiley and Sons.

Open Access Article. Published on 18 September 2018. Downloaded on 21/02/2026 10:11:12 PM.
This article is licensed under a Creative Commons Attribution-NonCommercial 3.0 Unported Licence.

Spinel-type MFe_2O_4 ferrites (M = Mn, Ni, Zn, or Co in divalent state and Fe in +3 oxidation state) also exhibit strong magnetic properties with excellent structural and thermal stability, which are highly dependent on the microstructure and cation distribution. To improve the magnetism as well as the activity of ferrites, the partial replacement of Fe^{3+} in MFe_2O_4 with transition metal cations (*e.g.*, Ru^{3+}) was successfully attempted without destroying the spinel structure.[344] The resulting doped ferrite catalysts were successfully applied for biomass upgrading reactions. Furthermore, Fe-based nanoalloys and Fe_3O_4 supported catalysts have found considerable applicability in biomass valorisation due to synergistic metal–metal and metal–support interactions, along with improved magnetic properties.[344–346] In the following sections, the catalytic applications of magnetic catalysts studied for biomass valorisation are thoroughly discussed, based on two categories, namely core–shell and non-core–shell iron oxide based catalysts. In addition, a summary of the interesting catalytic results obtained in magnetic iron oxides catalysed biomass conversions is presented in Table 4.

5.2 Core–shell Fe_3O_4 based magnetic catalysts

Various coating materials, such as SiO_2, γ-Al_2O_3, Nb_2O_5–SiO_2, organosilica, carbon, polymers, and hydroxyapatite have been used for the preparation of core–shell iron oxide based magnetic catalysts.[347,348] Primary applications of these catalysts in biomass valorisation refer to cellulose transformation, lignin fragmentation, and further upgrading of hereby obtained depolymerised (model) compounds.

5.2.1 Upgrading of carbohydrates-containing and -derived compounds. Cellulose is a major component of non-edible lignocellulose biomass (Fig. 6). Therefore, its effective valorisation is considered as a promising route towards renewable chemicals production.[349] Zhang *et al.*[332] developed a Fe_3O_4@carbon–SO_3H catalyst with a magnetic Fe_3O_4 core encapsulated in a sulfonated carbon shell for hydrolysis of cellulose. The catalyst showed a good activity, with 48.6% cellulose conversion and 25.3% glucose yield at moderate reaction conditions. Reusability studies revealed a small decrease in cellulose conversion from 48.6% to 45% after three cycles of the catalyst, due to leaching of acidic species (entry 1, Table 4). Xiong *et al.*[350] also studied the hydrolysis of cellulose using a functionalised core–shell Fe_3O_4@SiO_2–SO_3H catalyst. A 73.2% yield of reducing sugars was obtained and the magnetically recovered catalyst was efficiently reused for six times without much loss in product yields (entry 2, Table 4). In another work, a similar type of catalyst, *i.e.* Fe_3O_4@SiO_2–SO_3H, was tested for one-pot production of HMF from glucose.[340] A 70.5% yield of HMF with 98% glucose conversion was obtained at optimised reaction conditions. A noticeable decrease in HMF yields from 70.5% to 60.4% was noticed after five recycles of the catalyst, due to accumulation of oligomeric products on the active sites and leaching of acidic species (entry 3, Table 4). A magnetic nanocomposite, prepared by covering the Fe_3O_4 core with a Nb_2O_5–SiO_2 shell using either precipitation or sol–gel methods, was also recently reported for the one-pot transformation of cellulose to lactic acid.[351] A 43.7% yield of lactic acid, with about 95% cellulose conversion was obtained at optimised reaction conditions. A small decrease in product yields was noticed after three recycles of the catalyst, due to accumulation of reaction substrates on the catalytic active sites (entry 4, Table 4). The catalytic performances were directly correlated to the nature of the catalytic sites (Nb═O and/or Nb–O–H), which could be controlled by the niobium content and the applied preparation route. A facile green process was developed for the immobilisation of Pd NPs on core–shell magnetic Fe_3O_4@carbon microspheres without using any reductant and capping reagents.[352] The resulting catalyst showed a high activity and good stability for the oxidation of HMF into FDCA. Several reaction variables, such as temperature, solvent, and base amount were optimised to achieve a 86.7% yield of FDCA, which slightly decreased to 83.7% after five recycles of the catalyst (entry 5, Table 4).

Functionalised Ru-based magnetic catalysts were developed by combining propylamine functionalised SiO_2 coated magnetic Fe_3O_4 NPs with grafted cationic Ru.[353] The developed magnetic catalysts are able to convert cellulose into various important platform molecules, including glycerol. The catalyst exhibited 67.3% and 44.4% of cellulose conversion and glycerol yield, respectively, with a stable catalytic performance for at least two recycles (entry 6, Table 4). This is a key advantage over Nb@AlF_3, a typical diluted magnetic oxide, which also exhibited good performances in cellulose valorisation.[354] A similar type of Ru-based magnetic catalysts also demonstrated high efficiencies for the oxidation of levulinic acid to succinic acid (conversion = 59–79%, selectivity = 96–98%)[355] as well as for the cascade conversion of glucose to succinic acid (87.5% yield of succinic acid at nearly complete conversion of glucose).[356]

A novel ''inside-to-outside'' synthesis strategy was developed for the synthesis of bifunctional magnetic Ru–SO_3H nanoreactors.[357] Ru NPs were stabilised on yolk–shell nanoarchitectures composed of a Fe_3O_4 core and a sulfoacid-containing mesoporous organosilica (PMO) shell (Fig. 41a). The obtained magnetic nanoreactors exhibited various attractive properties, including a highly porous structure with uniform mesopores ($\sim$3.8 nm), superior BET surface areas ($>$350 m^2 g^{-1}), high dispersion of Ru NPs, and enhanced magnetisation. The participation of both Ru NPs and SO_3H moieties in catalytic reactions was confirmed by a one-pot conversion of cellulose to isosorbide (Fig. 41b). About 58% yield of isosorbide was achieved at optimised reaction conditions, which however considerably decreased with the repeated use of the catalyst (entry 7, Table 4). Yang *et al.*[358] developed several magnetic base catalysts, composed of functionalised SiO_2-coated magnetic Fe_3O_4 NPs and various organic bases. The resulting magnetic catalysts effectively catalysed the isomerization of glucose to fructose with reasonable good yields in water medium. A 1,2-enediol intermediate mechanism was proposed, which involves the removal of a proton at the C-2 position of glucose by the magnetic base catalyst. The catalytic performance of phosphotungstic acid (PHA) immobilised on a core–shell Fe_3O_4@SiO_2 magnetic catalyst was investigated for the

Open Access Article. Published on 18 September 2018. Downloaded on 21/02/2026 10:11:12 PM.
This article is licensed under a Creative Commons Attribution-NonCommercial 3.0 Unported Licence.

Table 4 Catalytic applications of the most significant magnetic iron oxide based materials in biomass valorisation

Entry	Catalyst	Reaction	Product	Reaction conditions	Catalytic activity: Conv. (%)	Catalytic activity: Yield (%)	Recycling results	Ref.
1	Fe_3O_4@carbon–SO_3H	Hydrolysis of cellulose	Glucose	50 mg cellulose, 150 mg catalyst, 10 mL H_2O, 140 °C, 12 h	48.6	25.3	3 (small decrease in cellulose conversion from 48.6% to 45%, due to leaching of acidic species)	332
2	Fe_3O_4@SiO_2–SO_3H	Hydrolysis of cellulose	Reducing sugar	160 mg cellulose, 100 mg catalyst, 2 g ionic liquid & 27 mg H_2O, 130 °C, 8 h	—	73.2	6 (small decrease in product yields from 73.2% to 69.4%)	350
3	Fe_3O_4@SiO_2–SO_3H	Glucose dehydration	HMF[a]	1 : 4 vol ratio of water/methyl isobutyl ketone, 140 °C, 24 h	98	70.5	5 (noticeable decrease in HMF yields from 70.5% to 60.4%, due to accumulation of oligomeric products on the active sites and leaching of acid species)	340
4	Fe_3O_4@Nb_2O_5–SiO_2	Hydrolysis of cellulose	Lactic acid	50 mg cellulose, 50 mg catalyst, 15 mL water, 180 °C, 24 h	95	43.7	3 (small decrease in lactic acid yields, due to accumulation of reaction substrates on the catalytic active sites)	351
5	Pd/Fe_3O_4@carbon	Oxidation of HMF	FDCA[b]	0.4 mmol HMF, 40 mg catalyst, 0.2 mmol K_2CO_3, 8 mL water, 80 °C, O_2 (30 mL min^{-1}), 6 h	98.4	86.7	5 (very small decrease in FDCA yields from 86.7% to 83.7%)	352
6	Ru(III)/Fe_3O_4@SiO_2–NH_2	Cellulose upgrading	Glycerol	140 mg cellulose, 60 mg catalyst, 5 mL water, 180 °C, 2 h	67.3	44.4	2 (stable catalytic activity)	353
7	Ru@Fe_3O_4@void@PMO–SO_3H[c]	Hydrogenolysis of cellulose	Isosorbide	60 mg cellulose, 60 mg catalyst, 30 mL H_2O, 6 MPa H_2, 220 °C, 2 h	98	58	4 (considerable decrease in isosorbide yields)	357
8	Fe_3O_4@SiO_2@PHA[d]	Dehydration of glucose	HMF	0.5 g glucose, 2 g catalyst, 15 mL dimethylformamide, 130 °C, 1 MPa N_2 at 130 °C, 3 h	59.8	30.4	5 (considerable decrease in HMF yields, due to leaching of acid species)	359
9	Fe_3O_4@SiO_2–HPW[e]	Etherification of HMF	EMF[f]	1 mmol HMF, 150 mg catalyst, 5 mL ethanol, 100 °C, 11 h, N_2 atm	97.9	83.2	6 (small decrease in EMF yields from 83.2% to 78.8%)	46
10	Fe_3O_4@Al_2O_3–BAIL–Al[g]	Dehydration of xylose	Furfural	100 mg xylose, 40 mg catalyst, 3 mL dimethyl sulfoxide, 140 °C, 3 h	97.3	67.5	5 (noticeable decrease in furfural yields from 67.5% to 58.7%, due to accumulation of reaction substrates on the catalytic active sites)	360
11	0.3% Pd–Fe_3O_4–PPP[h]	Hydrogenation of furfural	Furfuryl alcohol	2 mL furfural, 48 mL i-propanol, 120 °C, 60 bar H_2, 450 min	98.8	98	5 (stable catalytic activity)	361
12	γ-Fe_2O_3@HAP[i]	Hydrogenation of furfural	Furfuryl alcohol	1 mmol furfural, 40 mg catalyst, 15 mL of i-propanol, 180 °C, 10 bar N_2, 10 h	96.2	91.7	6 (stable catalytic activity)	362
13	γ-Fe_2O_3@HAP–Pd(0)	HMF oxidation	FDCA	0.4 mmol HMF, 40 mg catalyst, 0.2 mmol K_2CO_3, 8 mL water, 100 °C, O_2 (30 mL min^{-1}), 6 h	97	92.9	5 (minor loss of FDCA yields from 92.9% to 90.7%, due to mass loss of the catalyst during recovery/purification steps)	343
14	Fe_3O_4@SiO_2–NH_2–Ru(III)	HMF oxidation	DFF[j]	100 mg HMF, 150 mg catalyst, 7 mL toluene, 110 °C, O_2 (20 mL min^{-1}), 4 h	99.3	86.4	6 (small decrease in DFF yields from 86.4% to 80.8%)	363
15	Fe_3O_4@SiO_2–NH_2–VO^{2+} & Fe_3O_4@SiO_2–NH_2–Cu^{2+} as cocatalyst	HMF oxidation	DFF	0.8 mmol HMF, 100 mg Fe_3O_4@SiO_2–NH_2–VO^{2+}, 30 mg Fe_3O_4@SiO_2–NH_2–Cu^{2+}, 40 mL toluene, 110 °C, 2.8 bar O_2, 1 h	98.7	85.5	4 (small decrease in DFF yields from 85.5% to 81.2%)	48
16	Fe_3O_4@SiO_2–TEMPO[k]	HMF oxidation	DFF	1 mmol HMF, 2 mol% catalyst, 5 mol% *tert*-butyl nitrite, 75 mg acetic acid, 2 mL toluene, 50 °C, 18 h, 1 atm O_2	—	> 99	5 (stable catalytic activity up to four recycles and then a rapid decrease in DFF yield (77%) after 5th recycle)	364
17	WO_3HO–VO(salten)–SiO_2@Fe_3O_4	Dehydration-oxidation of fructose	DFF	(i) 1 mmol fructose, 100 mg catalyst, 80 °C, iso-propanol, 1 h (ii) 1 mmol H_2O_2, 60 °C, 15 h	—	71	5 (minor loss in DFF yields)	365
18	Fe_3O_4@Nb_2O_5@Co@Re	Lignin fragmentation	Lignin fragments (EG and PG)[l]	10 mg lignin, 20 mg catalyst, 2.5 mL H_2O, 180 °C, 10 bar H_2 at RT, 6 h	—	85	6 (stable catalytic activity)	347
19	Ru–Fe_3O_4–SiO_2 (5 wt% Ru)	Hydrogenolysis of cellulose		300 mg cellulose, 70 mg catalyst, 30 mL water, 255 °C, 60 bar H_2 at RT, 50 min	100	19 (EG)	3 (stable catalytic activity)	371

Open Access Article. Published on 18 September 2018. Downloaded on 21/02/2026 10:11:12 PM.
This article is licensed under a Creative Commons Attribution-NonCommercial 3.0 Unported Licence.

Table 4 (*continued*)

Entry	Catalyst	Reaction	Product	Reaction conditions	Catalytic activity		Recycling results	Ref.
					Conv. (%)	Yield (%)		
20 (PG)								
20	Fe_3O_4@SBA–SO_3H	Hydrolysis of cellulose[m]	Glucose	1 g cellulose, 1.5 g catalyst, 15 mL H_2O, 150 °C, 3 h	—	50	3 (stable catalytic activity)	373
21	Fe_3O_4/Mn_3O_4	Oxidation of HMF	DFF	1 mmol HMF, 160 mg catalyst, 7 mL dimethylformamide, 120 °C, O_2 (20 mL min^{-1}), 4 h	99.8	82.1	6 (small decrease in DFF yields from 82.1% to 78.9%, due to mass loss of the catalyst during recovery/purification steps)	375
22	Fe_3O_4–CoO_x	Oxidation of HMF	FDCA	70 mg HMF, 100 mg catalyst, 4 mL dimethyl sulfoxide, 0.5 mL of 70% aqueous *t*-butyl hydroperoxide, 80 °C, 12 h	97.2	68.6	2 (stable catalytic activity)	330
23	$MnFe_2O_4$	Oxidation of HMF	FDCA	1 mmol HMF, 0.015 g cm^{-3} catalyst, 100 °C, 9 mmol *t*-butyl hydroperoxide, 5 h	100	85	4 (stable catalytic activity)	376
24	$NiFe_2O_4$	Hydrogenation of furfural	Furfuryl alcohol	2 mmol furfural, 60 mg catalyst, 10 mL of 2-propanol (hydrogen source), 180 °C, 6 h	99	94	5 (stable catalytic activity)	345

[a] HMF – 5-hydroxymethylfurfural. [b] FDCA – 2,5-furandicarboxylic acid. [c] PMO – sulfoacid-containing mesoporous organosilica. [d] PHA – phosphotungstic acid. [e] HPW – phosphotungstic acid. [f] EMF – 5-ethoxymethylfurfural. [g] BAIL-Al – bifunctional acidic ionic liquid of metal Al substituted. [h] PPP – poly(pyridylphenylene). [i] HAP – hydroxyapatite. [j] DFF – 2,5-diformylfuran. [k] TEMPO – 2,2,6,6-tetramethylpiperidine-*N*-oxide. [l] EG – ethylene glycol and PG – propylene glycol. [m] Amorphous cellulose.

Fig. 41 (a) Detailed synthesis strategy for magnetic Ru–SO_3H nanoreactor and (b) its application in one-pot conversion of cellulose to isosorbide. Reproduced with permission from ref. 357. Copyright (2018) Royal Society of Chemistry.

direct synthesis of HMF from glucose.[359] The obtained catalytic activity of Fe_3O_4@SiO_2@PHA was comparable to that of a homogeneous PHA catalyst. About 30.4% yield of HMF was obtained at optimised reaction conditions. However, a considerable decrease in HMF yields was noticed after five recycles of the catalyst, due to leaching of acidic species (entry 8, Table 4). Etherification of fructose and HMF to 5-ethoxymethylfurfural (EMF) was investigated using a phosphotungstic acid immobilised core–shell Fe_3O_4@SiO_2 catalyst.[46] The resulting catalyst showed excellent activity with 83.2% and 54.8% yields of EMF from etherification of HMF and fructose, respectively. Only a small decrease in EMF yields from 83.2% to 78.8% was found after six recycles of the catalyst (entry 9, Table 4).

The selective dehydration of xylose to furfural was studied using a bifunctional magnetic catalyst composed of an immobilised acid ionic liquid of metal Al substituted onto the surface of Fe_3O_4@γ-Al_2O_3.[360] A 67.5% yield of furfural with 97.3% xylose conversion was obtained, attributed to abundant amounts of both Brønsted and Lewis acid sites in the developed catalyst. Reusability studies revealed a considerable decrease in furfural yields from 67.5% to 58.7% after five recycles of the catalyst, due to accumulation of reaction substrates on the catalytic active sites (entry 10, Table 4). The selective hydrogenation of furfural to furfuryl alcohol was studied using a magnetic Fe(NiFe)O_4@SiO_2 catalyst, synthesised by a facile

This journal is © The Royal Society of Chemistry 2018

Open Access Article. Published on 18 September 2018. Downloaded on 21/02/2026 10:11:12 PM.
This article is licensed under a Creative Commons Attribution-NonCommercial 3.0 Unported Licence.

co-precipitation method.[2] Good catalytic results were obtained with a more than 93% yield of furfuryl alcohol. A tentative mechanism *via* a non-hydrogen spillover route was proposed in this work. Highly dispersed nickel species played a pivotal role in the dissociation of H_2 into a proton and a hydride, hence enabling the superior catalytic performance of Fe(NiFe)O_4@SiO_2 for furfural hydrogenation. Polymer stabilised Pt- and Pd-containing Fe_3O_4 NPs were also studied for the selective hydrogenation of furfural to furfuryl alcohol.[361] Two types of polymers, namely polyphenylquinoxaline (PPQ) and polypyridylphenylene (PPP) were used in this work. A higher catalytic activity was observed in the case of hyperbranched PPP-based catalyst compared to that obtained with linear PPQ, which was ascribed to the improved accessibility of catalytic species in PPP-based catalyst. In other words, the longer distance between Pd and Fe_3O_4 NPs in the case of the PPP-stabilised catalyst endows a higher yield to furfuryl alcohol (98%), with a stable catalytic performance even after five recycles of the 0.3% Pd–Fe_3O_4–PPP catalyst (entry 11, Table 4). Alternatively, the catalytic transfer hydrogenation of furfural into furfuryl alcohol with alcohols as hydrogen donor was investigated using a hydroxyapatite-encapsulated magnetic γ-Fe_2O_3 (γ-Fe_2O_3@HAP) catalyst.[362] Results indicated iso-propanol as the best hydrogen donor for the transfer hydrogenation of furfural. A 91.7% yield of furfuryl alcohol was obtained at optimised reaction conditions, which was maintained even after six recycles of the γ-Fe_2O_3@HAP catalyst (entry 12, Table 4).

A Pd(0) immobilised γ-Fe_2O_3@HAP catalyst was prepared by the exchange of Pd^{2+} with Ca^{2+} in γ-Fe_2O_3@HAP, followed by the reduction of Pd^{2+} to Pd(0) using $NaBH_4$.[343] The synthesised catalyst was tested for the selective aerobic oxidation of HMF into FDCA. The effect of solvent, base, molar ratio of base to HMF, oxidising agent, catalyst loading, and the reaction temperature was studied for this reaction. About 97% HMF conversion, with a 92.9% FDCA yield was obtained in water after 6 h reaction time at 100 °C. Reusability studies showed a very small decrease in FDCA yields from 92.9% to 90.7% after five recycles of the catalyst, due to mass loss of the catalyst during recovery/purification steps (entry 13, Table 4). Similarly, a Ru exchanged γ-Fe_2O_3@HAP catalyst was developed for the aerobic oxidation of HMF to DFF.[339] A high yield of DFF (89%) at nearly complete conversion of HMF was obtained in this work. In addition, the direct conversion of fructose to DFF was performed, which follows two consecutive steps. The first step involves the dehydration of fructose to HMF (90% yield) over a magnetic acid catalyst (Fe_3O_4@SiO_2–SO_3H). Subsequently, the oxidation of HMF to DFF (79% yield based on fructose) is carried out using γ-Fe_2O_3@HAP-Ru, after removal of Fe_3O_4@SiO_2–SO_3H from the reaction mixture with a magnet. Wang *et al.*[363] also studied the aerobic oxidation of HMF to DFF using a Ru(III) catalyst immobilised on a core–shell Fe_3O_4@SiO_2–NH_2 catalyst. The developed catalyst showed a good performance with 99.3% conversion of HMF and 86.4% yield of DFF after 4 h. The magnetically recovered catalyst can be reused for at least six times, with a small decrease in DFF yields from 86.4% to 80.8% (entry 14, Table 4). In contrast, Liao *et al.*[48]

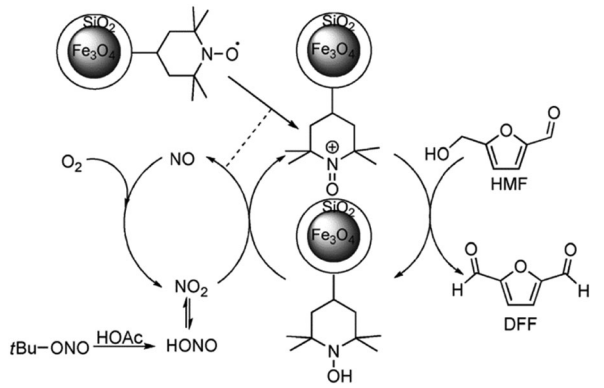

Fig. 42 Proposed reaction pathway for the aerobic oxidation of 5-hydroxymethylfurfural (HMF) into 2,5-diformylfuran (DFF) using a Fe_3O_4@SiO_2-TEMPO catalyst. Reproduced with permission from ref. 364. Copyright (2014) John Wiley and Sons.

used non-noble metals *i.e.*, Cu^{2+} and VO^{2+} immobilised on amino modified Fe_3O_4@SiO_2 (Fe_3O_4@SiO_2–NH_2–Cu^{2+} and Fe_3O_4@SiO_2–NH_2–VO^{2+}) for the production of DFF *via* HMF oxidation. The reaction is highly dependent on the nature of the solvent. A 98.7% conversion of HMF with 85.5% yield of DFF was obtained over the combination of both catalysts. Only a small decrease in DFF yields from 85.5% to 81.2% was found after four recycles of the catalysts (entry 15, Table 4). In another work, 2,2,6,6-tetramethylpiperidine-*N*-oxide (TEMPO) immobilised on Fe_3O_4@SiO_2 was studied for the oxidation of HMF into DFF.[364] Herein, *tert*-butyl nitrite and acetic acid were used as additive and co-catalyst, respectively. Quantitative yields of DFF were obtained with excellent chemoselectivity (>99%) and a tentative reaction mechanism was proposed as shown in Fig. 42. Interestingly, a stable catalytic activity was observed up to four recycles of the catalyst, with a rapid decrease in DFF yield (77%) after the 5th recycle (entry 16, Table 4). A bifunctional magnetic catalyst (WO_3HO-VO(salten)–SiO_2@Fe_3O_4) was developed for the one-pot conversion of fructose to DFF.[365] Two types of functional sites *i.e.*, (i) tungstic acid for fructose dehydration to HMF and (ii) an oxovanadium complex for HMF oxidation to DFF were covalently bonded to the core–shell Fe_3O_4@SiO_2 NPs. The resulting catalyst demonstrated good activity in the conversion of fructose to DFF (71% yield), with a minor loss in catalytic activity after five recycles (entry 17, Table 4).

5.2.2 Upgrading of non-carbohydrate compounds. In view of the challenges associated with first- and second-generation biofuels, the production of third-generation biofuels from marine biomass (*e.g.*, microalgae) has gained a great deal of attention. Ascribed benefits of marine biomass include a high content of lipids and carbohydrates without lignin, rapid growth, and a more effective CO_2 remediation.[47] However, studies estimated that the current production of biodiesel from algae is still 2.5 times as energy intensive as conventional diesel production. Therefore, Chiang *et al.*[47] developed a novel core–shell Fe_3O_4@SiO_2 magnetic catalyst functionalised with a strong base, triazabicyclodecene (TBD). Interestingly, the resulting

Open Access Article. Published on 18 September 2018. Downloaded on 21/02/2026 10:11:12 PM.
This article is licensed under a Creative Commons Attribution-NonCommercial 3.0 Unported Licence.

catalyst was not only found to be effective in the one-pot conversion of microalgae to biodiesel but also facilitated algae harvesting because of its magnetic feature. Three types of algae sources, such as dried algae, algae oil, and concentrate algae were used in this work. The base functionalised magnetic catalyst exhibited tremendous performance with a maximum biodiesel yield of 97.1%. Alternatively, several studies reported the immobilisation of lipase on magnetic Fe_3O_4@SiO_2 NPs for the production of biodiesel *via* transesterification.[366–370] Different types of lipase sources, such as *Candida Antarctica*, *Pseudomonas cepacia*, and *Aspergillus niger* have been used. The enzyme immobilised magnetic Fe_3O_4@SiO_2 catalysts exhibited reasonably good efficiencies for the production of biodiesel *via* transesterification of triglycerides with alcohols. Opris *et al.*[347] studied the role of the composition and deposition method of rhenium on the catalytic efficiency of a multifunctional Fe_3O_4@Nb_2O_5@Co@Re catalyst for lignin fragmentation. The catalyst (2%Co@3%Re) synthesised *via* an impregnation method showed the best performance with a 85% yield of lignin-derived fragments. Reusability studies revealed a remarkable stable catalytic activity even after six recycles of the catalyst (entry 18, Table 4).

5.3 Non-core–shell iron-based magnetic catalysts

In this section, applications of non-core–shell iron-based magnetic catalysts, such as Fe_3O_4 supported metals, mixed oxides, spinel ferrites, and nanoalloys are discussed within the context of biomass conversion.

5.3.1 Upgrading of carbohydrates-containing and -derived compounds. Biomass-derived polyols, such as ethylene glycol and propylene glycol are important building blocks for the production of liquid fuels, emulsifiers, surfactants, and pharmaceuticals.[371] A promising pathway to produce these polyols is cascade hydrogenolysis of cellulose over magnetic catalysts. In view of this, Manaenkov *et al.*[371] developed finely dispersed Ru NPs (average particle size of 2 nm) on Fe_3O_4–SiO_2 with various Ru nominal loadings of 1, 3, and 5 wt% for the one-pot hydrogenolysis of cellulose in subcritical water. The developed catalysts (especially 5 wt% Ru loaded catalyst) showed good cellulose conversions and product selectivities, hereby outperforming a commercial Ru/C catalyst, ascribed to the constructive effect of Fe_3O_4 on the redox couple of Ru^0/Ru^{4+}. The reaction temperature, reaction time, and the Ru loading play a decisive role in the selectivity of ethylene glycol and propylene glycol. Moreover, a stable catalytic activity was noticed even after three recycles of the Ru–Fe_3O_4–SiO_2 catalyst (5 wt% Ru amount) in hydrogenolysis of cellulose (entry 19, Table 4). Similar type of magnetic Ru/Fe_3O_4–SiO_2 catalysts were also studied for the hydrogenation of a solution of furfural, phenol, and acetic acid.[372] Conversions and product selectivities were highly dependent on the reaction temperature and pH of the solution. A sulfonated magnetic Fe_3O_4@SBA-SO_3H solid acid showed a stable catalytic activity for hydrolytic conversion of cellulose, achieving about 50% yield of glucose even after three recycles of the catalyst (entry 20, Table 4).[373] However, the attached sulfonic groups were susceptible to leaching in water at reaction temperatures above 130 °C.[374]

An efficient catalytic protocol for the aerobic oxidation of HMF to DFF was developed using a magnetic Fe_3O_4 supported Mn_3O_4 catalyst.[375] A 82.1% yield of DFF at nearly complete conversion of HMF was obtained at optimised reaction conditions. The magnetic catalyst can be reused for at least six times and only a small decrease in DFF yields from 82.1% to 78.9% was found, due to inevitable mass loss of the catalyst during recovery/purification steps (entry 21, Table 4). A nanosized magnetic Fe_3O_4–CoO_x catalyst also showed a good activity for the oxidation of HMF, but here FDCA is the major product with *t*-BuOOH as the oxidant.[330] Several reaction parameters were optimised and a 68.6% yield of FDCA was obtained after 12 h reaction, which can be maintained for two recycles of the catalyst (entry 22, Table 4). In another work, a spinel structured magnetic $MnFe_2O_4$ catalyst was tested for the oxidation of HMF to FDCA using *t*-BuOOH as the oxidant.[376] About 85% yield of FDCA was obtained at 100 °C in 5 h over the spinel $MnFe_2O_4$ catalyst, which was much higher than that obtained with Fe_3O_4–CoO_x.[330] A remarkable stable catalytic activity was observed even after four recycles of $MnFe_2O_4$ catalyst in HMF oxidation (entry 23, Table 4). This high catalytic performance was ascribed to the presence of variable Mn oxidation states in the spinel $MnFe_2O_4$ catalyst. Interestingly, a multicomponent $ZnFe_{1.65}Ru_{0.35}O_4$ magnetic catalyst, prepared *via* a simple alkaline co-precipitation method, was able to selectively produce either DFF or FDCA from aerobic oxidation of HMF under variable reaction conditions.[344] Excellent yields of DFF (93.5%) and FDCA (91.2%) were obtained at different optimised reaction conditions. In addition, the one-pot cascade conversion of fructose to DFF or FDCA was also performed. A functionalised reduced graphene oxide (r-GO–SO_3H) based magnetic catalyst was tested for the dehydration of fructose to HMF. The catalyst was then recovered from the reaction mixture using an external magnet.[344] Subsequent oxidation of the produced HMF towards DFF or FDCA was then performed in the presence of a $ZnFe_{1.65}Ru_{0.35}O_4$ catalyst. He *et al.*[345] studied the catalytic transfer hydrogenation of furfural over a nickel ferrite ($NiFe_2O_4$) catalyst using 2-propanol as both the hydrogen source and the solvent. An excellent yield of furfuryl alcohol (94%) was obtained at 180 °C after 6 h reaction and the catalyst was reused for five recycles without loss of catalytic performance (entry 24, Table 4).

5.3.2 Upgrading of non-carbohydrate compounds. Magnetic FeB, NiB, and FeNiB nanoalloys were examined for catalytic transfer hydrogenation of acetophenone (lignin model compound) using supercritical ethanol as the hydrogen donor as well as the reaction solvent.[377] Among them, the multicomponent FeNiB catalyst showed the best performance, reaching a 74% conversion and 84% selectivity to ethylbenzene. FeNiB catalyst was also tested for the deoxygenation of aliphatic hydroxyl and carbonyl groups in organosolv lignin. A nanosized K/ZrO_2/γ-Fe_2O_3 base catalyst was studied for the production of biodiesel *via* transesterification of soybean oil.[378] Characterisation studied revealed the formation of unique granular nano-structures with particle sizes of 15–25 nm and superior ferromagnetic property. A 93.6 wt% yield of biodiesel was obtained at mild reaction

 This journal is © The Royal Society of Chemistry 2018

Open Access Article. Published on 18 September 2018. Downloaded on 21/02/2026 10:11:12 PM.
This article is licensed under a Creative Commons Attribution-NonCommercial 3.0 Unported Licence.

conditions and the catalyst was recycled up to six times. A minor progressive decrease in biodiesel yield was noticed, due to leaching of active sites. Hollow fibre structured magnetic CaO/α-Fe catalysts, synthesised by an organic gel-thermal decomposition method, were studied for the transesterification of rapeseed oil with methanol to produce biodiesel.[379] The effect of molar ratios of metal ions, annealing atmospheres, and annealing temperatures on the structural and morphological properties of the catalyst was investigated. A 95.7% biodiesel yield was obtained at optimised conditions and the catalyst, recovered by magnetic field, maintained a 85.2% biodiesel yield after as many as 20 recycles.

Several heterogeneous magnetic biocatalysts (enzyme immobilised magnetic NPs) were found to exhibit good catalytic activities for the production of glycerol carbonate from glycerol and dimethyl carbonate.[380,381] The lipase enzyme was covalently attached to magnetic NPs *via* 1-ethyl-3-(3-dimethylaminopropyl)-carbodiimide or glutaraldehyde.[382] The developed magnetic biocatalysts showed about 3-fold higher catalytic efficiency (3.52×10^5 h^{-1} TOF) than the free lipase (1.16×10^5 h^{-1} TOF), which was explained as a beneficial effect of the lipase immobilisation and the resulting lipase–Fe_3O_4 interactions.[382,383] Similar catalytic performances were also achieved when starting from "crude" glycerol feed extracted during biodiesel synthesis.[384] The efficiency of these magnetic biocatalysts has also been proven for the transesterification of oils extracted from soybean, sunflower, rape, corn, olive, and palm.[385]

5.4 Conclusions of magnetic iron oxide-based catalysts

The reported examples in this section clearly reveal that the facile recovery of functionalised magnetic nanocatalysts using an external magnetic field is a notable advantage over conventional catalysts. This prevents the use of further steps to remove the catalyst from complex reaction mixture, allowing the efficient recyclability in successive cycles. Notwithstanding, magnetic iron oxide based catalysts still suffer from several drawbacks in terms of synthesis and stability.[50,372,386,387] For instance, developing a facile one-pot method for large-scale production of functionalised Fe_3O_4 based materials, especially core–shell catalysts, is a very challenging task. This is because each constituent material contains disparate properties, hence requires different reaction conditions as well as multi-steps for the synthesis of functionalised Fe_3O_4 catalysts. In addition, the instability/dissolution of magnetic NPs during longer time catalytic reactions as well as the leaching of functional sites under harsh reaction conditions remain the major problems in several biomass upgrading reactions. Although core–shell Fe_3O_4 based catalysts exhibit good stability, concerns associated with the necessity of complex synthesis processes and high production costs limit their applications in several catalytic applications including biomass upgrading. Alternatively, non-core–shell Fe_3O_4 catalysts (Fe_3O_4 supported metals, spinel ferrites, *etc.*) are easy to prepare and also show good catalytic stability in biomass conversions. Therefore, more research efforts should be undertaken towards developing novel non-core–shell Fe_3O_4 catalysts with the required catalytic properties, which is of great significance from both scientific and practical viewpoints.

6. Conclusions and future prospects

In view of global warming impact on humankind as well as on the biosphere, the use of biomass alternative to fossil fuels for renewable chemicals production is a hot research topic of the 21st century. Biomass is a promising renewable energy that can be derived from various sustainable sources, including lignocellulose, lipids, starch, and aquatic plants. A large number of value-added chemicals and high-energy density fuels can be produced from biomass using appropriate technologies based on biological, thermal, and chemical processes. Among them, chemical processing of biomass (*e.g.*, hydrolysis, fast pyrolysis, hydroprocessing, oxidation, (trans)esterification, amination, dehydration, isomerisation, *etc.*) has attracted tremendous attention as the resulting products can exhibit relatively equating characteristics to petroleum-based products, driving towards a more sustainable economy and carbon-neutral society.

Catalysis plays a central role in bio-refinery chemical processes. Compared to homogenous catalysts, heterogeneous catalysts can provide promising greener routes for efficient biomass upgrading. Handiness of various feasible synthesis methods, non-toxicity, high stability, and efficient recovery/reusability are some of the key benefits of heterogeneous solid catalysts. The development of multifunctional heterogeneous catalysts with ample amounts of acid, base or redox active sites is vital for achieving higher reaction rates, especially in cascade biomass processes. Recent advances in materials science and catalysis have provided several novel strategies for the development of new appealing catalytic materials, such as carbon materials, metal–organic frameworks, solid phase ionic liquids, and magnetic iron oxides. A distinctive feature of these catalytic materials is to accommodate abundant acid–base as well as redox functional species, hence enabling biomass conversion reactions in a one-pot cascade approach.

In this review, the unique catalytic properties of carbon materials, metal–organic frameworks, solid phase ionic liquids, and magnetic iron oxides were highlighted towards catalytic biomass upgrading. Several potential routes developed for the immobilisation of acid–base and redox functional species on particular sites of above-listed catalysts were discussed in detail. Finally, the subsequent effects of functionalisation on one-pot cascade processes as well as on other types of vital reactions that normally take place in bio-refineries were thoroughly discussed. It can be concluded that the distinctive properties of catalysts play an essential role for robust functionalisation, hence improved catalytic activities in biomass valorisation. For instance, both *ex situ* and *in situ* functionalisation are possible in the case of carbon materials. The presence of abundant surface defects and residual O-containing groups, for example in activated carbon, graphene, and carbon nanotubes, allows efficient *ex situ* functionalisation with acid–base and/or redox active phases.[35,79,130] On the other hand, the use of biomass-derived molecules (*e.g.*, glycerol and glucose) as catalyst precursors facilitates *in situ* functionalisation.[85,204] In the case of MOFs, organic ligands offer facile routes to

Open Access Article. Published on 18 September 2018. Downloaded on 21/02/2026 10:11:12 PM.
This article is licensed under a Creative Commons Attribution-NonCommercial 3.0 Unported Licence.

introduce acid–base functional molecules,[219] while robust porous cavities afford ample room for the encapsulation of metal NPs.[225] ILs fundamentally contain various kinds of synergistic interactions, resulting from organic cations and (in)organic anions, which play a crucial role in stabilising immobilised functional species.[284] In addition to the benefits of facile recovery/recyclability, the core–shell or polymer encapsulated magnetic iron oxides allow efficient ionic exchange with the active transition metals, attributed to the presence of abundant surface exchangeable species (*e.g.*, –OH and Ca^{2+}).[47,339,343] It must be noted here that most of the biomass upgrading reactions reported in this review are performed on the laboratory scale. This does not necessarily imply industrial relevance, but will provide useful information towards developing large-scale biorefineries in terms of catalyst selection, reaction conditions needed, tailoring activity/selectivity, and potentials to regenerate the catalyst activity.

Although tremendous progress has been achieved towards development of efficient functionalised heterogeneous catalysts for biomass valorisation, further advances are still necessary in view of sustainable bio-refinery industry. Hence, to guide future research in the respective fields we would like to propose an interesting 'PYSSVR' concept, which means P – production cost, Y – yield, S – stability, S – selectivity, V – versatility, and R – reusability (Fig. 43).

(1) Production cost: efforts should be made to minimise catalyst production costs. Especially, high synthesis costs of CNTs, graphene, MOFs, and ILs limits their practical applications in biomass upgrading. A promising solution to tackle this problem is the use of low-cost and renewable precursors. For instance, a variety of economical carbon-based catalysts with abundant functional sites can be developed *via* carbonisation of biomass substrates as discussed in Section 2.8.[82–84] The subsequent use of these catalysts in biomass upgrading can greatly improve process economy and sustainability. Moreover, one-pot synthesis of functionalised heterogeneous catalysts *via in situ* functionalisation as well as the utilisation of non-noble metals can help to reduce catalyst production costs.

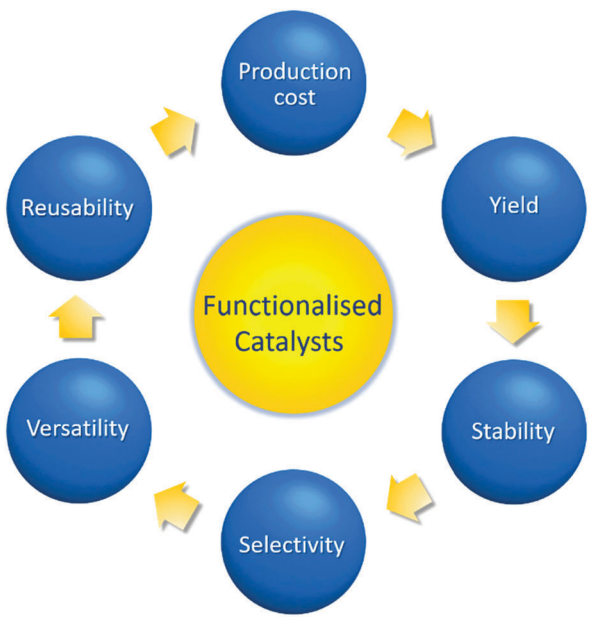

Fig. 43 Promising features of functionalised heterogeneous catalysts for a more sustainable biomass valorisation.

(2) Yield: it is also crucial to improve production yields of functionalised heterogeneous catalysts, while maintaining their unique properties. In this context, the selected preparation method must be simple, cost-effective, eco-friendly (*i.e.* avoiding hazardous organic reagents/solvents) and able to scaled-up. Compared with gas- and solid-phase synthesis methods, efforts needs to be strengthened towards developing wet chemical preparation routes as they can be efficiently modified for economical mass production of solid catalysts.

(3) Stability: hydrothermal stability of functionalised catalysts under harsh aqueous conditions is very important, because water is the preferred reaction medium for many bio-refinery processes. This review emphasised several potential strategies to improve hydrothermal stability of the catalysts, including doping of heteroatoms (*e.g.*, nitrogen) in carbon,[186] developing carbon-silica composites,[160–162] selective encapsulation/anchoring of active phases in MOFs,[245,246] incorporation of ILs into the polymeric substrates,[313] and designing robust core–shell Fe_3O_4@SiO_2 catalysts.[47]

(4) Selectivity: tailoring the selectivity of functionalised catalysts towards a particular product in biomass upgrading is essential to control the formation of unwanted by-products as well as to minimise energy-intensive steps required for the separation/purification of reaction substrates. This can be achieved by selectively anchoring functional species on particular sites of heterogeneous catalysts, which may direct the specificity of interaction with the biomass molecules, hence preferred reaction pathway and formation of desirable products.

(5) Versatility: it is also vital to develop functionalised heterogeneous catalysts, with versatile applications in biomass upgrading. Several examples of this kind are highlighted in this review, including sulfonated silica–carbon nanocomposites (cellulose hydrolysis[160] and fructose ethanolysis[162]), SO_3H functionalised MIL-101(Cr) MOF (fructose-to-HMF[220] and furfuryl alcohol-to-ethyl levulinate[249]), and Fe_3O_4@SiO_2–SO_3H (glucose-to-HMF[340] and cellulose-to-reducing sugar[350]). For an improved bio-based economy, developing a more number of versatile catalysts with multiple active sites is an urgent task.

(6) Reusability: above all, efficient reusability of the catalysts is of paramount importance in order to avoid post-reaction steps, minimise waste disposal and energy consumption, as well as maximise the productivity. Owing to excellent paramagnetic properties, magnetic iron oxide based catalysts can be efficiently recovered from reaction mixtures using a magnet without affecting their physicochemical properties. Hence, efforts should be directed towards developing composite catalysts consisting of magnetic iron oxides with functionalised carbon materials, MOFs, or ILs. This appealing approach may combine the unique catalytic properties of the respective components, with the magnetic properties of iron oxides, hence avoiding recycling concerns associated with the conventional catalysts. This route may further lead to significantly improved

 This journal is © The Royal Society of Chemistry 2018

Open Access Article. Published on 18 September 2018. Downloaded on 21/02/2026 10:11:12 PM.
This article is licensed under a Creative Commons Attribution-NonCommercial 3.0 Unported Licence.

catalytic activities in biomass upgrading, due to availability of abundant functional active sites.

More stimulating research efforts are therefore needed to develop state-of-the-art functionalised heterogeneous catalysts, with necessary functional active sites and various key features as listed in Fig. 43 for a more sustainable biomass valorisation. In this context, the present comprehensive review may provide a systematic background for further advances towards economic mass production of versatile functionalised heterogeneous catalysts for a viable bio-refinery industry.

Conflicts of interest

There are no conflicts to declare.

Acknowledgements

This project has received funding from the European Union's Horizon 2020 research and innovation programme under the Marie Skłodowska-Curie grant agreement number-747968 (project acronym: CATLIGCAR). SVDB acknowledges the internal funds of KU Leuven for a postdoctoral mandate (PDM). VIP kindly acknowledge UEFISCDI for financial support (projects PN-III-P4-ID-PCE-2016-0146 and 32PCCDI-2018). BFS would like to thank BIOFACT Excellence of Science project as well as SPICEY (VLAIO SBO Flemish Government) project.

References

1 L. T. Mika, E. Cséfalvay and Á. Németh, *Chem. Rev.*, 2018, **118**, 505–613.
2 A. Halilu, T. H. Ali, A. Y. Atta, P. Sudarsanam, S. K. Bhargava and S. B. A. Hamid, *Energy Fuels*, 2016, **30**, 2216–2226.
3 A. Wittstock and M. Bäumer, *Acc. Chem. Res.*, 2014, **47**, 731–739.
4 W. Schutyser, T. Renders, S. Van den Bosch, S. F. Koelewijn, G. T. Beckham and B. F. Sels, *Chem. Soc. Rev.*, 2018, **47**, 852–908.
5 B. Mallesham, P. Sudarsanam, G. Raju and B. M. Reddy, *Green Chem.*, 2013, **15**, 478–489.
6 K. Sordakis, C. Tang, L. K. Vogt, H. Junge, P. J. Dyson, M. Beller and G. Laurenczy, *Chem. Rev.*, 2018, **118**, 372–433.
7 G. P. Peters, C. Le Quéré, R. M. Andrew, J. G. Canadell, P. Friedlingstein, T. Ilyina, R. B. Jackson, F. Joos, J. I. Korsbakken, G. A. McKinley, S. Sitch and P. Tans, *Nat. Clim. Change*, 2017, **7**, 848–850.
8 R. Snoeckx and A. Bogaerts, *Chem. Soc. Rev.*, 2017, **46**, 5805–5863.
9 http://www.cop21.gouv.fr/.
10 https://ec.europa.eu/clima/policies/international/paris_protocol/energy_en.
11 S. Van de Vyver, J. Geboers, P. A. Jacobs and B. F. Sels, *ChemCatChem*, 2011, **3**, 82–94.
12 M. Dusselier, M. Mascal and B. F. Sels, *Top. Curr. Chem.*, 2014, **353**, 1–40.
13 J. A. Geboers, S. Van de Vyver, R. Ooms, B. Op De Beeck, P. A. Jacobs and B. F. Sels, *Catal. Sci. Technol.*, 2011, **1**, 714–726.
14 D. M. Alonso, J. Q. Bond and J. A. Dumesic, *Green Chem.*, 2010, **12**, 1493–1513.
15 P. S. Reddy, P. Sudarsanam, B. Mallesham, G. Raju and B. M. Reddy, *J. Ind. Eng. Chem.*, 2011, **17**, 377–381.
16 S. Santoro, F. Ferlin, L. Luciani, L. Ackermann and L. Vaccaro, *Green Chem.*, 2017, **19**, 1601–1612.
17 X. Zhang, K. Rajagopalan, H. Lei, R. Ruan and B. K. Sharma, *Sustainable Energy Fuels*, 2017, **1**, 1664–1699.
18 W. Y. Hernandez, J. Lauwaert, P. Van Der Voort and A. Verberckmoes, *Green Chem.*, 2017, **19**, 5269–5302.
19 W. Liu, W. Li, H. Jiang and H. Yu, *Chem. Rev.*, 2017, **117**, 6367–6398.
20 P. Lamers, R. Hoefnagels, M. Junginger, C. Hamelinck and A. Faaij, *GCB Bioenergy*, 2015, **7**, 618–634.
21 X. Lian, Y. Xue, Z. Zhao, G. Xu, S. Han and H. Yu, *Int. J. Energy Res.*, 2017, **41**, 1798–1816.
22 T. Ennaert, J. Van Aelst, J. Dijkmans, R. De Clercq, W. Schutyser, M. Dusselier, D. Verboekend and B. F. Sels, *Chem. Soc. Rev.*, 2016, **45**, 584–611.
23 A. Corma, S. Iborra and A. Velty, *Chem. Rev.*, 2007, **107**, 2411–2502.
24 A. Aronne, M. Di Serio, R. Vitiello, N. J. Clayden, L. Minieri, C. Imparato, A. Piccolo, P. Pernice, P. Carniti and A. Gervasini, *J. Phys. Chem. C*, 2017, **121**, 17378–17389.
25 T. Kitanosono, K. Masuda, P. Xu and S. Kobayashi, *Chem. Rev.*, 2018, **118**, 679–746.
26 F. Yang, D. Deng, X. Pan, Q. Fu and X. Bao, *Natl. Sci. Rev.*, 2015, **2**, 183–201.
27 P. Munnik, P. E. de Jongh and K. P. de Jong, *Chem. Rev.*, 2015, **115**, 6687–6718.
28 A. Kokel, C. Schäfer and B. Török, *Green Chem.*, 2017, **19**, 3729–3751.
29 Y. Lin and G. W. Huber, *Energy Environ. Sci.*, 2009, **2**, 68–80.
30 B. Karimi, F. Mansouri and H. M. Mirzaei, *ChemCatChem*, 2015, **7**, 1736–1789.
31 M. J. Climent, A. Corma, S. Iborra and M. J. Sabater, *ACS Catal.*, 2014, **4**, 870–891.
32 A. Corma, S. B. A. Hamid, S. Iborra and A. Velty, *ChemSusChem*, 2008, **1**, 85–90.
33 M. Tao, D. Zhang, H. Guan, G. Huang and X. Wang, *Sci. Rep.*, 2016, **6**, 29840.
34 S. Song, L. Di, G. Wu, W. Dai, N. Guan and L. Li, *Appl. Catal., B*, 2017, **205**, 393–403.
35 E. Lam and J. H. T. Luong, *ACS Catal.*, 2014, **4**, 3393–3410.
36 A. Herbst and C. Janiak, *CrystEngComm*, 2017, **19**, 4092–4117.
37 A. Herbst and C. Janiak, *New J. Chem.*, 2016, **40**, 7958–7967.
38 A. A. Ibrahim, A. Lin, F. Zhang, K. M. AbouZeid and M. S. El-Shall, *ChemCatChem*, 2017, **9**, 469–480.
39 B. Xin and J. Hao, *Chem. Soc. Rev.*, 2014, **43**, 7171–7187.
40 S. Zhang, J. Zhang, Y. Zhang and Y. Deng, *Chem. Rev.*, 2017, **117**, 6755–6833.

Open Access Article. Published on 18 September 2018. Downloaded on 21/02/2026 10:11:12 PM.
This article is licensed under a Creative Commons Attribution-NonCommercial 3.0 Unported Licence.

41 H. Li, P. S. Bhadury, B. Song and S. Yang, *RSC Adv.*, 2012, **2**, 12525–12551.
42 Q. Wang, W. Hou, S. Li, J. Xie, J. Li, Y. Zhou and J. Wang, *Green Chem.*, 2017, **19**, 3820–3830.
43 K. L. Luska, P. Migowski and W. Leitner, *Green Chem.*, 2015, **17**, 3195–3206.
44 P. Ferrini and R. Rinaldi, *Angew. Chem., Int. Ed.*, 2014, **53**, 8634–8639.
45 Q. Song, F. Wang, J. Cai, Y. Wang, J. Zhang, W. Yu and J. Xu, *Energy Environ. Sci.*, 2013, **6**, 994–1007.
46 S. Wang, Z. Zhang, B. Liu and J. Li, *Catal. Sci. Technol.*, 2013, 2104–2112.
47 Y. Chiang, S. Dutta, C. Chen, Y. Huang, K. Lin, J. C. S. Wu, N. Suzuki, Y. Yamauchi and K. C. W. Wu, *ChemSusChem*, 2015, **8**, 789–794.
48 L. Liao, Y. Liu, Z. Li, J. Zhuang, Y. Zhou and S. Chen, *RSC Adv.*, 2016, **6**, 94976–94988.
49 Z. Zhang, J. Song and B. Han, *Chem. Rev.*, 2017, **117**, 6834–6880.
50 B. Liu and Z. Zhang, *ACS Catal.*, 2016, **6**, 326–338.
51 H. Li, Z. Fang, R. L. Smith Jr. and S. Yang, *Prog. Energy Combust. Sci.*, 2016, **55**, 98–194.
52 V. Trombettoni, D. Lanari, P. Prinsen, R. Luque, A. Marrocchi and L. Vaccaro, *Prog. Energy Combust. Sci.*, 2018, **65**, 136–162.
53 L. Liu and A. Corma, *Chem. Rev.*, 2018, **118**, 4981–5079.
54 A. Villa, N. Dimitratos, C. E. Chan-Thaw, C. Hammond, G. M. Veith, D. Wang, M. Manzoli, L. Prati and G. J. Hutchings, *Chem. Soc. Rev.*, 2016, **45**, 4953–4994.
55 D. N. Durgasri, T. Vinodkumar, P. Sudarsanam and B. M. Reddy, *Catal. Lett.*, 2014, **144**, 971–979.
56 M. H. Amin, S. Putla, S. Bee Abd Hamid and S. K. Bhargava, *Appl. Catal., A*, 2015, **492**, 160–168.
57 B. Ren, P. Sudarsanam, A. E. Kandjani, B. Hillary, M. H. Amin, S. K. Bhargava and L. A. Jones, *Electroanalysis*, 2018, **30**, 928–936.
58 J. C. Yang, M. W. Small, R. V. Grieshaber and R. G. Nuzzo, *Chem. Soc. Rev.*, 2012, **41**, 8179–8194.
59 Q. Wu, L. Yang, X. Wang and Z. Hu, *Acc. Chem. Res.*, 2017, **50**, 435–444.
60 A. Lu, G. Hao, Q. Sun, X. Zhang and W. Li, *Macromol. Chem. Phys.*, 2012, **213**, 1107–1131.
61 M. Titirici, R. J. White, N. Brun, V. L. Budarin, D. S. Su, F. del Monte, J. H. Clark and M. J. MacLachlan, *Chem. Soc. Rev.*, 2015, **44**, 250–290.
62 W. Xin and Y. Song, *RSC Adv.*, 2015, **5**, 83239–83285.
63 E. Pérez-Mayoral, V. Calvino-Casilda and E. Soriano, *Catal. Sci. Technol.*, 2016, **6**, 1265–1291.
64 S. Zhu, J. Wang and W. Fan, *Catal. Sci. Technol.*, 2015, **5**, 3845–3858.
65 V. Georgakilas, J. A. Perman, J. Tucek and R. Zboril, *Chem. Rev.*, 2015, **115**, 4744–4822.
66 P. Zhang, H. Zhu and S. Dai, *ChemCatChem*, 2015, **7**, 2788–2805.
67 D. Yu, E. Nagelli, F. Du and L. Dai, *J. Phys. Chem. Lett.*, 2010, **1**, 2165–2173.
68 J. L. Figueiredo, *J. Mater. Chem. A*, 2013, **1**, 9351–9364.
69 R. Zhong and B. F. Sels, *Appl. Catal., B*, 2018, **236**, 518–545.
70 S. Van de Vyver, J. Geboers, M. Dusselier, H. Schepers, T. Vosch, L. Zhang, G. Van Tendeloo, P. A. Jacobs and B. F. Sels, *ChemSusChem*, 2010, **3**, 698–701.
71 L. Liu, Y. Zhu, M. Su and Z. Yuan, *ChemCatChem*, 2015, **7**, 2765–2787.
72 H. Yang, R. Nie, W. Xia, X. Yu, D. Jin, X. Lu, D. Zhou and Q. Xia, *Green Chem.*, 2017, **19**, 5714–5722.
73 P. Chen, F. Yang, A. Kostka and W. Xia, *ACS Catal.*, 2014, **4**, 1478–1486.
74 M. A. Patel, F. Luo, M. R. Khoshi, E. Rabie, Q. Zhang, C. R. Flach, R. Mendelsohn, E. Garfunkel, M. Szostak and H. He, *ACS Nano*, 2016, **10**, 2305–2315.
75 J. M. R. Gallo, R. Alamillo and J. A. Dumesic, *J. Mol. Catal. A: Chem.*, 2016, **422**, 13–17.
76 J. Bedia, J. M. Rosas, J. Márquez, J. Rodríguez-Mirasol and T. Cordero, *Carbon*, 2009, **47**, 286–294.
77 J. Tessonnier, A. Villa, O. Majoulet, D. S. Su and R. Schlögl, *Angew. Chem., Int. Ed.*, 2009, **48**, 6543–6546.
78 H. Liu, J. Chen, L. Chen, Y. Xu, X. Guo and D. Fang, *ACS Sustainable Chem. Eng.*, 2016, **4**, 3140–3150.
79 Y. Wang, Z. Rong, Y. Wang, T. Wang, Q. Du, Y. Wang and J. Qu, *ACS Sustainable Chem. Eng.*, 2017, **5**, 1538–1548.
80 F. de Clippel, M. Dusselier, S. Van de Vyver, L. Peng, P. A. Jacobs and B. F. Sels, *Green Chem.*, 2013, **15**, 1398–1430.
81 F. de Clippel, M. Dusselier, R. Van Rompaey, P. Vanelderen, J. Dijkmans, E. Makshina, L. Giebeler, S. Oswald, G. V. Baron, J. F. M. Denayer, P. P. Pescarmona, P. A. Jacobs and B. F. Sels, *J. Am. Chem. Soc.*, 2012, **134**, 10089–10101.
82 Q. Ma, Y. Yu, M. Sindoro, A. G. Fane, R. Wang and H. Zhang, *Adv. Mater.*, 2017, **29**, 1605361.
83 S. Kang, J. Ye, Y. Zhang and J. Chang, *RSC Adv.*, 2013, **3**, 7360–7366.
84 J. Laohapornchaiphan, C. B. Smith and S. M. Smith, *Chem. – Asian J.*, 2017, **12**, 3178–3186.
85 B. L. A. Prabhavathi Devi, K. V. Lakshmi, K. N. Gangadhar, R. B. N. Prasad, P. S. Sai Prasad, B. Jagannadh, P. P. Kundu, G. Kumari and C. Narayana, *ChemistrySelect*, 2017, **2**, 1925–1931.
86 P. Serp and B. Machado, *Nanostructured Carbon Materials for Catalysis*, RSC Catalysis Series No. 23, The Royal Society of Chemistry, UK, 2015, ch. 1, pp. 1–45.
87 B. M. Upton and A. M. Kasko, *Chem. Rev.*, 2016, **116**, 2275–2306.
88 M. S. Singhvi, S. Chaudhari and D. V. Gokhale, *RSC Adv.*, 2014, **4**, 8271–8277.
89 C. Li, X. Zhao, A. Wang, G. W. Huber and T. Zhang, *Chem. Rev.*, 2015, **115**, 11559–11624.
90 R. Rinaldi, R. Jastrzebski, M. T. Clough, J. Ralph, M. Kennema, P. C. A. Bruijnincx and B. M. Weckhuysen, *Angew. Chem., Int. Ed.*, 2016, **55**, 8164–8215.
91 S. Van den Bosch, W. Schutyser, R. Vanholme, T. Driessen, S. F. Koelewijn, T. Renders, B. De Meester, W. J. J. Huijgen, W. Dehaen, C. M. Courtin, B. Lagrain, W. Boerjan and B. F. Sels, *Energy Environ. Sci.*, 2015, **8**, 1748–1763.

Open Access Article. Published on 18 September 2018. Downloaded on 21/02/2026 10:11:12 PM.
This article is licensed under a Creative Commons Attribution-NonCommercial 3.0 Unported Licence.

92 W. Schutyser, S. Van den Bosch, T. Renders, T. De Boe, S. F. Koelewijn, A. Dewaele, T. Ennaert, O. Verkinderen, B. Goderis, C. M. Courtin and B. F. Sels, *Green Chem.*, 2015, **17**, 5035–5045.
93 T. Renders, S. Van den Bosch, T. Vangeel, T. Ennaert, S. Koelewijn, G. Van den Bossche, C. M. Courtin, W. Schutyser and B. F. Sels, *ACS Sustainable Chem. Eng.*, 2016, **4**, 6894–6904.
94 T. Renders, W. Schutyser, S. Van den Bosch, S. Koelewijn, T. Vangeel, C. M. Courtin and B. F. Sels, *ACS Catal.*, 2016, **6**, 2055–2066.
95 S. Van den Bosch, W. Schutyser, S. F. Koelewijn, T. Renders, C. M. Courtin and B. F. Sels, *Chem. Commun.*, 2015, **51**, 13158–13161.
96 E. M. Anderson, M. L. Stone, R. Katahira, M. Reed, G. T. Beckham and Y. Román-Leshkov, *Joule*, 2017, **1**, 613–622.
97 I. Kumaniaev, E. Subbotina, J. Sävmarker, M. Larhed, M. V. Galkin and J. S. M. Samec, *Green Chem.*, 2017, **19**, 5767–5771.
98 B. Op de Beeck, M. Dusselier, J. Geboers, J. Holsbeek, E. Morré, S. Oswald, L. Giebeler and B. F. Sels, *Energy Environ. Sci.*, 2015, **8**, 230–240.
99 A. Deneyer, T. Ennaert, G. Cavents, J. Dijkmans, J. Vanneste, C. M. Courtin, M. Dusselier and B. F. Sels, *Green Chem.*, 2016, **18**, 5594–5606.
100 Y. Luo, J. Yi, D. Tong and C. Hu, *Green Chem.*, 2016, **18**, 848–857.
101 W. Daengprasert, P. Boonnoun, N. Laosiripojana, M. Goto and A. Shotipruk, *Ind. Eng. Chem. Res.*, 2011, **50**, 7903–7910.
102 S. Shen, C. Wang, B. Cai, H. Li, Y. Han, T. Wang and H. Qin, *Fuel*, 2013, **113**, 644–649.
103 A. Shrotri, H. Kobayashi, A. Tanksale, A. Fukuoka and J. Beltramini, *ChemCatChem*, 2014, **6**, 1349–1356.
104 J. Y. Park, M. A. Kim, S. J. Lee, J. Jung, H. M. Jang, P. P. Upare, Y. K. Hwang, J. Chang and J. K. Park, *J. Mater. Sci.*, 2015, **50**, 334–343.
105 S. G. Wettstein, J. Q. Bond, D. M. Alonso, H. N. Pham, A. K. Datye and J. A. Dumesic, *Appl. Catal., B*, 2012, **117–118**, 321–329.
106 C. Li, G. Xu, Y. Zhai, X. Liu, Y. Ma and Y. Zhang, *Fuel*, 2017, **203**, 23–31.
107 E. Sairanen, R. Karinen and J. Lehtonen, *Catal. Lett.*, 2014, **144**, 1839–1850.
108 X. Jin, P. S. Thapa, B. Subramaniam and R. V. Chaudhari, *ACS Sustainable Chem. Eng.*, 2016, **4**, 6037–6047.
109 Y. T. Kim, J. A. Dumesic and G. W. Huber, *J. Catal.*, 2013, **304**, 72–85.
110 Z. Gao, C. Li, G. Fan, L. Yang and F. Li, *Appl. Catal., B*, 2018, **226**, 523–533.
111 J. Li, J. Liu, H. Zhou and Y. Fu, *ChemSusChem*, 2016, **9**, 1339–1347.
112 M. Rivière, N. Perret, D. Delcroix, A. Cabiac, C. Pinel and M. Besson, *ACS Sustainable Chem. Eng.*, 2018, **6**, 4076–4085.
113 O. O. Ayodele, F. A. Dawodu, D. Yan, H. Dong, J. Xin and S. Zhang, *ChemistrySelect*, 2017, **2**, 4219–4225.
114 Y. Zhai, C. Li, G. Xu, Y. Ma, X. Liu and Y. Zhang, *Green Chem.*, 2017, **19**, 1895–1903.
115 J. Ji, H. Guo, C. Li, Z. Qi, B. Zhang, T. Dai, M. Jiang, C. Ren, A. Wang and T. Zhang, *ChemCatChem*, 2018, **10**, 415–421.
116 H. Zeng, D. Cao, Z. Qiu and C. J. Li, *Angew. Chem., Int. Ed.*, 2018, **57**, 3752–3757.
117 H. Lai, Y. Chou, M. Lee and K. A. Lin, *Chem. Eng. J.*, 2018, **332**, 717–726.
118 A. Bjelić, M. Grilc and B. Likozar, *Chem. Eng. J.*, 2018, **333**, 240–259.
119 J. Engelhardt, P. Lyu, P. Nachtigall, F. Schüth and Á. M. García, *ChemCatChem*, 2017, **9**, 1985–1991.
120 B. Mallesham, P. Sudarsanam and B. M. Reddy, *Catal. Sci. Technol.*, 2014, **4**, 803–813.
121 P. Sudarsanam, B. Mallesham, A. N. Prasad, P. S. Reddy and B. M. Reddy, *Fuel Process. Technol.*, 2013, **106**, 539–545.
122 X. Fu, J. Chen, X. Song, Y. Zhang, Y. Zhu, J. Yang and C. Zhang, *J. Am. Oil Chem. Soc.*, 2015, **92**, 495–502.
123 P. Chanchaochai, P. Boonnoun, N. Laosiripojana, M. Goto, B. Jongsomjit, J. Panpranot, O. Mekasuwandumrong and A. Shotipruk, *Chem. Eng. Commun.*, 2013, **200**, 1542–1552.
124 B. Mallesham, P. Sudarsanam and B. M. Reddy, *Ind. Eng. Chem. Res.*, 2014, **53**, 18775–18785.
125 S. B. A. Hamid, N. A. Daud, D. D. Suppiah, W. A. Yehya, P. Sudarsanam and S. K. Bhargava, *Polyhedron*, 2016, **120**, 154–161.
126 J. Dou, B. Zhang, H. Liu, J. Hong, S. Yin, Y. Huang and R. Xu, *Appl. Catal., B*, 2016, **180**, 78–85.
127 A. K. Geim and K. S. Novoselov, *Nat. Mater.*, 2007, **6**, 183–191.
128 E. Furimsky, *Ind. Eng. Chem. Res.*, 2017, **56**, 11359–11371.
129 B. Qiu, M. Xing and J. Zhang, *Chem. Soc. Rev.*, 2018, **47**, 2165–2216.
130 C. Su and K. P. Loh, *Acc. Chem. Res.*, 2013, **46**, 2275–2285.
131 V. K. Das, Z. B. Shifrina and L. M. Bronstein, *J. Mater. Chem. A*, 2017, **5**, 25131–25143.
132 P. P. Upare, J. Yoon, M. Y. Kim, H. Kang, D. W. Hwang, Y. K. Hwang, H. H. Kung and J. Chang, *Green Chem.*, 2013, **15**, 2935–2943.
133 H. Han, H. Zhao, Y. Liu, Z. Li, J. Song, W. Chu and Z. Sun, *RSC Adv.*, 2017, **7**, 3790–3795.
134 P. A. Russo, S. Lima, V. Rebuttini, M. Pillinger, M. Willinger, N. Pinna and A. A. Valente, *RSC Adv.*, 2013, **3**, 2595–2603.
135 C. Xiao, T. Goh, Z. Qi, S. Goes, K. Brashler, C. Perez and W. Huang, *ACS Catal.*, 2016, **6**, 593–599.
136 T. Zhang, Y. Ge, X. Wang, J. Chen, X. Huang and Y. Liao, *ACS Omega*, 2017, **2**, 3228–3240.
137 A. V. Nakhate and G. D. Yadav, *ACS Sustainable Chem. Eng.*, 2016, **4**, 1963–1973.
138 H. Wang, Y. Wang, T. Deng, C. Chen, Y. Zhu and X. Hou, *Catal. Commun.*, 2015, **59**, 127–130.
139 X. Jin, L. Dang, J. Lohrman, B. Subramaniam, S. Ren and R. V. Chaudhari, *ACS Nano*, 2013, **7**, 1309–1316.
140 J. Cheng, Y. Qiu, J. Zhang, R. Huang, W. Yang and Z. Fan, *Bioresour. Technol.*, 2017, **244**, 569–574.
141 X. Guo, J. Guan, B. Li, X. Wang, X. Mu and H. Liu, *Sci. Rep.*, 2015, **5**, 16451.

Open Access Article. Published on 18 September 2018. Downloaded on 21/02/2026 10:11:12 PM.
This article is licensed under a Creative Commons Attribution-NonCommercial 3.0 Unported Licence.

142 M. Melchionna, S. Marchesan, M. Prato and P. Fornasiero, *Catal. Sci. Technol.*, 2015, **5**, 3859–3875.
143 S. A. Miners, G. A. Rance and A. N. Khlobystov, *Chem. Soc. Rev.*, 2016, **45**, 4727–4746.
144 Y. Guo and J. Chen, *ChemPlusChem*, 2016, **80**, 1760–1768.
145 J. Chen, J. Zhong, Y. Guo and L. Chen, *RSC Adv.*, 2015, **5**, 5933–5940.
146 C. Zhou, W. Deng, X. Wan, Q. Zhang, Y. Yang and Y. Wang, *ChemCatChem*, 2015, **7**, 2853–2863.
147 D. S. Park, D. Yun, T. Y. Kim, J. Baek, Y. S. Yun and J. Yi, *ChemSusChem*, 2013, **6**, 2281–2289.
148 L. P. P. Sukma and E. W. Qian, *Environ. Prog. Sustainable Energy*, 2018, **37**, 850–860.
149 K. N. Sorokina, O. P. Taran, T. B. Medvedeva, Y. V. Samoylova, A. V. Piligaev and V. N. Parmon, *ChemSusChem*, 2017, **10**, 562–574.
150 S. Zhang, Z. Zheng, C. Zhao and L. Zhang, *ACS Omega*, 2017, **2**, 6123–6130.
151 D. Song, S. An, B. Lu, Y. Guo and J. Leng, *Appl. Catal., B*, 2015, **179**, 445–457.
152 J. Lee, J. Jung, H. J. Kim, T. Kim, K. Kim and E. E. Kwon, *ACS Sustainable Chem. Eng.*, 2017, **5**, 7433–7438.
153 L. Peng, A. Philippaerts, X. Ke, J. Van Noyen, F. De Clippel, G. Van Tendeloo, P. A. Jacobs and B. F. Sels, *Catal. Today*, 2010, **150**, 140–146.
154 U. Díaz, D. Brunel and A. Corma, *Chem. Soc. Rev.*, 2013, **42**, 4083–4097.
155 R. Liu, Y. Shi, Y. Wan, Y. Meng, F. Zhang, D. Gu, Z. Chen, B. Tu and D. Zhao, *J. Am. Chem. Soc.*, 2006, **128**, 11652–11662.
156 J. Xu, A. Wang, X. Wang, D. Su and T. Zhang, *Nano Res.*, 2011, **4**, 50–60.
157 P. Valle-Vigón, M. Sevilla and A. B. Fuertes, *Appl. Surf. Sci.*, 2012, **261**, 574–583.
158 P. A. Russo, M. M. Antunes, P. Neves, P. V. Wiper, E. Fazio, F. Neri, F. Barreca, L. Mafra, M. Pillinger, N. Pinna and A. A. Valente, *Green Chem.*, 2014, **16**, 4292–4305.
159 L. Fang, K. Zhang, L. Chen and P. Wu, *Chin. J. Catal.*, 2013, **34**, 932–941.
160 S. Van de Vyver, L. Peng, J. Geboers, H. Schepers, F. de Clippel, C. J. Gommes, B. Goderis, P. A. Jacobs and B. F. Sels, *Green Chem.*, 2010, **12**, 1560–1563.
161 R. Zhong, L. Peng, F. de Clippel, C. Gommes, B. Goderis, X. Ke, G. Van Tendeloo, P. A. Jacobs and B. F. Sels, *ChemCatChem*, 2015, **7**, 3047–3058.
162 R. Zhong, F. Yu, W. Schutyser, Y. Liao, F. de Clippel, L. Peng and B. F. Sels, *Appl. Catal., B*, 2017, **206**, 74–88.
163 L. Fang, K. Zhang, X. H. Li, H. H. Wu and P. Wu, *Chin. J. Catal.*, 2012, **33**, 114–122.
164 R. Zhong, L. Peng, R. I. Iacobescu, Y. Pontikes, R. Shu, L. Ma and B. F. Sels, *ChemCatChem*, 2017, **9**, 65–69.
165 W. Song, Z. Chen, W. Lai, I. Rodríguez-Ramos, X. Yi, W. Weng and W. Fang, *Appl. Catal., A*, 2017, **540**, 21–30.
166 S. Van de Vyver, J. Geboers, W. Schutyser, M. Dusselier, P. Eloy, E. Dornez, J. W. Seo, C. M. Courtin, E. M. Gaigneaux, P. A. Jacobs and B. F. Sels, *ChemSusChem*, 2012, **5**, 1549–1558.
167 T. van Haasterecht, C. C. I. Ludding, K. P. de Jong and J. H. Bitter, *J. Catal.*, 2014, **319**, 27–35.
168 Y. Xu, P. Jiang and Q. Li, *Acta Phys. -Chim. Sin.*, 2013, **29**, 1041–1047.
169 T. Zhang, W. Li, Z. Xu, Q. Liu, Q. Ma, H. Jameel, H. Chang and L. Ma, *Bioresour. Technol.*, 2016, **209**, 108–114.
170 Q. Liu, F. Yang, Z. Liu and G. Li, *J. Ind. Eng. Chem.*, 2015, **26**, 46–54.
171 Y. Wang, F. Delbecq, W. Kwapinski and C. Len, *Mol. Catal.*, 2017, **438**, 167–172.
172 P. Wataniyakul, P. Boonnoun, A. T. Quitain, M. Sasaki, T. Kida, N. Laosiripojana and A. Shotipruk, *Catal. Commun.*, 2018, **104**, 41–47.
173 X. Qi, Y. Lian, L. Yan and R. L. Smith, *Catal. Commun.*, 2014, **57**, 50–54.
174 Z. Sun, M. Tao, Q. Zhao, H. Guang, T. Shi and X. Wang, *Cellulose*, 2015, **22**, 675–682.
175 Y. Bai, L. Xiao and R. Sun, *Cellulose*, 2014, **21**, 2327–2336.
176 S. Dora, T. Bhaskar, R. Singh, D. V. Naik and D. K. Adhikari, *Bioresour. Technol.*, 2012, **120**, 318–321.
177 L. J. Konwar, P. Mäki-Arvela, E. Salminen, N. Kumar, A. J. Thakur, J. Mikkola and D. Deka, *Appl. Catal., B*, 2015, **176–177**, 20–35.
178 A. D. C. Fraga, C. P. B. Quitete, V. L. Ximenes, E. F. Sousa-Aguiar, I. M. Fonseca and A. M. B. Rego, *J. Mol. Catal. A: Chem.*, 2016, **422**, 248–257.
179 Y. Bai, L. Xiao and R. Sun, *Biomass Bioenergy*, 2015, **75**, 245–253.
180 P. K. Khatri, N. Karanwal, S. Kaul and S. L. Jain, *Tetrahedron Lett.*, 2015, **56**, 1203–1206.
181 J. Zhao, C. Zhou, C. He, Y. Dai, X. Jia and Y. Yang, *Catal. Today*, 2016, **264**, 123–130.
182 Q. Wang, J. Hao and Z. Zhao, *Aust. J. Chem.*, 2018, 24–31.
183 J. Zhang and J. Chen, *J. Energy Chem.*, 2016, **25**, 747–753.
184 X. Liu, B. Zhang, B. Fei, X. Chen, J. Zhang and X. Mu, *Faraday Discuss.*, 2017, **202**, 79–98.
185 P. Sudarsanam, L. Katta, G. Thrimurthulu and B. M. Reddy, *J. Ind. Eng. Chem.*, 2013, **19**, 1517–1524.
186 M. Li, X. Xu, Y. Gong, Z. Wei, Z. Hou, H. Li and Y. Wang, *Green Chem.*, 2014, **16**, 4371–4377.
187 M. M. Zainol, N. A. S. Amin and M. Asmadi, *Fuel Process. Technol.*, 2017, **167**, 431–441.
188 J. Bedia, J. M. Rosas, D. Vera, J. Rodríguez-Mirasol and T. Cordero, *Catal. Today*, 2010, **158**, 89–96.
189 S. B. Abd Hamid, M. M. Ambursa, P. Sudarsanam, L. H. Voon and S. K. Bhargava, *Catal. Commun.*, 2017, **94**, 18–22.
190 M. M. Ambursa, T. H. Ali, H. V. Lee, P. Sudarsanam, S. K. Bhargava and S. B. A. Hamid, *Fuel*, 2016, **180**, 767–776.
191 M. M. Ambursa, P. Sudarsanam, L. H. Voon, S. B. A. Hamid and S. K. Bhargava, *Fuel Process. Technol.*, 2017, **162**, 87–97.
192 S. Gbadamasi, T. H. Ali, L. H. Voon, A. Y. Atta, P. Sudarsanam, S. K. Bhargava and S. B. Abd Hamid, *RSC Adv.*, 2016, **6**, 25992–26002.
193 X. Liu, L. Xu, G. Xu, W. Jia, Y. Ma and Y. Zhang, *ACS Catal.*, 2016, **6**, 7611–7620.

Open Access Article. Published on 18 September 2018. Downloaded on 21/02/2026 10:11:12 PM.
This article is licensed under a Creative Commons Attribution-NonCommercial 3.0 Unported Licence.

194 M. Zhang, A. Sun, Y. Meng, L. Wang, H. Jiang and G. Li, *Catal. Surv. Asia*, 2015, **19**, 61–67.
195 J. R. Kastner, J. Miller, D. P. Geller, J. Locklin, L. H. Keith and T. Johnson, *Catal. Today*, 2012, **190**, 122–132.
196 I. F. Nata, M. D. Putra, C. Irawan and C. Lee, *J. Environ. Chem. Eng.*, 2017, **5**, 2171–2175.
197 W. Lou, Q. Guo, W. Chen, M. Zong, H. Wu and T. J. Smith, *ChemSusChem*, 2012, **5**, 1533–1541.
198 K. Ngaosuwan, J. G. Goodwin and P. Prasertdham, *Renewable Energy*, 2016, **86**, 262–269.
199 L. J. Konwar, R. Das, A. J. Thakur, E. Salminen, P. Mäki-Arvela, N. Kumar, J. Mikkola and D. Deka, *J. Mol. Catal. A: Chem.*, 2014, **388–389**, 167–176.
200 K. Malins, J. Brinks, V. Kampars and I. Malina, *Appl. Catal., A*, 2016, **519**, 99–106.
201 F. Zhang, X. Tian, Z. Fang, M. Shah, Y. Wang, W. Jiang and M. Yao, *Energy Convers. Manage.*, 2017, **142**, 107–116.
202 H. H. Mardhiah, H. C. Ong, H. H. Masjuki, S. Lim and Y. L. Pang, *Energy Convers. Manage.*, 2017, **144**, 10–17.
203 F. A. Dawodu, O. O. Ayodele, J. Xin and S. Zhang, *J. Chem. Technol. Biotechnol.*, 2014, **89**, 1898–1909.
204 C. Wang, F. Yuan, L. Liu, X. Niu and Y. Zhu, *ChemPlusChem*, 2015, **80**, 1657–1665.
205 P. S. Reddy, P. Sudarsanam, G. Raju and B. M. Reddy, *Catal. Commun.*, 2010, **11**, 1224–1228.
206 P. S. Reddy, P. Sudarsanam, G. Raju and B. M. Reddy, *J. Ind. Eng. Chem.*, 2012, **18**, 648–654.
207 P. Sudarsanam, B. Mallesham, P. S. Reddy and B. M. Reddy, *J. Chem. Sci. Technol.*, 2013, **2**, 161–168.
208 M. Tao, H. Guan, X. Wang, Y. Liu and R. Louh, *Fuel Process. Technol.*, 2015, **138**, 355–360.
209 C. Ban, W. Jeon, G. Park, H. C. Woo and D. H. Kim, *ChemCatChem*, 2017, **9**, 329–337.
210 Q. Yan, C. Wan, J. Liu, J. Gao, F. Yu, J. Zhang and Z. Cai, *Green Chem.*, 2013, **15**, 1631–1640.
211 B. F. Machado and P. Serp, *Catal. Sci. Technol.*, 2012, **2**, 54–75.
212 C. Huang, C. Li and G. Shi, *Energy Environ. Sci.*, 2012, **5**, 8848–8868.
213 Q. Zhu and Q. Xu, *Chem. Soc. Rev.*, 2014, **43**, 5468–5512.
214 O. Fleker, A. Borenstein, R. Lavi, L. Benisvy, S. Ruthstein and D. Aurbach, *Langmuir*, 2016, **32**, 4935–4944.
215 Y. Zhou, Y. Chen, Y. Hu, G. Huang, S. Yu and H. Jiang, *Chem. – Eur. J.*, 2014, **20**, 14976–14980.
216 X. Li, A. K. Tjiptoputro, J. Ding, J. M. Xue and Y. Zhu, *Catal. Today*, 2017, **279**, 77–83.
217 L. Zhu, X. Liu, H. Jiang and L. Sun, *Chem. Rev.*, 2017, **117**, 8129–8176.
218 M. Yabushita, P. Li, T. Islamoglu, H. Kobayashi, A. Fukuoka, O. K. Farha and A. Katz, *Ind. Eng. Chem. Res.*, 2017, **56**, 7141–7148.
219 J. Jiang and O. M. Yaghi, *Chem. Rev.*, 2015, **115**, 6966–6997.
220 J. Chen, K. Li, L. Chen, R. Liu, X. Huang and D. Ye, *Green Chem.*, 2014, **16**, 2490–2499.
221 J. Jiang, F. Gándara, Y. Zhang, K. Na, O. M. Yaghi and W. G. Klemperer, *J. Am. Chem. Soc.*, 2014, **136**, 12844–12847.
222 Y. Kuwahara, H. Kango and H. Yamashita, *ACS Sustainable Chem. Eng.*, 2017, **5**, 1141–1152.
223 V. Pascanu, A. Bermejo Gómez, C. Ayats, A. E. Platero-Prats, F. Carson, J. Su, Q. Yao, M. À. Pericàs, X. Zou and B. Martín-Matute, *ACS Catal.*, 2015, **5**, 472–479.
224 L. Ning, S. Liao, H. Cui, L. Yu and X. Tong, *ACS Sustainable Chem. Eng.*, 2018, **6**, 135–142.
225 Y. Guo, Y. Li, J. Chen and L. Chen, *Catal. Lett.*, 2016, **146**, 2041–2052.
226 T. B. Čelič, M. Grilc, B. Likozar and N. N. Tušar, *ChemSusChem*, 2015, **8**, 1703–1710.
227 Y. Wang, Y. Miao, S. Li, L. Gao and G. Xiao, *Mol. Catal.*, 2017, **436**, 128–137.
228 Y. Wang, S. Sang, W. Zhu, L. Gao and G. Xiao, *Chem. Eng. J.*, 2016, **299**, 104–111.
229 P. Hester, S. Xu, W. Liang, N. Al-Janabi, R. Vakili, P. Hill, C. A. Muryn, X. Chen, P. A. Martin and X. Fan, *J. Catal.*, 2016, **340**, 85–94.
230 G. Zi, Z. Yan, Y. Wang, Y. Chen, Y. Guo, F. Yuan, W. Gao, Y. Wang and J. Wang, *Carbohydr. Polym.*, 2015, **115**, 146–151.
231 P. Huang and L. Yan, *Chin. J. Chem. Phys.*, 2016, **29**, 742–748.
232 B. Murillo, B. Zornoza, O. de la Iglesia, C. Téllez and J. Coronas, *J. Catal.*, 2016, **334**, 60–67.
233 S. Huang, K. Yang, X. Liu, H. Pan, H. Zhang and S. Yang, *RSC Adv.*, 2017, **7**, 5621–5627.
234 X. Lu, L. Wang and X. Lu, *Catal. Commun.*, 2018, **110**, 23–27.
235 A. Chatterjee, X. Hu and F. L. Lam, *Catal. Today*, 2018, **314**, 137–146.
236 C. Lucarelli, S. Galli, A. Maspero, A. Cimino, C. Bandinelli, A. Lolli, J. Velasquez Ochoa, A. Vaccari, F. Cavani and S. Albonetti, *J. Phys. Chem. C*, 2016, **120**, 15310–15321.
237 A. Rapeyko, K. S. Arias, M. J. Climent, A. Corma and S. Iborra, *Catal. Sci. Technol.*, 2017, **7**, 3008–3016.
238 O. Kikhtyanin, D. Kubička and J. Čejka, *Catal. Today*, 2015, **243**, 158–162.
239 L. Ning, S. Liao, X. Liu, L. Yu, X. Zhuang and X. Tong, *J. Catal.*, 2017, **352**, 480–490.
240 F. G. Cirujano, A. Corma and F. X. Llabrés i Xamena, *Chem. Eng. Sci.*, 2015, **124**, 52–60.
241 I. Larasati, D. Winarni, F. R. Putri, Q. A. Hanif and W. W. Lestari, *IOP Conf. Ser.: Mater. Sci. Eng.*, 2017, **214**, 012006.
242 F. G. Cirujano, A. Corma and F. X. Llabrés i Xamena, *Catal. Today*, 2015, **257**, 213–220.
243 Q. Yuan, D. Zhang, L. V. Haandel, F. Ye, T. Xue, E. J. M. Hensen and Y. Guan, *J. Mol. Catal. A: Chem.*, 2015, **406**, 58–64.
244 S. B. A. Hamid, N. Basiron, W. A. Yehye, P. Sudarsanam and S. K. Bhargava, *Polyhedron*, 2016, **120**, 124–133.
245 Z. Hu, Y. Peng, Y. Gao, Y. Qian, S. Ying, D. Yuan, S. Horike, N. Ogiwara, R. Babarao, Y. Wang, N. Yan and D. Zhao, *Chem. Mater.*, 2016, **28**, 2659–2667.
246 R. Oozeerally, D. L. Burnett, T. W. Chamberlain, R. I. Walton and V. Degirmenci, *ChemCatChem*, 2018, **10**, 706–709.

Open Access Article. Published on 18 September 2018. Downloaded on 21/02/2026 10:11:12 PM.
This article is licensed under a Creative Commons Attribution-NonCommercial 3.0 Unported Licence.

247 Y. Su, G. Chang, Z. Zhang, H. Xing, B. Su, Q. Yang, Q. Ren, Y. Yang and Z. Bao, *AIChE J.*, 2016, **62**, 4403–4417.
248 M. Liu, Y. Zhang, E. Zhu, P. Jin, K. Wang, J. Zhao, C. Li and Y. Yan, *ChemistrySelect*, 2017, **2**, 10413–10419.
249 X. Liu, H. Li, H. Zhang, H. Pan, S. Huang, K. Yang and S. Yang, *RSC Adv.*, 2016, **6**, 90232–90238.
250 Z. Hasan, J. W. Jun and S. H. Jhung, *Chem. Eng. J.*, 2015, **278**, 265–271.
251 W. Xie, X. Yang and P. Hu, *Catal. Lett.*, 2017, **147**, 2772–2782.
252 J. Chen, S. Wang, J. Huang, L. Chen, L. Ma and X. Huang, *ChemSusChem*, 2013, **6**, 1545–1555.
253 S. Wang, J. Chen and L. Chen, *Catal. Lett.*, 2014, **144**, 1728–1734.
254 Z. Lin, X. Cai, Y. Fu, W. Zhu and F. Zhang, *RSC Adv.*, 2017, **7**, 44082–44088.
255 D. Zhang, F. Ye, Y. Guan, Y. Wang and E. J. M. Hensen, *RSC Adv.*, 2014, **4**, 39558–39564.
256 R. Insyani, D. Verma, S. M. Kim and J. Kim, *Green Chem.*, 2017, **19**, 2482–2490.
257 J. Chen, R. Liu, Y. Guo, L. Chen and H. Gao, *ACS Catal.*, 2015, **5**, 722–733.
258 F. Zhang, Y. Jin, Y. Fu, Y. Zhong, W. Zhu, A. A. Ibrahim and M. S. El-Shall, *J. Mater. Chem. A*, 2015, **3**, 17008–17015.
259 H. Yu, Z. Guo, Y. Zang, Y. Jin, T. Shi, G. Tu, C. Xu, Y. Fu, F. Zhang, J. Xie and W. Zhu, *Adv. Sci. Lett.*, 2017, **23**, 5821–5823.
260 F. Zhang, S. Zheng, Q. Xiao, Y. Zhong, W. Zhu, A. Lin and M. Samy El-Shall, *Green Chem.*, 2016, **18**, 2900–2908.
261 Q. Guan, B. Wang, X. Chai, J. Liu, J. Gu and P. Ning, *Fuel*, 2017, **205**, 130–141.
262 X. Fang, Y. Shi, K. Wu, J. Liang, Y. Wu and M. Yang, *RSC Adv.*, 2017, **7**, 40581–40590.
263 R. Fang, R. Luque and Y. Li, *Green Chem.*, 2017, **19**, 647–655.
264 R. Fang, R. Luque and Y. Li, *Green Chem.*, 2016, **18**, 3152–3157.
265 P. Jin, Y. Zhang, Y. Chen, J. Pan, X. Dai, M. Liu, Y. Yan and C. Li, *J. Taiwan Inst. Chem. Eng.*, 2017, **75**, 59–69.
266 Y. Su, C. Chen, X. Zhu, Y. Zhang, W. Gong, H. Zhang, H. Zhao and G. Wang, *Dalton Trans.*, 2017, **46**, 6358–6365.
267 B. Mallesham, P. Sudarsanam, B. V. S. Reddy and B. M. Reddy, *Appl. Catal., B*, 2016, **181**, 47–57.
268 L. Zheng, X. Li, W. Du, D. Shi, W. Ning, X. Lu and Z. Hou, *Appl. Catal., B*, 2017, **203**, 146–153.
269 A. Li, K. Shen, J. Chen, Z. Li and Y. Li, *Chem. Eng. Sci.*, 2017, **166**, 66–76.
270 H. Zhang, J. Nai, L. Yu and X. W. D. Lou, *Joule*, 2017, **1**, 77–107.
271 T. Torimoto, T. Tsuda, K. Okazaki and S. Kuwabata, *Adv. Mater.*, 2010, **22**, 1196–1221.
272 M. Koel, *Crit. Rev. Anal. Chem.*, 2005, **35**, 177–192.
273 V. I. Pârvulescu and C. Hardacre, *Chem. Rev.*, 2007, **107**, 2615–2665.
274 Q. Zhang, S. Zhang and Y. Deng, *Green Chem.*, 2011, **13**, 2619–2637.
275 A. M. Da Costa Lopes and R. Bogel-Lukasik, *ChemSusChem*, 2015, **8**, 947–965.
276 A. S. Amarasekara, *Chem. Rev.*, 2016, **116**, 6133–6183.
277 C. C. Weber, A. F. Masters and T. Maschmeyer, *Org. Biomol. Chem.*, 2013, **11**, 2534–2542.
278 Y. Wang, Z. Gu, W. Liu, Y. Yao, H. Wang, X. Xia and W. Li, *RSC Adv.*, 2015, **5**, 60736–60744.
279 H. Zhou, L. Yang, W. Li, F. Wang, W. Li, J. Zhao, X. Liang and H. Liu, *Ind. Eng. Chem. Res.*, 2012, **51**, 13173–13181.
280 H. Olivier-Bourbigou, L. Magna and D. Morvan, *Appl. Catal., A*, 2010, **373**, 1–56.
281 L. Han, H. Li, S. Choi, M. Park, S. Lee, Y. Kim and D. Park, *Appl. Catal., A*, 2012, **429–430**, 67–72.
282 J. Zhu, B. He, J. Huang, C. Li and T. Ren, *Microporous Mesoporous Mater.*, 2018, **260**, 190–200.
283 D. R. MacFarlane, J. M. Pringle, K. M. Johansson, S. A. Forsyth and M. Forsyth, *Chem. Commun.*, 2006, 1905–1917.
284 K. L. Luska, P. Migowski, S. El Sayed and W. Leitner, *ACS Sustainable Chem. Eng.*, 2016, **4**, 6186–6192.
285 H. Li, Q. Zhang, X. Liu, F. Chang, Y. Zhang, W. Xue and S. Yang, *Bioresour. Technol.*, 2013, **144**, 21–27.
286 Z. Wu, C. Chen, Q. Guo, B. Li, Y. Que, L. Wang, H. Wan and G. Guan, *Fuel*, 2016, **184**, 128–135.
287 E. Benazzi, A. Hirschauer, J. F. Joly, H. Olivier and J. Y. Berhard, EP0553009, 1993.
288 C. P. Mehnert, R. A. Cook, N. C. Dispenziere and M. Afeworki, *J. Am. Chem. Soc.*, 2002, **124**, 12932–12933.
289 T. Selvam, A. Machoke and W. Schwieger, *Appl. Catal., A*, 2012, **445–446**, 92–101.
290 M. Haumann and A. Riisager, *Chem. Rev.*, 2008, **108**, 1474–1497.
291 B. Wiredu and A. S. Amarasekara, *Catal. Commun.*, 2014, **48**, 41–44.
292 C. Zhang, Z. Fu, B. Dai, S. Zen, Y. Liu, Q. Xu, S. R. Kirk and D. Yin, *Cellulose*, 2014, **21**, 1227–1237.
293 H. Xu, H. Zhao, H. Song, Z. Miao, J. Yang, J. Zhao, N. Liang and L. Chou, *J. Mol. Catal. A: Chem.*, 2015, **410**, 235–241.
294 K. B. Sidhpuria, A. L. Daniel-da-Silva, T. Trindade and J. A. P. Coutinho, *Green Chem.*, 2011, **13**, 340–349.
295 X. Shi, M. Zhang, Y. Li and W. Zhang, *Green Chem.*, 2013, **15**, 3438–3445.
296 J. Miao, H. Wan and G. Guan, *Catal. Commun.*, 2011, **12**, 353–356.
297 K. L. Luska, A. Bordet, S. Tricard, I. Sinev, W. Grünert, B. Chaudret and W. Leitner, *ACS Catal.*, 2016, **6**, 3719–3726.
298 J. Yang, L. Zhou, X. Guo, L. Li, P. Zhang, R. Hong and T. Qiu, *Chem. Eng. J.*, 2015, **280**, 147–157.
299 V. Degirmenci, E. A. Pidko, P. C. M. M. Magusin and E. J. M. Hensen, *ChemCatChem*, 2011, **3**, 969–972.
300 V. Degirmenci and E. J. M. Hensen, *Environ. Prog. Sustainable Energy*, 2014, **33**, 657–662.
301 H. Li, S. Saravanamurugan, S. Yang and A. Riisager, *ACS Sustainable Chem. Eng.*, 2015, **3**, 3274–3280.
302 S. Kudo, N. Goto, J. Sperry, K. Norinaga and J. Hayashi, *ACS Sustainable Chem. Eng.*, 2017, **5**, 1132–1140.

 This journal is © The Royal Society of Chemistry 2018

Open Access Article. Published on 18 September 2018. Downloaded on 21/02/2026 10:11:12 PM.
This article is licensed under a Creative Commons Attribution-NonCommercial 3.0 Unported Licence.

303 Y. Sun, Q. Zhang, P. Zhang, D. Song and Y. Guo, *ACS Sustainable Chem. Eng.*, 2018, **6**, 6771–6782.
304 J. Sun, J. Yang, S. Li and X. Xu, *Catal. Commun.*, 2016, **83**, 35–38.
305 Y. Cao, H. Zhou and J. Li, *Renewable Sustainable Energy Rev.*, 2016, **58**, 871–875.
306 Z. Wu, C. Chen, H. Wan, L. Wang, Z. Li, B. Li, Q. Guo and G. Guan, *Energy Fuels*, 2016, **30**, 10739–10746.
307 H. Zhang, H. Li, H. Pan, X. Liu, K. Yang, S. Huang and S. Yang, *Energy Convers. Manage.*, 2017, **138**, 45–53.
308 M. K. Munshi, S. T. Lomate, R. M. Deshpande, V. H. Rane and A. A. Kelkar, *J. Chem. Technol. Biotechnol.*, 2010, **85**, 1319–1324.
309 M. H. Valkenberg, C. DeCastro and W. F. Holderich, *Green Chem.*, 2002, **4**, 88–93.
310 E. Salminen, P. Mäki-Arvela, P. Virtanen, T. Salmi and J. Mikkola, *Top. Catal.*, 2014, **57**, 1533–1538.
311 E. Salminen, P. Mäki-Arvela, P. Virtanen, T. Salmi, J. Wärnå and J. Mikkola, *Ind. Eng. Chem. Res.*, 2014, **53**, 20107–20115.
312 E. Salminen, L. Rujana, P. Mäki-Arvela, P. Virtanen, T. Salmi and J. Mikkola, *Catal. Today*, 2015, **257**, 318–321.
313 A. Eftekhari and T. Saito, *Eur. Polym. J.*, 2017, **90**, 245–272.
314 Y. Wang, J. Liu and C. Xia, *Tetrahedron Lett.*, 2011, **52**, 1587–1591.
315 J. Restrepo, R. Porcar, P. Lozano, M. I. Burguete, E. García-Verdugo and S. V. Luis, *ACS Catal.*, 2015, **5**, 4743–4750.
316 D. D. J. Liu and E. Y. X. Chen, *Biomass Bioenergy*, 2013, **48**, 181–190.
317 H. Li, X. He, Q. Zhang, F. Chang, W. Xue, Y. Zhang and S. Yang, *Energy Technol.*, 2013, **1**, 151–156.
318 H. Zhou, J. Song, X. Kang, J. Hu, Y. Yang, H. Fan, Q. Meng and B. Han, *RSC Adv.*, 2015, **5**, 15267–15273.
319 J. Zhang, S. Zhang, J. Han, Y. Hu and R. Yan, *Chem. Eng. J.*, 2015, **271**, 269–275.
320 W. Zhang, M. Li, J. Wang, Y. Zhao, S. Zhou and W. Xing, *Appl. Clay Sci.*, 2017, **146**, 167–175.
321 R. Wu, L. Song, G. Ma, Y. Su, Y. Hong, H. Wang and J. Li, *Catal. Lett.*, 2017, **147**, 2736–2744.
322 C. D. Hubbard, P. Illner and R. van Eldik, *Chem. Soc. Rev.*, 2011, **40**, 272–290.
323 P. Sudarsanam, B. Hillary, M. H. Amin, S. B. A. Hamid and S. K. Bhargava, *Appl. Catal., B*, 2016, **185**, 213–224.
324 Y. Li and W. Shen, *Chem. Soc. Rev.*, 2014, **43**, 1543–1574.
325 B. Hillary, P. Sudarsanam, M. H. Amin and S. K. Bhargava, *Langmuir*, 2017, **33**, 1743–1750.
326 D. Astruc, *Nanoparticles and Catalysis*, Wiley-VCH, Weinheim, 2008.
327 P. Sudarsanam, B. Hillary, B. Mallesham, B. G. Rao, M. H. Amin, A. Nafady, A. M. Alsalme, B. M. Reddy and S. K. Bhargava, *Langmuir*, 2016, **32**, 2208–2215.
328 S. Putla, M. H. Amin, B. M. Reddy, A. Nafady, K. A. Al Farhan and S. K. Bhargava, *ACS Appl. Mater. Interfaces*, 2015, **7**, 16525–16535.
329 P. Sudarsanam, B. Hillary, D. K. Deepa, M. H. Amin, B. Mallesham, B. M. Reddy and S. K. Bhargava, *Catal. Sci. Technol.*, 2015, **5**, 3496–3500.
330 S. Wang, Z. Zhang and B. Liu, *ACS Sustainable Chem. Eng.*, 2015, **3**, 406–412.
331 S. Shylesh, V. Schünemann and W. R. Thiel, *Angew. Chem., Int. Ed.*, 2010, **49**, 3428–3459.
332 C. Zhang, H. Wang, F. Liu, L. Wang and H. He, *Cellulose*, 2013, **20**, 127–134.
333 N. Mei and B. Liu, *Int. J. Hydrogen Energy*, 2016, **41**, 17960–17966.
334 V. Polshettiwar, R. Luque, A. Fihri, H. Zhu, M. Bouhrara and J. Basset, *Chem. Rev.*, 2011, **111**, 3036–3075.
335 A. Lu, E. L. Salabas and F. Schuth, *Angew. Chem., Int. Ed.*, 2007, **46**, 1222–1244.
336 J. Lee, Y. Lee, J. K. Youn, H. B. Na, T. Yu, H. Kim, S. Lee, Y. Koo, J. H. Kwak, H. G. Park, H. N. Chang, M. Hwang, J. Park, J. Kim and T. Hyeon, *Small*, 2008, **4**, 143–152.
337 V. Polshettiwar and R. S. Varma, *Green Chem.*, 2010, **12**, 743–754.
338 N. Candu, C. Rizescu, I. Podolean, M. Tudorache, V. I. Parvulescu and S. M. Coman, *Catal. Sci. Technol.*, 2015, **5**, 729–737.
339 Z. Zhang, Z. Yuan, D. Tang, Y. Ren, K. Lv and B. Liu, *ChemSusChem*, 2014, **7**, 3496–3504.
340 I. Elsayed, M. Mashaly, F. Eltaweel, M. A. Jackson and E. B. Hassan, *Fuel*, 2018, **221**, 407–416.
341 K. Rajkumari, J. Kalita, D. Das and L. Rokhum, *RSC Adv.*, 2017, **7**, 56559–56565.
342 A. Ramazani, M. Khoobi, F. Sadri, R. Tarasi, A. Shafiee, H. Aghahosseini and S. W. Joo, *Appl. Organomet. Chem.*, 2018, **32**, e3908.
343 Z. Zhang, J. Zhen, B. Liu, K. Lv and K. Deng, *Green Chem.*, 2015, **17**, 1308–1317.
344 Z. Yang, W. Qi, R. Su and Z. He, *Energy Fuels*, 2017, **31**, 533–541.
345 J. He, S. Yang and A. Riisager, *Catal. Sci. Technol.*, 2018, **8**, 790–797.
346 X. Long, P. Sun, Z. Li, R. Lang, C. Xia and F. Li, *Chin. J. Catal.*, 2015, **36**, 1512–1518.
347 C. Opris, B. Cojocaru, N. Gheorghe, M. Tudorache, S. M. Coman, V. I. Parvulescu, B. Duraki, F. Krumeich and J. A. van Bokhoven, *ACS Catal.*, 2017, **7**, 3257–3267.
348 C. Opris, B. Cojocaru, N. Gheorghe, M. Tudorache, S. M. Coman, V. I. Parvulescu, B. Duraki, F. Krumeich and J. A. van Bokhoven, *J. Catal.*, 2016, **339**, 209–227.
349 A. Negoi, I. T. Trotus, O. Mamula Steiner, M. Tudorache, V. Kuncser, D. Macovei, V. I. Parvulescu and S. M. Coman, *ChemSusChem*, 2013, **6**, 2090–2094.
350 Y. Xiong, Z. Zhang, X. Wang, B. Liu and J. Lin, *Chem. Eng. J.*, 2014, **235**, 349–355.
351 N. Candu, F. Anita, I. Podolean, B. Cojocaru, V. I. Parvulescu and S. M. Coman, *Green Process Synth.*, 2017, **6**, 255–264.
352 B. Liu, Y. Ren and Z. Zhang, *Green Chem.*, 2015, **17**, 1610–1617.
353 I. Podolean, A. Negoi, N. Candu, M. Tudorache, V. I. Parvulescu and S. M. Coman, *Top. Catal.*, 2014, **57**, 1463–1469.
354 V. Kuncser, S. M. Coman, E. Kemnitz and V. I. Parvulescu, *J. Appl. Phys.*, 2015, **117**, 17D724.

Open Access Article. Published on 18 September 2018. Downloaded on 21/02/2026 10:11:12 PM.
This article is licensed under a Creative Commons Attribution-NonCommercial 3.0 Unported Licence.

355 I. Podolean, V. Kuncser, N. Gheorghe, D. Macovei, V. I. Parvulescu and S. M. Coman, *Green Chem.*, 2013, **15**, 3077–3082.
356 I. Podolean, C. Rizescu, C. Bala, L. Rotariu, V. I. Parvulescu, S. M. Coman and H. Garcia, *ChemSusChem*, 2016, **9**, 2307–2311.
357 Y. Yang, W. Zhang, F. Yang, B. Zhou, D. Zeng, N. Zhang, G. Zhao, S. Hao and X. Zhang, *Nanoscale*, 2018, **10**, 2199–2206.
358 Q. Yang, S. Zhou and T. Runge, *J. Catal.*, 2015, **330**, 474–484.
359 Y. Wang, Z. Hu, G. Fan, J. Yan, G. Song and J. Li, *Waste Biomass Valorization*, 2018, DOI: 10.1007/s12649-018-0242-9.
360 C. Wu, W. Yuan, Y. Huang, Y. Xia, H. Yang, H. Wang and X. Liu, *Catal. Lett.*, 2017, **147**, 953–963.
361 K. Alibegovic, D. G. Morgan, Y. Losovyj, M. Pink, B. D. Stein, N. V. Kuchkina, E. S. Serkova, K. E. Salnikova, Z. B. Shifrina, V. G. Matveeva, E. M. Sulman and L. M. Bronstein, *ChemistrySelect*, 2017, **2**, 5485–5491.
362 F. Wang and Z. Zhang, *ACS Sustainable Chem. Eng.*, 2017, **5**, 942–947.
363 S. Wang, Z. Zhang, B. Liu and J. Li, *Ind. Eng. Chem. Res.*, 2014, **53**, 5820–5827.
364 B. Karimi, H. M. Mirzaei and E. Farhangi, *ChemCatChem*, 2014, **6**, 758–762.
365 N. Mittal, G. M. Nisola, L. B. Malihan, J. G. Seo, H. Kim, S. Lee and W. Chung, *RSC Adv.*, 2016, **6**, 25678–25688.
366 M. Raita, J. Arnthong, V. Champreda and N. Laosiripojana, *Fuel Process. Technol.*, 2015, **134**, 189–197.
367 M. R. Mehrasbi, J. Mohammadi, M. Peyda and M. Mohammadi, *Renewable Energy*, 2017, **101**, 593–602.
368 B. Thangaraj, Z. Jia, L. Dai, D. Liu and W. Du, *Arabian J. Chem.*, 2016, DOI: 10.1016/j.arabjc.2016.09.004.
369 Q. Zhang, Z. Zheng, C. Liu, C. Liu and T. Tan, *Colloids Surf., B*, 2016, **140**, 446–451.
370 M. Kalantari, M. Kazemeini and A. Arpanaei, *Biochem. Eng. J.*, 2013, **79**, 267–273.
371 O. V. Manaenkov, J. J. Mann, O. V. Kislitza, Y. Losovyj, B. D. Stein, D. G. Morgan, M. Pink, O. L. Lependina, Z. B. Shifrina, V. G. Matveeva, E. M. Sulman and L. M. Bronstein, *ACS Appl. Mater. Interfaces*, 2016, **8**, 21285–21293.
372 N. Cherkasov, V. Jadvani, J. Mann, Y. B. Losovyj, Z. B. Shifrina, L. M. Bronstein and E. V. Rebrov, *Fuel Process. Technol.*, 2017, **167**, 738–746.
373 D. Lai, L. Deng, J. Li, B. Liao, Q. Guo and Y. Fu, *ChemSusChem*, 2011, **4**, 55–58.
374 T. Komanoya, H. Kobayashi, K. Hara, W. Chun and A. Fukuoka, *Appl. Catal., A*, 2011, **407**, 188–194.
375 B. Liu, Z. Zhang, K. Lv, K. Deng and H. Duan, *Appl. Catal., A*, 2014, **472**, 64–71.
376 A. B. Gawade, A. V. Nakhate and G. D. Yadav, *Catal. Today*, 2018, **309**, 119–125.
377 Y. N. Regmi, J. K. Mann, J. R. McBride, J. Tao, C. E. Barnes, N. Labbé and S. C. Chmely, *Catal. Today*, 2018, **302**, 190–195.
378 K. Liu, R. Wang and M. Yu, *RSC Adv.*, 2017, **7**, 51814–51821.
379 L. Lin, S. Vittayapadung, X. Li, W. Jiang and X. Shen, *Environ. Prog. Sustainable Energy*, 2013, **32**, 1255–1261.
380 M. Tudorache, L. Protesescu, S. Coman and V. I. Parvulescu, *Green Chem.*, 2012, **14**, 478–482.
381 M. Tudorache, G. Ghemes, A. Nae, E. Matei, I. Mercioniu, E. Kemnitz, B. Ritter, S. Coman and V. I. Parvulescu, *Cent. Eur. J. Chem.*, 2014, **12**, 1262–1270.
382 M. Tudorache, L. Protesescu, A. Negoi and V. I. Parvulescu, *Appl. Catal., A*, 2012, **437–438**, 90–95.
383 M. Tudorache, A. Negoi, L. Protesescu and V. I. Parvulescu, *Appl. Catal., B*, 2014, **145**, 120–125.
384 M. Tudorache, A. Nae, S. Coman and V. I. Parvulescu, *RSC Adv.*, 2013, **3**, 4052–4058.
385 M. Tudorache, A. Negoi, B. Tudora and V. I. Parvulescu, *Appl. Catal., B*, 2014, **146**, 274–278.
386 D. Wang and D. Astruc, *Chem. Rev.*, 2014, **114**, 6949–6985.
387 M. Shokouhimehr, *Catalysts*, 2015, **5**, 534–560.

 This journal is © The Royal Society of Chemistry 2018